

HIGH-FREQUENCY TRANSFORMER MODEL

FOR

SWITCHING TRANSIENT STUDIES

by

SUTHEP CHIMKLAI

B.Eng., Chulalongkorn University, 1977

M.Sc. in EE., Carnegie Mellon University, 1984

A THESIS SUBMITTED IN PARTIAL FULFILLMENT OF

THE REQUIREMENTS FOR THE DEGREE OF

DOCTOR OF PHILOSOPHY

in

THE FACULTY OF GRADUATE STUDIES

Department of Electrical Engineering

We accept this thesis as conforming

to the required standard

THE UNIVERSITY OF BRITISH COLUMBIA

April 11, 1995

© Suthep Chimklai, 1995

In presenting this thesis in partial fulfilment of the requirements for an advanced degree at the University of British Columbia, I agree that the Library shall make it freely available for reference and study. I further agree that permission for extensive copying of this thesis for scholarly purposes may be granted by the head of my department or by his or her representatives. It is understood that copying or publication of this thesis for financial gain shall not be allowed without my written permission.

(Signature)

Department of Electrical Engineering

The University of British Columbia
Vancouver, Canada

Date April 20, 1995

ABSTRACT

The objective of this thesis is to develop a simplified high-frequency model for three-phase, two- and three-winding transformers. The model is an extension of the classical 60 Hz model which includes two important factors prevailing in transformers under transient conditions: stray capacitances which cause transformers to resonate and frequency dependent characteristics of the leakage flux and winding resistances due to skin effects. The model is not aimed to represent internal details of the transformer and only lumped circuit parameters are used in order to simulate terminal behaviours of the transformer. However, it is different from other terminal models in that it is not just an impedance or admittance black box derived from measured transfer functions. Only the meaningful parameters which correspond to the physical components in the real transformer are included in the model.

The short-circuit impedances T-form of the classical model is retained which makes it possible to separate the frequency-dependent series branch from the constant-valued capacitances. In addition, it enables the model to be built at the coil level which is independent of winding connections. The model stray capacitances are placed at the corresponding coils terminals. If they link two coils they will be split into two halves with one half connected at the upper ends and the other half at the lower ends. The frequency

dependent series branch is divided into sections corresponding to various sections in the transformer coil which can be assumed uniform. An RL equivalent network is used to synthesise the frequency dependent behaviour of each section. The values of R's and L's are calculated from minimum-phase-shift approximations which guarantees numerical stability of the resulting network. With the use of symmetrical components, mathematical complications of fitting mutual impedance functions are avoided and also the number of impedance functions to be fitted by rational functions is reduced.

A number of short-circuit tests on the actual power transformers installed in the Thailand 's power system were performed to determine the parameters of the model. The frequency responses calculated from the model are compared with the tests. Also, a time-domain test was conducted and the result was used for comparison with the simulation from the model.

TABLE OF CONTENTS

ABSTRACT		ii
TABLE OF CONTENTS		iv
LIST OF ILLUSTRATIONS		vi
LIST OF TABLES		x
ACKNOWLEDGMENT		xii
Chapter One	INTRODUCTION	1
	1. Previous Work	3
	2. Proposed Model	10
Chapter Two	NON-FREQUENCY DEPENDENT PART	14
	1. Stray capacitances in Three-Phase Transformer	14
	2. Types of Stray Capacitances	16
	3. Discrete-Time Model	20
	4. Capacitance Model for Multi-Resonance Transformer	23
	5. Implementaiton of Interwinding Capacitance Modification	34
Chapter Three	MODELLING OF FREQUENCY DEPENDENT COMPONENTS	36
	1. Short-Circuit Responses of Transformers	36
	2. Equivalent Network Representation for $Z_{winding}$	39
	3. Discretization of Equivalent Network for $Z_{winding}$	44

	4. Updating History Terms	50
Chapter Four	THE COMPLETE MODEL	53
	1. Discrete-time Model in Sequence Domain	54
	2. Discrete-time Model in Phase Co-ordinates	59
	3. Nodal Admittance Matrix	64
Chapter Five	MEASUREMENTS AND NUMERICAL RESULTS	68
	1. Measurement of Frequency Dependent Leakage Impedance	68
	2. Measurement of Stray Capacitances	84
Chapter Six	NUMERICAL EXAMPLES	90
	1. Two-winding Transformer	90
	2. Three-winding Transformer	112
	3. Simulation of Transient Recovery Voltage	137
Chapter Seven	PROPOSED FUTURE WORK	141
Chapter Eight	CONCLUSIONS	143
	REFERENCE LIST	145
Appendix 1	FITTING OF THE IMPEDANCE FUNCTION	148

LIST OF ILLUSTRATIONS

Figure		Page
1.1	Amplitude frequency response of a 50 MVA 115/23 kV transformer versus calculated impedance from its 60 Hz model	2
1.2	Transformer model developed by [2]	6
1.3	P. T. M. Vaessen's high frequency transformer model	7
1.4	The proposed transformer model which consists of the non-frequency dependent stray capacitances and the frequency dependent part	10
2.1	A cutaway view of a single phase, two-winding transformer	14
2.2	Stray capacitances in a three-phase, three-winding transformer	15
2.3	Stray capacitances in any phase of a three-phase, three-winding transformer	17
2.4	Impedance of stray capacitances in the 115/23 kV, 50 MVA transformer	18
2.5	Phase-to-phase capacitances in a three-phase transformer	19
2.6	Discrete time representation of a capacitance	20
2.7	Stray capacitances in a single phase, two-winding transformer	21
2.8	Representation of interwinding capacitances for a two-winding transformer	24
2.9	Transformation of a three-winding transformer into a delta representation	27
2.10	Equivalent circuit after interwinding capacitances have been moved to the same side as the leakage impedances	31

Figure		Page
3.1	Typical short-circuit frequency response of a transformer	37
3.2	Frequency dependent characteristics of the real part of the series impedance $Z_{winding}$	39
3.3	RLC synthesis network to approximate $Z_{winding}$	44
3.4	Discretization of a section of the equivalent network for $Z_{winding}$	46
4.1	Discrete-time equivalent circuit for a sequence model of a transformer	54
4.2	Transformer node labelling for external network connection	65
5.1	Measurement of positive-sequence impedance in a Yd transformer	75
5.2	Application of the Capacitance & D. F. Bridge to measure stray capacitances in a transformer	85
5.3	Measurement of the sum of interwinding and winding-to-ground capacitances in a three-winding, three-phase transformer with CB100	86
6.1	Transformer capacitance impedance measured with an Impedance Analyser	92
6.2	Schematic of short-circuit frequency response tests	94
6.3	Real part of short-circuit impedance (zero-sequence) for the two-winding transformer	95
6.4	Short-circuit impedance (zero-sequence) for the two-winding transformer	96
6.5	Short-circuit impedances (positive-sequence) of the two-winding transformer measured on different windings	99
6.6	Real part of the short-circuit impedance (positive-sequence) for the two-winding transformer	100
6.7	Transformer short-circuit impedance (positive-sequence) for the two-winding transformer	101

Figure	Page
6.8 Fitting of the real part of the Z_{winding} impedance for the zero-sequence circuit of the two-winding transformer	104
6.9 Fitting of the magnitude and phase angle of the frequency dependent Z_{winding} impedance for the zero-sequence circuit of the two-winding transformer	105
6.10 Fitting of the real part of the Z_{winding} impedance for the positive-sequence circuit of the two-winding transformer	108
6.11 Fitting of the magnitude and phase angle of the frequency dependent Z_{winding} impedance for the positive-sequence circuit of the two-winding transformer	109
6.12 Impulse response test	111
6.13 Effective stray capacitances of a three-winding transformer during the short-circuit tests	114
6.14 Fitting of the short-circuit impedance measured on the low-voltage side with the high and tertiary-voltage windings short-circuited (zero-sequence)	115
6.15 Fitting of the short-circuit impedance measured on the high-voltage side with the low and tertiary-voltage windings short-circuited (zero-sequence)	116
6.16 Fitting of the short-circuit impedance measured on the low-voltage side with only the tertiary-voltage winding short-circuited (zero-sequence)	117
6.17 Fitting of the short-circuit impedance measured on the tertiary-voltage side with the high and low-voltage windings short-circuited (positive-sequence)	118
6.18 Fitting of the short-circuit impedance measured on the tertiary-voltage side with only the high-voltage winding short-circuited (positive-sequence)	119

Figure	Page
6.19 Fitting of the short-circuit impedance measured on the tertiary-voltage side with only the low-voltage winding short-circuited (positive-sequence)	120
6.20 Fitting of the sum of the high and low-voltage winding impedances (zero-sequence)	124
6.21 Fitting of the sum of the high and tertiary-voltage winding impedances (zero-sequence)	125
6.22 Fitting of the sum of the low and tertiary-voltage winding impedances (zero-sequence)	126
6.23 Fitting of the sum of the high and low-voltage winding impedances (positive-sequence)	127
6.24 Fitting of the sum of the high and tertiary-voltage winding impedances (positive-sequence)	128
6.25 Fitting of the sum of the low and tertiary-voltage winding impedances (positive-sequence)	129
6.26 Fitting of the winding impedance of the high-voltage winding (positive-sequence)	136
6.27 Winding impedance of the low-voltage winding (positive-sequence)	138
6.28 Winding impedance of the tertiary-voltage winding (positive-sequence)	139
6.29 Transient recovery voltage in a circuit breaker after clearing a fault	140
7.1 Capacitance model with dielectric losses	141
A1.1 Equivalent network representation of the frequency dependent branch of the sequence model	148

LIST OF TABLES

Table		Page
1.1	Comparison of the no. impedance functions required by the proposed model and the Ontario Hydro's model for a three-phase transformer	4
1.2	No. of history terms to be updated in the proposed model and in the Ontario Hydro's model	5
3.1	Summary of discrete-time models for inductances and capacitances using trapezoidal and backward Euler integration rules	45
6.1	Measured values of capacitances for the tested transformer	91
6.2	Parameters of the zero-sequence short-circuit equivalent network for the tested two-winding transformer	97
6.3	Parameters of the positive-sequence short-circuit equivalent network for the tested two-winding transformer	102
6.4	Parameters of the zero-sequence $Z_{winding}$ impedance for the tested two-winding transformer	106
6.5	Parameters of the positive-sequence $Z_{winding}$ impedance for the tested two-winding transformer	110
6.6	Measured values of capacitances for the three-winding transformer	113
6.7	Parameters of the zero-sequence short-circuit equivalent network for the tested three-winding transformer	121
6.8	Parameters of the positive-sequence short-circuit equivalent network for the tested three-winding transformer	122

6.9	Parameters of the zero-sequence Z_{winding} impedance for the tested three-winding transformer	130
6.10	Parameters of the positive-sequence Z_{winding} impedance for the tested three-winding transformer	131

ACKNOWLEDGMENT

I would like to thank the Electricity Generating Authority of Thailand (EGAT) which granted me the opportunity to come to Canada on an education leave. I would like also to thank Mr. Siridat Glankhamdee, Director of Systems Planning Department, for his very much appreciated guidance regarding my research work.

A very special thank you to the Canadian International Development Agency (CIDA) for providing me the scholarship for my graduate study at UBC.

My deepest gratitude to Dr. José R. Martí, my advisor, for initiating the research idea and for his supervision afterwards. During the entire course of my study, I received invaluable suggestions, support and time from him. With his constant encouragement, my achievements are even more special to me.

To all the professors whose courses I attended. I learned a lot from them during the time I did my coursework. I found their lectures extremely worthwhile for my research work.

To my special friend Supatra for her excellent work on transformer data which was a key to the success of my project. I will always hold this exceptional friendship in high regard.

To all my friends in the Power Group who in one way or another contributed to the accomplishment of my study, I sincerely thank all of them.

Last but not least, I want to thank my wife Porntip for her understanding and patience. Without these, I would have not been able to stay in Canada until the end of my study program.

Chapter One

INTRODUCTION

Switching transients have been a concern in most power utilities. They could cause damages to various equipment in the power system. The problem may be prevented or avoided if simulations on the power system under various transient conditions can be conducted with sufficient accuracy so that the effects of the transient can be predicted in advance. However, simulation studies need good models of the electrical equipment including power transformers which are very common in the power system. Unfortunately, a mathematical model of the power transformer is not common, and a general model is being under research by many interested people.

When the power transformer is in operation, it will be subject to both steady-state and transient conditions. At steady state, the coupling in the transformer is primarily due to the inductive interaction of various coils. Under this circumstance, the transformer may be accurately modelled with inductances and resistances without the need to include any capacitances. The low frequency model is good for an electromagnetic transients study if the frequency components under consideration are below a certain frequency limit. For example, the low frequency model of the 50 MVA, 115/23 kV power transformer whose data are used in this thesis will be good to about 5 kHz, as shown in fig. 1.1. At a higher

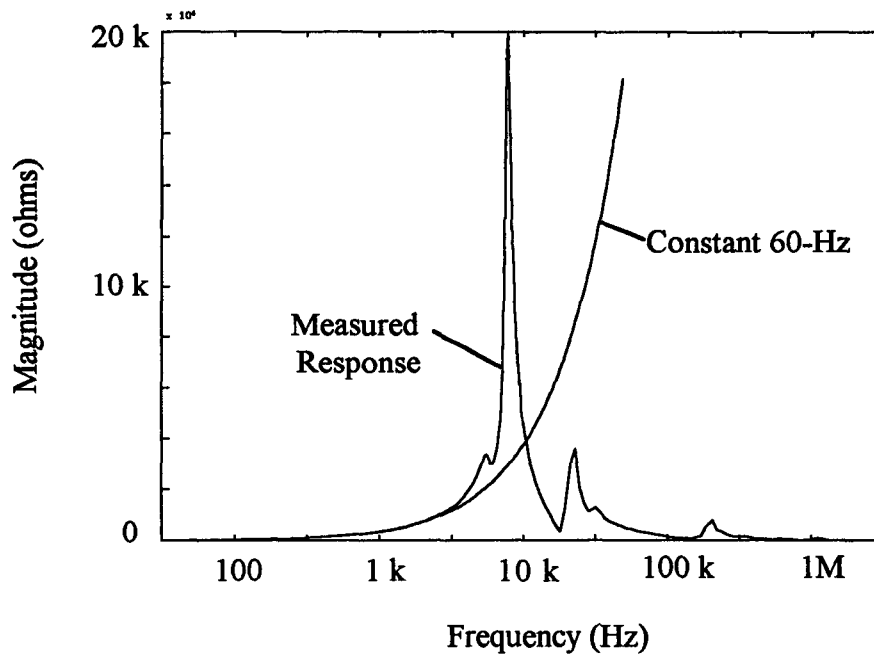


Fig. 1.1 Amplitude frequency response of a 50 MVA 115/23 KV transformer versus the calculated impedance from its 60 Hz model.

frequency range, such as switching frequencies, the low frequency model should be modified so as to improve its accuracy.

In recent years, many authors have presented a number of good transformer models. Nonetheless, some of these models are limited to single phase transformer while some others are "black box" representations. The problems which are mostly encountered in transformer modelling are numerical stability, difficulty in data acquisition to realise parameters for the model, size of the matrix to describe the model, and complexity of the model itself which requires sophisticated knowledge of electromagnetic theory. This implies that further improvements are still required before satisfactory models finally

become available. The proposed model in this thesis is designed to be simple, easy to implement and requires minimum understanding of electromagnetic theory, yet it is sufficiently accurate. The model can be used in various analyses associated with switching transients such as surge arresters selection, insulation level evaluation, etc. In addition, the model may be used to carry out simulations under different transient conditions to investigate causes of problems which already occurred or are expected to take place without the need to conduct the actual field tests. Before further details of the proposed model are discussed, it is helpful to look back at some of the previous works in transformer modelling.

1. Previous Work

It may be accurate to say that there are hundreds of transformer models which have been proposed for transient simulation studies. However, the objective of this thesis is on improving EMTP models. Therefore, transformer models will be grouped into EMTP models and models belonging to other sources.

1.1 EMTP

A high frequency model for EMTP has been recently developed by Ontario Hydro, Canada [1]. This model was derived from the nodal admittance matrix equation which relates transformer currents and voltages at its external terminals. For example, a wye-delta-wye transformer in which the delta winding has no accessible terminals is modelled by a

[6x6] matrix equation. This representation is in contrast with the proposed model in this thesis in which the modelling of transformers begins at the coil level.

In Ontario Hydro's model, the coupling between different windings of the same phase is averaged so as to make use of the symmetrical components transformation. The distinct elements of the admittance matrix after transformation which are needed to be fitted by rational functions are reduced to $m(m+1)$ from $3m(3m+1)/2$, where m is the no. of windings. Comparison of the no. of impedance functions required by the proposed model and Ontario Hydro's model is given in table 1.1 below.

Table 1.1--Comparison of the no. of impedance functions required by the proposed model and Ontario Hydro's model for a three-phase transformer

No. of windings	Proposed model	Ontario Hydro's	Times
2	2	6	3
3	6	12	2

Even though it is required to fit only $m(m+1)$ elements, the total number of measurements required is still $3m(3m+1)/2$. Therefore, the transformation only saves fitting time not the time spent for measurements.

In terms of time-domain solution costs, the differences are even greater. For example, for a three-phase two-winding transformer, only 3 history terms are needed to be

updated in the proposed model. Whereas in Ontario's Hydro model, 12 history terms must be updated due to the use of a pi-equivalent circuit which requires 12 impedances for the complete three-phase two winding transformer. The savings of simulation time in the proposed model is clearly demonstrated in table 1.2.

Table 1.2--No. of history terms to be updated in the proposed model and in Ontario Hydro's model

No. of windings	Proposed model	Ontario Hydro's	Times
2	3	12	4
3	9	27	3

1.2 Other Models

There are a number of models developed by other sources. However, they may be classified into 2 major groups: the terminal models and the detailed models.

1.2.1 Terminal Models

Most of the previous works in transformer modelling fall into this type. Some of these works are:

(a) M. D'Amore, et al., [2] modelled a transformer as a two port network consisting of a series impedance $Z(s)$ and a parallel capacitance connected at the output port, as

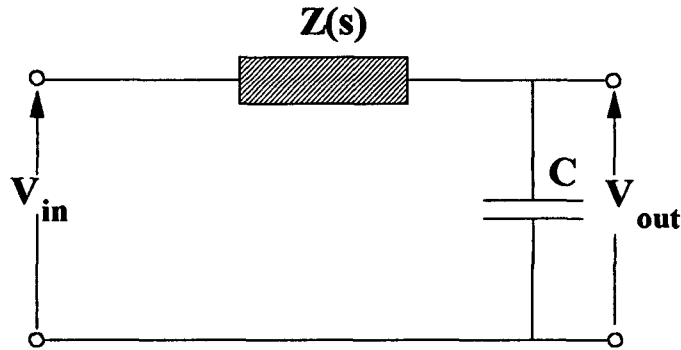


Fig 1.2 Transformer model developed by [2].

shown in fig. 1.2. A number of networks for $Z(s)$, made up of R, L and C's were used to reproduce the voltage gain functions of single and double resonance transformers. There was no restriction in the sign of the R, L, C parameters used. Consequently, there is no guarantee of numerical stability in the model. Furthermore, the choice of $Z(s)$ which would produce more than two resonances was not shown in the work.

(b) P. T. M. Vaessen [3] also constructed a transformer model from the voltage function. He used a two-port network consisting of two ideal transformers to duplicate each peak in the voltage gain function. Many such two-port networks were connected in parallel if multiple peaks were to be matched. The diagram of Vaessen's model is shown in fig. 1.3.

(c) R. C. Degeneff [4] proposed a transformer model which was made of RL parallel components as the basic building block. The model was constructed by joining a pair of transformer terminals with one RL parallel block and also from each terminal to

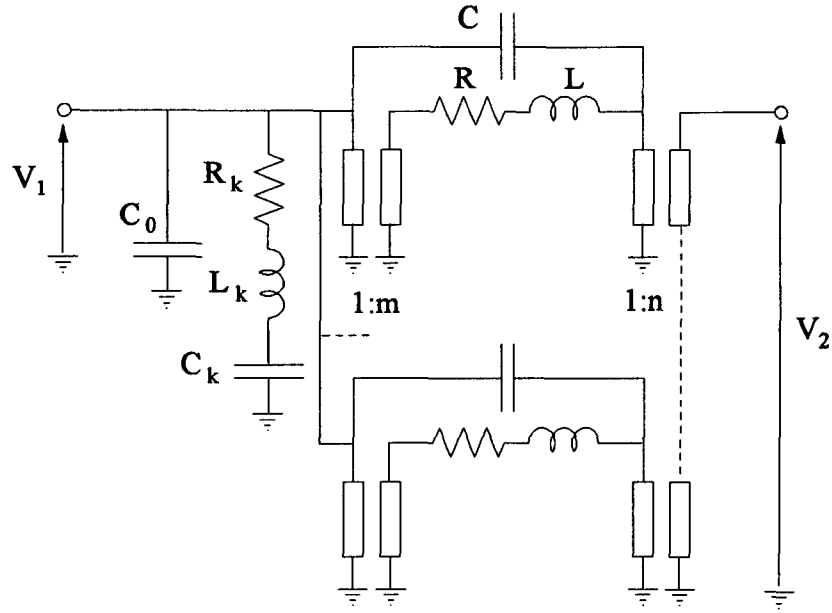


Fig. 1.3 P. T. M. Vaessen's high frequency transformer model.

ground. In his paper, he demonstrated the model for a 250 MVA single phase auto-transformer with tertiary winding. For this single phase transformer where the common winding was grounded, there were a total of five terminals including ground to be considered. The total number of RL parallel branches required to build the model was ten, or $0.5(n-1)n$ - where n is the number of terminals in the model. This type of model would be almost impossible to realise for the three-phase transformer because the number of branches required would be too many. Furthermore, losses were not included in the model.

(d) T. Adielson et al. [5] developed a transformer model from a matrix equation which describes a multi-winding transformer as n magnetically coupled coils. The model was designed for transient studies within the frequency range of tens of kHz. Adielson

proposed the separate modelling of stray capacitances from the frequency dependent part of the transformer model. However, he used an RLC equivalent circuit to represent the frequency dependent part without consideration on numerical stability. He stated in his paper that he encountered many cases of numerical problems in the time-domain simulations.

(e) CIGRE WG 33.02 Report [6] presented several models for transient studies. Each model was designed to serve the study within a particular frequency range. The effects of stray capacitances, frequency dependency of the windings and leakage flux were introduced. These models, therefore, were more accurate for transient studies than the 60 Hz model. However, the frequency dependent effect of the winding was represented by only RL parallel branches which is not sufficient to represent a transformer with multi-resonance characteristics.

The models described in (a) to (e) above were developed for the single phase transformer. Most of them, except in (e), were based on the concept of the black box, without paying attention to the internal conditions of the transformer under transients. We believe the transformer model should be more representative of the real transformer. It should be general and every parameter constituting the model should be included only if it is related to what it would represent in the real transformer. This is the core idea of the model proposed in this thesis.

1.2.2 Detailed Model

Not many works are devoted to modelling the transformer in detail. Two of these works are reviewed here:

(a) R. C. Degeneff [7] has worked at modelling a transformer at the turn level. Each turn of the coil was represented with a loss resistance, a turn-to-turn capacitance and an inductance with loss. Also the capacitive coupling of the turn to ground was taken into account and was represented with a capacitance with loss. The parameters for the model were obtained from measurements.

(b) Francisco de Leon and Adam Semlyen [8, 18], instead of finding the transformer parameters from measurements, applied electromagnetic field theory to calculate the winding leakage inductance and capacitance on a turn basis from the knowledge of the physical layout of the transformer. Not only was the leakage impedance modelled in detail, the iron core was also mathematically represented and included in the overall model.

Models of this type are good for the study of internal winding stresses. The difficulty which may be encountered is that detailed transformer data are not normally made available by the manufacturers. Also, the size of the matrices involved is too large to make it practical to interface the transformer model with the EMTP.

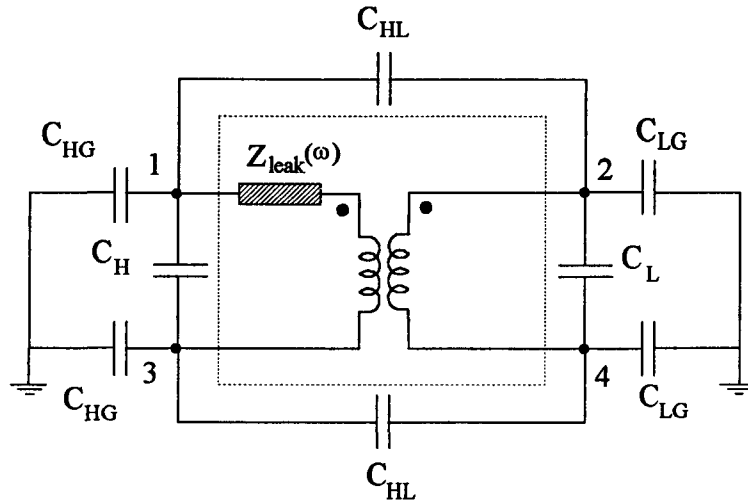


Fig. 1.4 The proposed transformer model which consists of the non-frequency dependent stray capacitances (outside the dotted frame) and the frequency dependent part (inside the dotted frame).

2. Proposed Model

The proposed transformer model could be classified as belonging to the group of "terminal models" but the principles upon which the model is developed are totally different. The model is not a direct translation from the admittance matrix equation nor a black box. On the contrary, the admittance matrix equation could be derived from the model. The model is made to be representative of the real transformer in a simplified way. That is, the real physical components in a transformer under transient conditions are incorporated into the model with the use of lumped R, L and C components. The two main factors influencing the behaviour of the transformer at high frequencies which are - 1) the stray

capacitances and 2) the frequency dependence of the leakage flux and losses due to skin effect are taken into consideration. These two components are separately treated in the proposed model which can be seen in fig. 1.4.

The magnetising effects such as saturation and hysteresis in the core are not considered. Under switching frequencies, these effects have a lesser influence and can be disregarded [5].

Stray capacitances are assumed to be constant and are represented in the model by non-frequency dependent capacitances connected between the outside terminals of the model. Unlike other previous models in which "mathematically equivalent" capacitances are connected between any two terminals possible, only the physical capacitances are considered in the proposed model. No fictitious capacitances are then present to complicate the model.

Leakage fluxes and losses are represented in the same way as it is found in the traditional transformer model. They constitute a series branch of resistances and inductances but both elements are now frequency dependent. In the model, this frequency dependent branch is subdivided into a number of sections, each associated with a resonance region in the transformer response. Each frequency dependent section is approximated with a rational function of the minimum-phase-shift type. With the use of symmetrical components to decouple the model into three sequence-models, direct fitting of the mutual impedances is avoided. The mutual impedances are non-minimum-phase-shift functions and very strict conditions regarding the location of poles and zeroes of

approximating rational functions would have to be satisfied to prevent numerical stability problems [13]. RLC equivalent networks, each consisting of a capacitance connected in parallel with a branch of a resistance connected in series with an RL parallel circuit, are used to synthesise the rational functions. The resistance of the series branch of the RLC equivalent network corresponds to the dc resistance of each coil section the network is representing.

For the frequency range up to the first resonance peak, several RL parallel circuits are used in the section so as to reproduce the transition from low frequency to the first resonance peak more effectively.

In the real transformer, there are capacitances between each turn and between turns on one coil to the others. The former are lumped at the coil terminals and the latter are lumped across each section in the model. Detailed discussion on this issue will be presented later in chapter 2.

Modelling the transformer this way has the following advantages:

- 1) The model is simple yet representative of the real transformer.
- 2) The model is numerically stable because only minimum-phase-shift functions are considered.
- 3) The number of impedances to be synthesised is minimal. Only two impedances are required to be fit in a three-phase, two-winding transformer and only six for a three-winding transformer. This can be accomplished with the use of symmetrical components.

4) The representation is independent of the particular external connection among windings (wye, delta, etc.) The connection is taken care of by node labelling at the EMTP level.

In the proposed model, short-circuit tests and capacitance measurements are needed for calculations of the model parameters. For this thesis, the experiments were carried out at the high-voltage laboratory of the Electricity Generating Authority of Thailand. The type of experiments needed for the model were proposed by the author.

Chapter Two

NON-FREQUENCY DEPENDENT PART

1. Stray Capacitances in Three-Phase Transformer

The non-frequency dependent parts of the proposed transformer model are the stray capacitances which exist in every transformer. Fig. 2.1 shows a simplified cutaway view of a single-phase, two-winding transformer. The high voltage and the low voltage windings are shown as two concentric cylinders. In this arrangement, there is capacitive coupling between the high voltage and the low voltage coils as there would be between

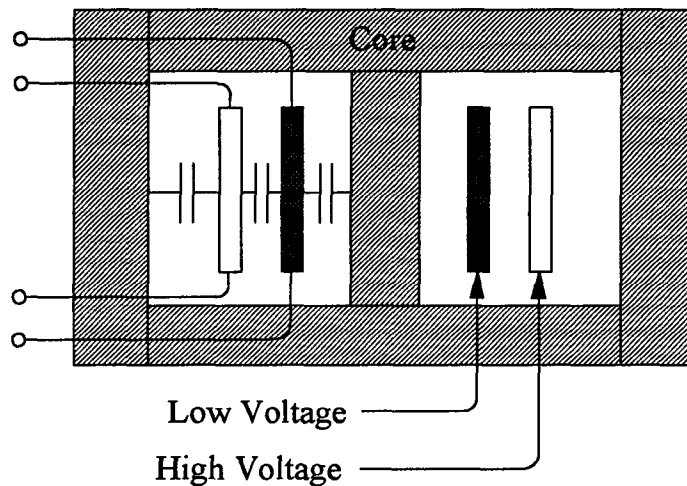


Fig. 2.1 A cutaway view of a single phase, two-winding transformer.

any two concentric metallic cylinders. Also, the cylinders and the ground (core and tank) act as capacitors and there will be capacitances from transformer coils to ground. There is another type of stray capacitance which is not shown in fig. 2.1. This capacitance is the turn-to-turn capacitance which is distributed throughout each transformer coil. In the case of three phase transformers, there are also capacitances between outer windings on different phases. Ideally, the stray capacitances for a three-phase, three-winding transformer will be as shown in fig. 2.2 which is drawn to represent a transformer with three-limb core. In each phase, there exist capacitances between the inside winding to the core, the

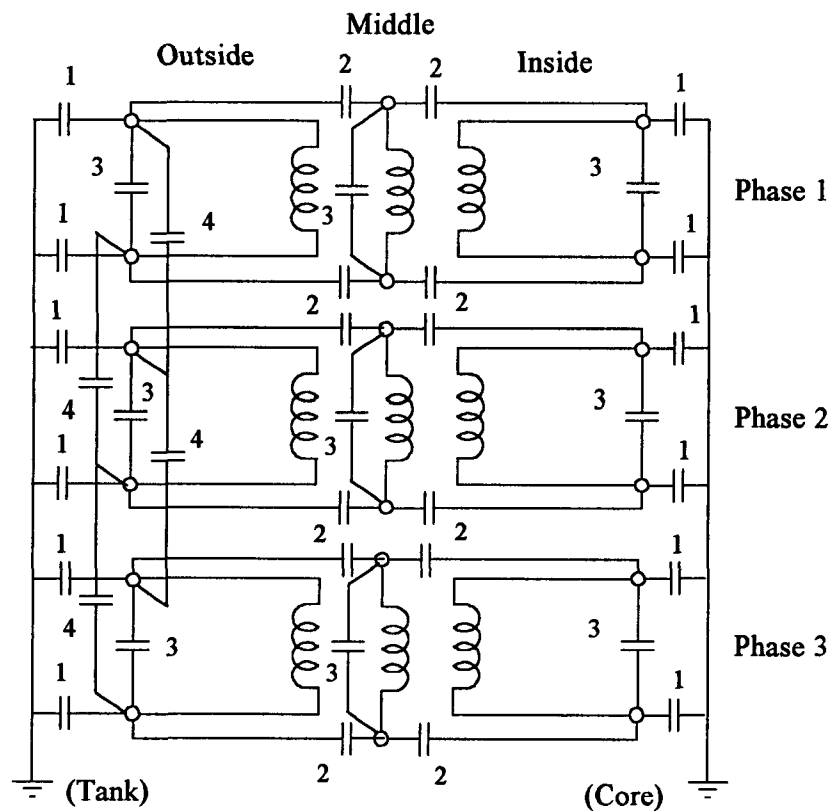


Fig. 2.2 Stray capacitances in a three-phase, three-winding transformer.

middle winding to the inside and the outside windings, and between the outside winding and the transformer tank, as well as between the outside coil on the middle limb to the corresponding coils on the other two outer limbs. In addition, there exists additional capacitances which are not shown in fig. 2.2. For example, there are some small capacitances from the outside coil to the inside coil of the same phase and also between the outside coils of phase 1 and phase 3 as well.

2. Types of Stray Capacitances

Within the scope of this thesis, the capacitances will be lumped into the following four groups:

(1) Capacitances between windings on the same limb (phase) or "interwinding capacitances" (numbered 2 in fig. 2.2),

(2) Capacitances between windings and the tank and between windings and the core or "winding-to-ground capacitances" (numbered 1 in fig. 2.2),

(3) Capacitances between turns of the same coil or "turn-to-turn capacitances" (numbered 3 in fig. 2.2),

(4) Capacitances among the outer coils on different limbs (phases) to the windings on the other two limbs or "phase-to-phase capacitances" (numbered 4 in fig. 2.2).

The turn-to-turn capacitances are modelled as a single lumped capacitance connected between the two ends of the coil. The rest of the capacitances are split into two

equal parts. As shown in fig. 2.7, the winding-to-winding capacitances are connected between each pair of coils, while the winding-to-ground capacitances are connected from each end of the coil to ground. An alternative way of splitting the winding-to-ground capacitances has been worked out by Allan Greenwood [9]. He has shown that if one end of the coils is grounded, the effective winding-to-ground capacitance will be reduced to only one-third of the total value instead of one half. This idea was implemented in the software developed for the model. If, at any instant in time, a transformer coil is grounded, the

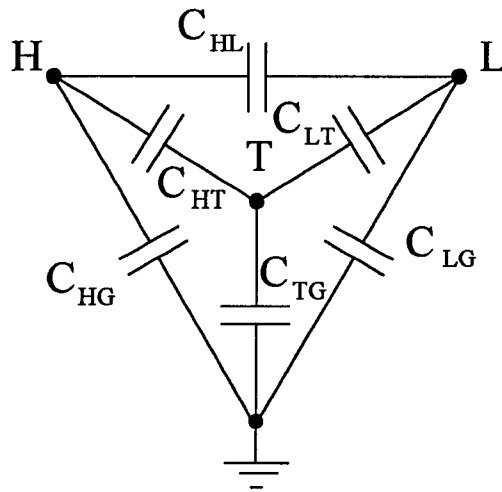


Fig. 2.3 Stray capacitances in any phase of a three-phase, three-winding transformer (turn-to-turn capacitances not shown).

winding-to-ground capacitances of that coil, which were previously composed of two equal parts of value one-half each, will both be changed to one-third.

If the three windings of a three-phase transformer are labelled as the high-voltage, the tertiary-voltage and the low-voltage windings, denoted by H, T and L respectively, the averaged stray capacitances which are formed between H, T, L and ground in any of the three phases will be as shown in fig. 2.3. Even though they belong to different phases, these capacitances are assumed to be equal (to their averaged values) so as to achieve a

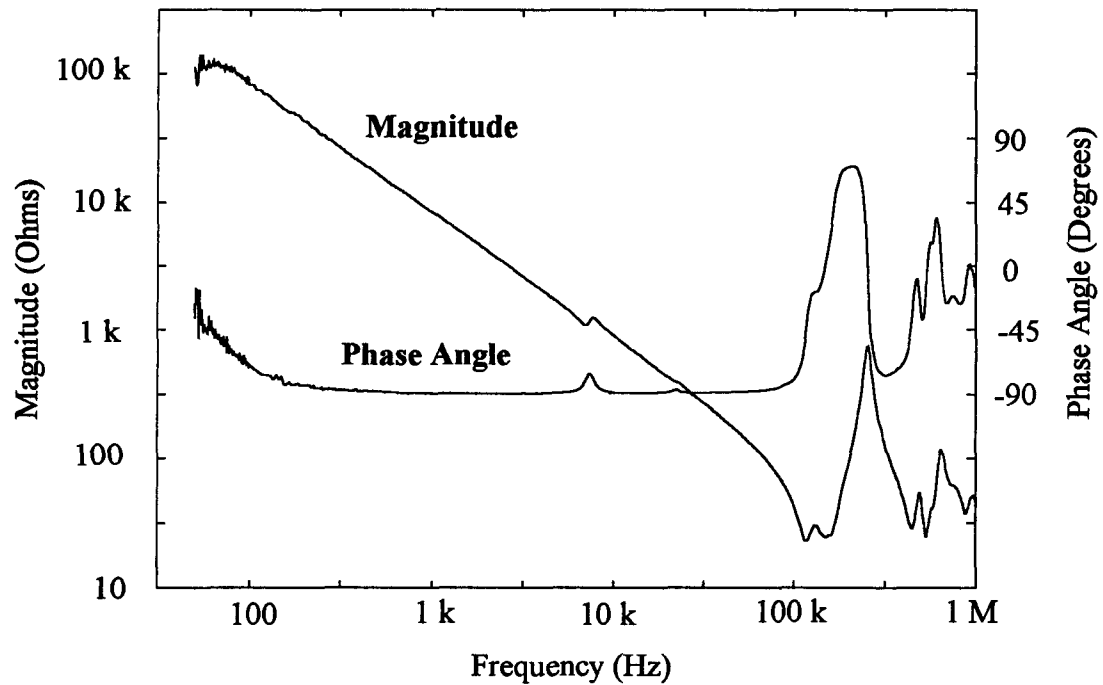


Fig. 2.4 Impedance of stray capacitances in a 115/23 kV, 50 MVA transformer.

balanced condition. For the same reason, the phase-to-phase capacitances, shown in fig. 2.5, are assumed also to be equal among each other.

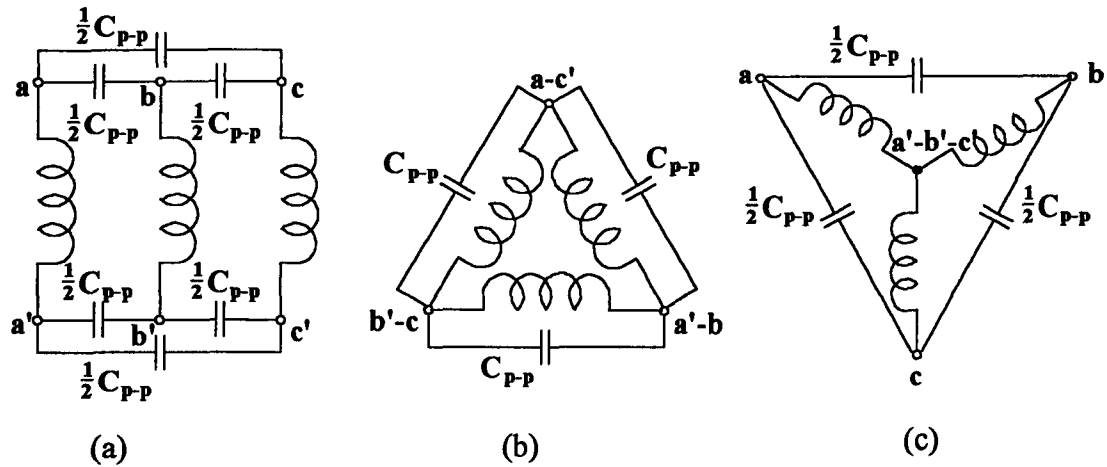


Fig. 2.5 Phase-to-phase capacitances in a three-phase transformer. (a) unconnected windings, (b) delta-connected windings and (c) wye-connected windings.

In the proposed model, all stray capacitances are assumed to be constant within the frequency range of interest (which is sufficiently high to cover switching transients). Although capacitance is frequency dependent to some extent, the idea of modelling stray capacitances as constant is not overly simplified. An analysis of the measured frequency response of stray capacitances shows that they are basically constant over a wide frequency range. Figure 2.4 shows an experimental measurement of the combined winding-to-ground and the winding-to-winding capacitances of a 115/23 kV, 50 MVA transformer. As can be seen in this graph, the capacitance is constant to about 100 kHz. The irregularities beyond 100 kHz may probably be due to inaccuracies in the measurements or to local resonances in the winding at high frequencies.

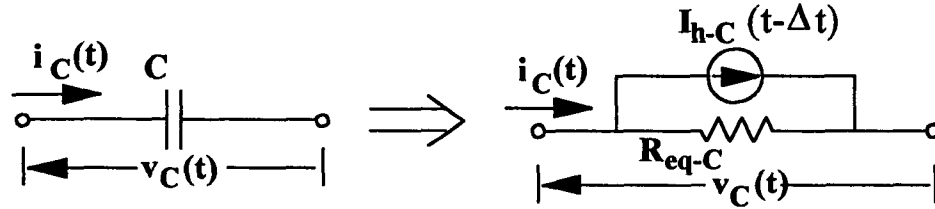


Fig. 2.6 Discrete-time representation of a capacitance.

Stray capacitances are modelled directly in the phase domain without the use of symmetrical components. Although, there is mutual coupling of stray capacitances between the three phases due to the phase-to-phase capacitances, it is not necessary to decouple them. Each of these capacitances can be represented as two equal capacitances and connected as shown in fig. 2.5 for wye or delta configuration of the outermost windings.

3. Discrete-Time Model

In the electromagnetic transient program, such as the EMTP, capacitances must be represented in discrete time form for a numerical step-by-step solution of the power system network with digital computers. The discrete-time model of a capacitance, shown in fig. 2.6, consists of a resistance and a current source connected in parallel. The values of the resistance and the current source depend on the integration rule used to discretize

the capacitance. If the trapezoidal rule is used, the resistance and the current source will be given by

$$R_{eq-C} = \frac{\Delta t}{2C} \quad (2.1)$$

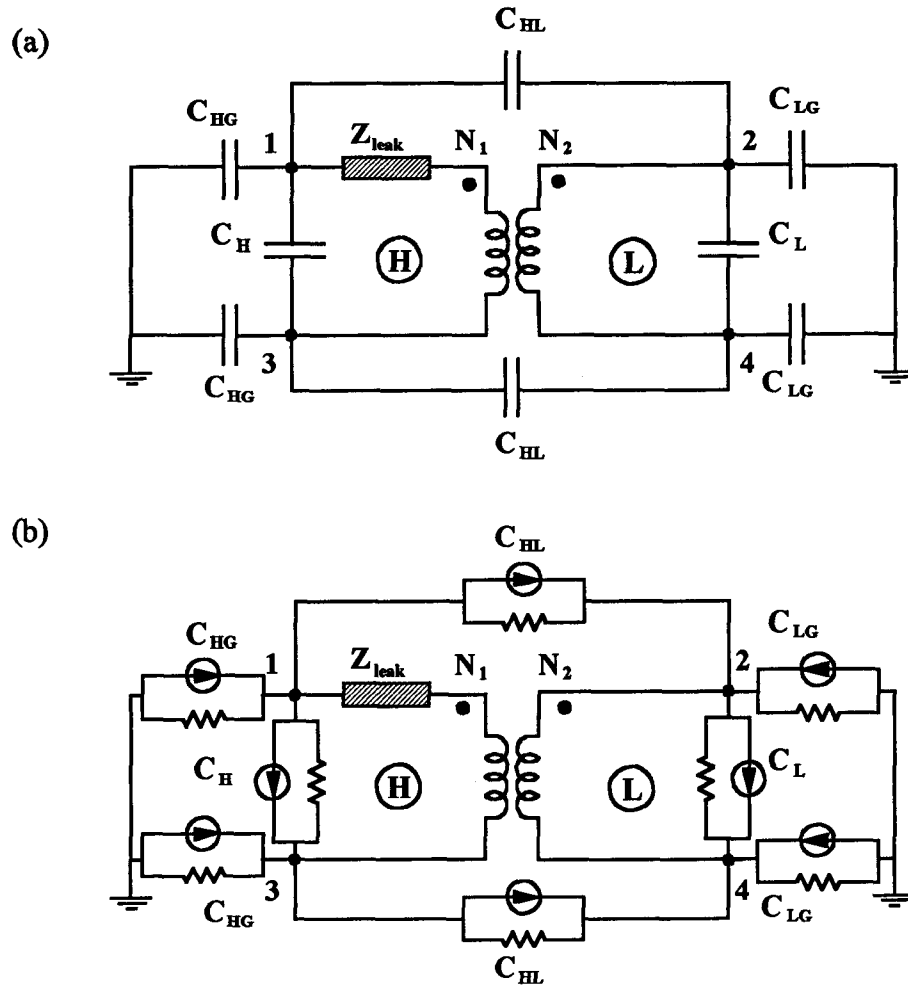


Fig. 2.7 Stray capacitances in a single phase, two-winding transformer. (a) Continuous time model, and (b) Discrete time model.

and,

$$I_{h-C}(t - \Delta t) = -\frac{2C}{\Delta t} \cdot v_C(t - \Delta t) - i_C(t - \Delta t) \quad (2.2)$$

where,

- $v_C(t)$ and $i_C(t)$ = voltages across the capacitance and current flowing into the capacitance, respectively,
- R_{eq-C} = equivalent internal resistance of the current source,
- $I_{h-C}(t - \Delta t)$ = known current source.

If the backward Euler is used, the parameters for the discretized capacitance will be,

$$R_{eq-C} = \frac{\Delta t}{C} \quad (2.3)$$

and,

$$I_{h-C}(t - \Delta t) = -\frac{C}{\Delta t} \cdot v_C(t - \Delta t) \quad (2.4)$$

An admittance matrix equation for the entire stray capacitances network can be formulated in the regular manner. Each diagonal element of the admittance matrix comes from the sum of all the admittances connected to that node and the off-diagonal elements are the negative of the admittances joining a pair of nodes. The external current entering a node will be added to the current vector on the right-hand side of the equation. Figure 2.7 illustrates the discrete-time model for the stray capacitances of a single phase, two winding transformer. C_{HL} is half the total winding-to-winding capacitance, C_{HG} is half the

total winding-to-ground capacitance for the high-voltage winding and so is C_{LG} for the low-voltage winding. C_H and C_L are the total turn-to-turn capacitances for the high and low-voltage winding, respectively. The model of fig. 2.7 is used to show how a nodal equation for stray capacitances can be formulated. An equation for the more complicated stray capacitances configuration of a three-phase transformer can be worked out in a similar fashion. The admittance matrix for the network of fig. 2.7, using the trapezoidal rule of integration, is as follows:

$$\frac{2}{\Delta t} \cdot \begin{bmatrix} C_{HG} + C_{HL} + C_H & -C_{HL} & -C_H & 0 \\ -C_{HL} & C_{HL} + C_{LG} + C_L & 0 & -C_L \\ -C_H & 0 & C_{HL} + C_{HG} + C_H & -C_{HL} \\ 0 & -C_L & -C_{HL} & C_{HL} + C_{LG} + C_L \end{bmatrix} \begin{bmatrix} v_1(t) \\ v_2(t) \\ v_3(t) \\ v_4(t) \end{bmatrix} = \begin{bmatrix} -I_{h1-G}(t - \Delta t) - I_{h1-3}(t - \Delta t) - I_{h1-2}(t - \Delta t) \\ I_{h1-2}(t - \Delta t) - I_{h2-4}(t - \Delta t) - I_{h2-G}(t - \Delta t) \\ I_{h1-3}(t - \Delta t) - I_{h3-G}(t - \Delta t) - I_{h3-4}(t - \Delta t) \\ I_{h2-4}(t - \Delta t) + I_{h3-4}(t - \Delta t) - I_{h4-G}(t - \Delta t) \end{bmatrix} \quad (2.5)$$

where,

$v_i(t)$ = voltage at terminal i of the transformer at the present time step,

$I_{h_{i-j}}(t - \Delta t)$ = current source at the previous time step resulting from discretizing the capacitance joining nodes i and j ,

Δt = duration of the time step.

4. Capacitance Model for Multi-Resonance Transformer

It should be noted that the capacitance model shown in fig. 2.7 produces only a single resonance during the short-circuit tests. In the short-circuit test, the transformer

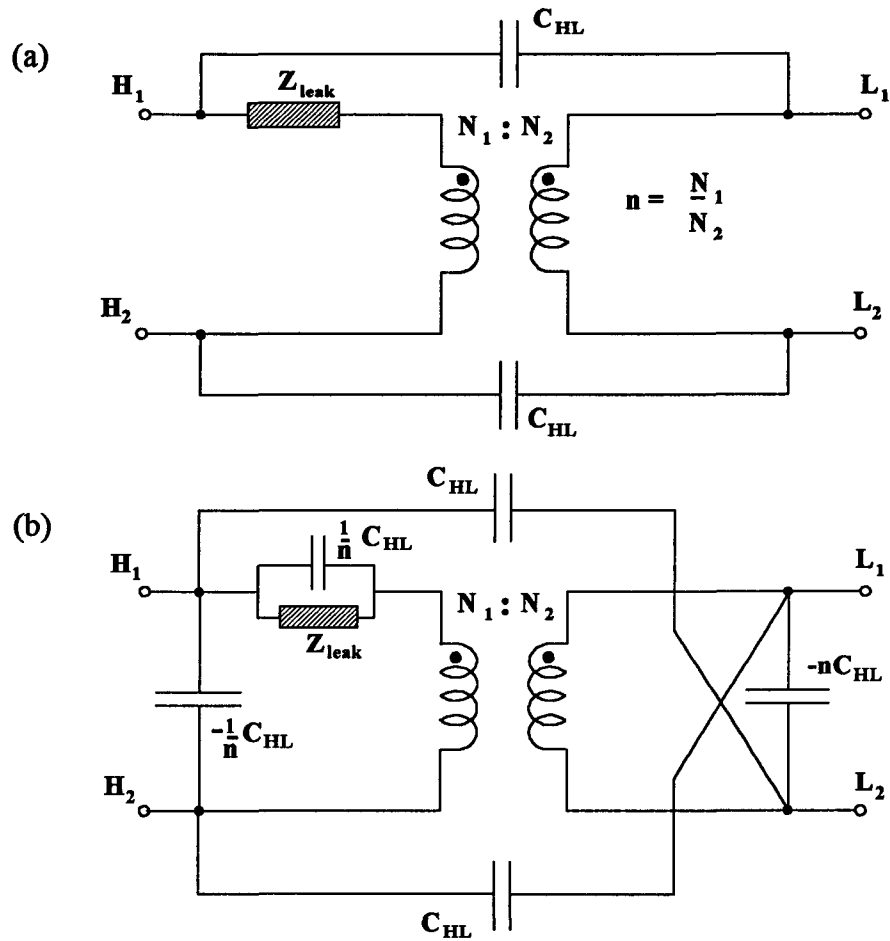


Fig. 2.8 Representation of interwinding capacitances for a two-winding transformer. (a) Original model and (b) The proposed modification.

model is reduced to an equivalent network consisting of a capacitance in parallel with the leakage impedance, $R(\omega) + j\omega L(\omega)$, which has only one resonance. It is more likely, however, for a transformer to have multiple resonances. These are due to non-uniform winding parts produced, for instance, by the presence of auxiliary tap changing windings [19]

and by voltage grading schemes [20], therefore, modifications are required to take this effect into consideration. In the two-winding transformer, the capacitances between the high voltage and low voltage winding can be moved to the side where Z_{leak} is located without altering the terminal characteristics of the model. The transferred capacitance can then be combined with the leakage impedance and treated as a single unit. This process is illustrated in fig. 2.8b.

4.1 Two-Winding Transformer

A matrix equation to describe the transformer of fig. 2.8a, in which the interwinding capacitance between the two coils is represented as two equal parts - each with half of the total capacitance value, is

$$\begin{bmatrix} I_{H_1} \\ I_{L_1} \\ I_{H_2} \\ I_{L_2} \end{bmatrix} = \begin{bmatrix} \frac{1}{Z_{leak}} + j\omega C_{HL} & \frac{-n}{Z_{leak}} - j\omega C_{HL} & \frac{-1}{Z_{leak}} & \frac{n}{Z_{leak}} \\ \frac{-n}{Z_{leak}} - j\omega C_{HL} & \frac{n^2}{Z_{leak}} + j\omega C_{HL} & \frac{n}{Z_{leak}} & \frac{-n^2}{Z_{leak}} \\ \frac{-1}{Z_{leak}} & \frac{n}{Z_{leak}} & \frac{1}{Z_{leak}} + j\omega C_{HL} & \frac{-n}{Z_{leak}} - j\omega C_{HL} \\ \frac{n}{Z_{leak}} & \frac{n}{Z_{leak}} & \frac{-n}{Z_{leak}} - j\omega C_{HL} & \frac{n^2}{Z_{leak}} + j\omega C_{HL} \end{bmatrix} \begin{bmatrix} V_{H_1} \\ V_{L_1} \\ V_{H_2} \\ V_{L_2} \end{bmatrix} \quad (2.6)$$

where,

I_{H_1} , I_{H_2} , I_{L_1} and I_{L_2} = currents entering nodes H_1 , H_2 , L_1 and L_2 , respectively,

V_{H_1} , V_{H_2} , V_{L_1} and V_{L_2} = voltages at nodes H_1 , H_2 , L_1 and L_2 , respectively,

C_{HL} = half of the interwinding capacitance between the high and low-voltage windings.

Similarly, from fig. 2.8b,

$$\begin{aligned}
\begin{bmatrix} I_{H_1} \\ I_{L_1} \\ I_{H_2} \\ I_{L_2} \end{bmatrix} &= \begin{bmatrix} \frac{1}{Z_{leak}} + j\omega \frac{C_{HL}}{n} & \frac{-n}{Z_{leak}} - j\omega C_{HL} & \frac{-1}{Z_{leak}} - j\omega \frac{C_{HL}}{n} & \frac{n}{Z_{leak}} + j\omega C_{HL} \\ \frac{-n}{Z_{leak}} - j\omega C_{HL} & \frac{n^2}{Z_{leak}} + j\omega n C_{HL} & \frac{n}{Z_{leak}} + j\omega C_{HL} & \frac{-n^2}{Z_{leak}} - j\omega n C_{HL} \\ \frac{-1}{Z_{leak}} - j\omega \frac{C_{HL}}{n} & \frac{n}{Z_{leak}} + j\omega C_{HL} & \frac{1}{Z_{leak}} + j\omega \frac{C_{HL}}{n} & \frac{-n}{Z_{leak}} - j\omega C_{HL} \\ \frac{n}{Z_{leak}} + j\omega C_{HL} & \frac{-n^2}{Z_{leak}} - j\omega n C_{HL} & \frac{-n}{Z_{leak}} - j\omega C_{HL} & \frac{n^2}{Z_{leak}} + j\omega n C_{HL} \end{bmatrix} \begin{bmatrix} V_{H_1} \\ V_{L_1} \\ V_{H_2} \\ V_{L_2} \end{bmatrix} \\
&+ j\omega \cdot \begin{bmatrix} C_{HL} - \frac{1}{n}C_{HL} & 0 & \frac{1}{n}C_{HL} & -C_{HL} \\ 0 & C_{HL} - nC_{HL} & -C_{HL} & nC_{HL} \\ \frac{1}{n}C_{HL} & -C_{HL} & C_{HL} - \frac{1}{n}C_{HL} & 0 \\ -C_{HL} & nC_{HL} & 0 & C_{HL} - nC_{HL} \end{bmatrix} \begin{bmatrix} V_{H_1} \\ V_{L_1} \\ V_{H_2} \\ V_{L_2} \end{bmatrix} \\
&= \begin{bmatrix} \frac{1}{Z_{leak}} + j\omega C_{HL} & \frac{-n}{Z_{leak}} - j\omega C_{HL} & \frac{-1}{Z_{leak}} & \frac{n}{Z_{leak}} \\ \frac{-n}{Z_{leak}} - j\omega C_{HL} & \frac{n^2}{Z_{leak}} + j\omega C_{HL} & \frac{n}{Z_{leak}} & \frac{-n^2}{Z_{leak}} \\ \frac{-1}{Z_{leak}} & \frac{n}{Z_{leak}} & \frac{1}{Z_{leak}} + j\omega C_{HL} & \frac{-n}{Z_{leak}} - j\omega C_{HL} \\ \frac{n}{Z_{leak}} & \frac{n}{Z_{leak}} & \frac{-n}{Z_{leak}} - j\omega C_{HL} & \frac{n^2}{Z_{leak}} + j\omega C_{HL} \end{bmatrix} \begin{bmatrix} V_{H_1} \\ V_{L_1} \\ V_{H_2} \\ V_{L_2} \end{bmatrix} \quad (2.7)
\end{aligned}$$

Equation 2.7 is exactly the same as equation 2.6. This indicates that the transformer model of fig. 2.8b is identical to that of fig. 2.8a with parameters as shown. Next, C_{HL}/n and Z_{leak} , which are now connected in parallel, will be combined into a new frequency dependent impedance which consists of R, L and C and will be, thereafter, referred to as " $Z_{winding}$ ".

4.2 Three-Winding Transformer

The same idea can be applied to a three-winding transformer but it takes more steps to get to the final result. The transformer without stray capacitances, which is

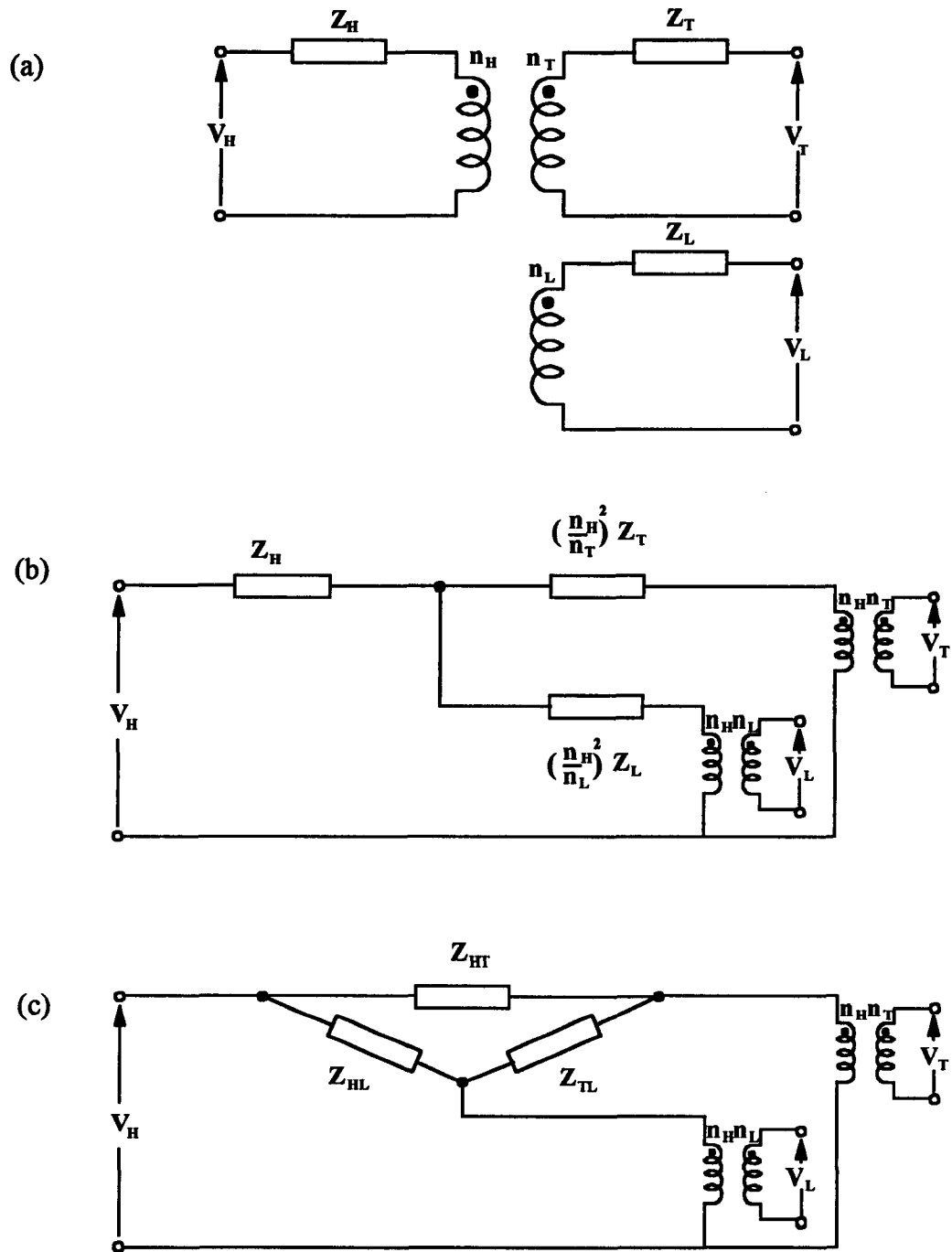


Fig. 2.9 Transformation of a three-winding transformer into a delta representation. (a) Transformer is modelled as three coupled coils, (b) Leakage impedances are referred to the V_H side, (c) Leakage impedances are transformed into a delta representation consisting of Z_{HT} , Z_{HL} and Z_{TL} .

initially modelled as a "T-circuit", must be transformed into a delta representation. The transformation process is shown in fig. 2.9. The model in fig. 2.9c can be described by a matrix equation, where all voltages and currents are associated with the winding, as follows:

$$\begin{bmatrix} I_H \\ \frac{n_T}{n_H} I_T \\ \frac{n_L}{n_H} I_L \end{bmatrix} = \begin{bmatrix} \frac{1}{Z_{HT}} + \frac{1}{Z_{HL}} & -\frac{1}{Z_{HT}} & -\frac{1}{Z_{HL}} \\ -\frac{1}{Z_{HT}} & \frac{1}{Z_{HT}} + \frac{1}{Z_{TL}} & -\frac{1}{Z_{TL}} \\ -\frac{1}{Z_{HL}} & -\frac{1}{Z_{TL}} & \frac{1}{Z_{HL}} + \frac{1}{Z_{TL}} \end{bmatrix} \begin{bmatrix} V_H \\ \frac{n_H}{n_T} \cdot V_T \\ \frac{n_H}{n_L} \cdot V_L \end{bmatrix} \quad (2.8)$$

or,

$$\begin{bmatrix} I_H \\ I_T \\ I_L \end{bmatrix} = \begin{bmatrix} \frac{1}{Z_{HT}} + \frac{1}{Z_{HL}} & -\frac{n_H}{n_T} \cdot \frac{1}{Z_{HT}} & -\frac{n_H}{n_L} \cdot \frac{1}{Z_{HL}} \\ -\frac{n_H}{n_T} \cdot \frac{1}{Z_{HT}} & \frac{n_H^2}{n_T^2} \cdot \left(\frac{1}{Z_{HT}} + \frac{1}{Z_{TL}} \right) & -\frac{n_H^2}{n_T n_L} \cdot \frac{1}{Z_{TL}} \\ -\frac{n_H}{n_L} \cdot \frac{1}{Z_{HL}} & -\frac{n_H^2}{n_T n_L} \cdot \frac{1}{Z_{TL}} & \frac{n_H^2}{n_L^2} \cdot \left(\frac{1}{Z_{HL}} + \frac{1}{Z_{TL}} \right) \end{bmatrix} \begin{bmatrix} V_H \\ V_T \\ V_L \end{bmatrix} \quad (2.9)$$

where,

- I_H, I_T and I_L = currents in high, tertiary and low-voltage windings, respectively,
- V_H, V_T and V_L = terminal voltages of high, tertiary and low-voltage windings, respectively,
- Z_{HT}, Z_{TL} and Z_{HL} = leakage impedance of high, tertiary and low-voltage windings, as represented in the delta configuration (fig. 2.9c),
- n_H, n_T and n_L = no. of turns of high, tertiary and low-voltage windings, respectively.

Equation 2.9 is not the nodal admittance matrix equation, therefore, it cannot be combined with the nodal equation indicated previously to describe the interwinding capacitances. However, a change in variables to express all the voltages and currents as node quantities takes only a small additional effort. Based on equation 2.9, the nodal admittance matrix equation for a three-winding transformer can be written as:

$$\begin{bmatrix} I_{H_1} \\ I_{T_1} \\ I_{L_1} \\ I_{H_2} \\ I_{T_2} \\ I_{L_2} \end{bmatrix} = \begin{bmatrix} [Y_D] & -[Y_D] \\ -[Y_D] & [Y_D] \end{bmatrix} \begin{bmatrix} V_{H_1} \\ V_{T_1} \\ V_{L_1} \\ V_{H_2} \\ V_{T_2} \\ V_{L_2} \end{bmatrix} \quad (2.10)$$

where,

$[Y_D]$ = admittance matrix of size $[3 \times 3]$ in equation 2.9,

1 and 2

designate variables associated with node 1 and node 2 of each winding. For example, I_{H_1} and I_{H_2} are the currents entering nodes H_1 and H_2 , where $I_{H_1} = I_H$, $I_{H_2} = -I_H$. Note that after the interwinding capacitances have been included, I_{H_1} is no longer equal to the negative of I_{H_2} .

The interwinding capacitances can be added to the transformer in fig. 2.9c in a similar fashion. This is shown in fig. 2.8a where half of the capacitance is connected from "node 1" of one winding to "node 1" of the other winding, and the other half is connected between their corresponding "node 2". After the interwinding capacitances are included, equation 2.10 becomes

$$\begin{bmatrix} I_{H_1} \\ I_{T_1} \\ I_{L_1} \\ I_{H_2} \\ I_{T_2} \\ I_{L_2} \end{bmatrix} = \begin{bmatrix} [Y_D] & -[Y_D] \\ -[Y_D] & [Y_D] \end{bmatrix} \begin{bmatrix} V_{H_1} \\ V_{T_1} \\ V_{L_1} \\ V_{H_2} \\ V_{T_2} \\ V_{L_2} \end{bmatrix} +$$

$$\begin{bmatrix} C_{HT} + C_{HL} & -C_{HT} & -C_{HL} & 0 & 0 & 0 \\ -C_{HT} & C_{HT} + C_{TL} & -C_{TL} & 0 & 0 & 0 \\ -C_{HL} & -C_{TL} & C_{HL} + C_{TL} & 0 & 0 & 0 \\ 0 & 0 & 0 & C_{HT} + C_{HL} & -C_{HT} & -C_{HL} \\ 0 & 0 & 0 & -C_{HT} & C_{HT} + C_{TL} & -C_{TL} \\ 0 & 0 & 0 & -C_{HL} & -C_{TL} & C_{HL} + C_{TL} \end{bmatrix} \begin{bmatrix} V_{H_1} \\ V_{T_1} \\ V_{L_1} \\ V_{H_2} \\ V_{T_2} \\ V_{L_2} \end{bmatrix} \quad (2.11)$$

where,

C_{HT} , C_{TL} and C_{HL} = one half of the high-to-tertiary, tertiary-to-low and high-to-low interwinding capacitances, respectively.

We consider now taking a portion of the interwinding capacitances and lumping them with the delta-equivalent leakage impedance, as shown in fig. 2.10a. In so doing, some extra capacitances are generated as by-products which must also be included in the equivalent circuit in order to retain similarity between the modified and original network (as shown in fig. 2.10b). All these fictitious capacitances can be chosen properly to be as follows:

$$\begin{aligned} C'_{HT} &= \frac{n_T}{n_H} \cdot C_{HT} \\ C'_{HL} &= \frac{n_L}{n_H} \cdot C_{HL} \\ C'_{TL} &= \frac{n_T \cdot n_L}{n_H^2} \cdot C_{TL} \end{aligned}$$

and,

$$C'_H = -\frac{n_T}{n_H} \cdot C_{HT} - \frac{n_L}{n_H} \cdot C_{HL}$$

$$C'_T = -\frac{n_H}{n_T} \cdot C_{HT} - \frac{n_L}{n_T} \cdot C_{TL}$$

$$C'_L = -\frac{n_H}{n_L} \cdot C_{HL} - \frac{n_T}{n_L} \cdot C_{TL}$$

According to this choice of capacitances, a matrix equation describing the transformer of fig. 2.10a can be expressed as:

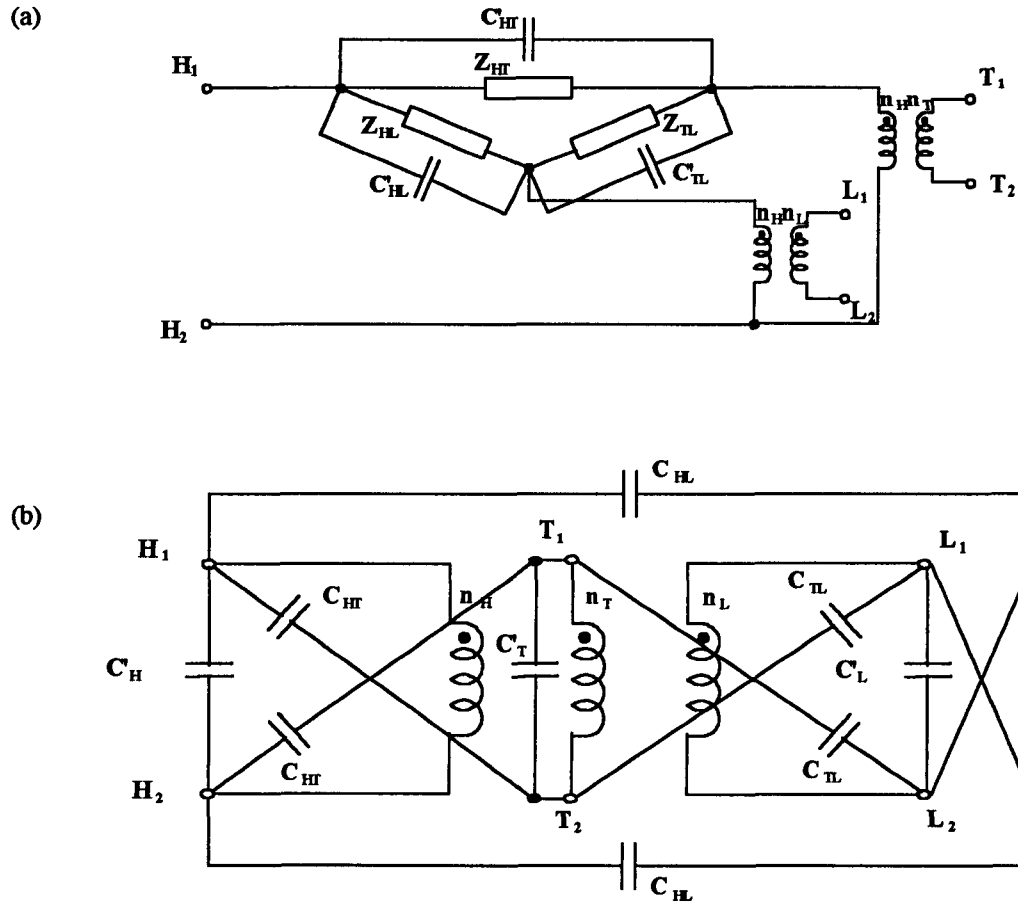


Fig. 2.10 Equivalent circuit after the interwinding capacitances have been moved to the same side as the leakage impedances. (a) Capacitances which will be lumped with the leakage impedances and (b) Additional capacitances resulting from the modification.

$$\begin{bmatrix} I_{H_1} \\ I_{T_1} \\ I_{L_1} \\ I_{H_2} \\ I_{T_2} \\ I_{L_2} \end{bmatrix} = \begin{bmatrix} [Y_D] & -[Y_D] \\ -[Y_D] & [Y_D] \end{bmatrix} \begin{bmatrix} V_{H_1} \\ V_{T_1} \\ V_{L_1} \\ V_{H_2} \\ V_{T_2} \\ V_{L_2} \end{bmatrix} \\
+ j\omega \cdot \begin{bmatrix} [Y'_D] & -[Y'_D] \\ -[Y'_D] & [Y'_D] \end{bmatrix} \begin{bmatrix} V_{H_1} \\ V_{T_1} \\ V_{L_1} \\ V_{H_2} \\ V_{T_2} \\ V_{L_2} \end{bmatrix} \\
+ j\omega \cdot \begin{bmatrix} [Y_{C_1}] & [Y_{C_2}] \\ [Y_{C_2}] & [Y_{C_1}] \end{bmatrix} \begin{bmatrix} V_{H_1} \\ V_{T_1} \\ V_{L_1} \\ V_{H_2} \\ V_{T_2} \\ V_{L_2} \end{bmatrix} \quad (2.12)$$

where,

$$[Y'_D] = \begin{bmatrix} C'_{HT} + C'_{HL} & -\frac{n_H}{n_T} C'_{HT} & -\frac{n_H}{n_L} C'_{HL} \\ -\frac{n_H}{n_T} C'_{HT} & \frac{n_H^2}{n_T^2} (C'_{HT} + C'_{TL}) & -\frac{n_H^2}{n_T n_L} C'_{TL} \\ -\frac{n_H}{n_L} C'_{HL} & -\frac{n_H^2}{n_T n_L} C'_{TL} & \frac{n_H^2}{n_L^2} (C'_{HL} + C'_{TL}) \end{bmatrix}, \\
= \begin{bmatrix} -C'_H & -C_{HT} & -C_{HL} \\ -C_{HT} & -C'_T & -C_{TL} \\ -C_{HT} & -C_{TL} & -C'_L \end{bmatrix},$$

$$[Y_{C_1}] = \begin{bmatrix} C'_H + C_{HL} + C_{HT} & 0 & 0 \\ 0 & C'_T + C_{TL} + C_{HT} & 0 \\ 0 & 0 & C'_L + C_{TL} + C_{HL} \end{bmatrix},$$

and

$$[Y_{C_2}] = \begin{bmatrix} -C'_H & -C_{HT} & -C_{HL} \\ -C_{HT} & C'_T & -C_{TL} \\ -C_{HL} & -C_{TL} & -C'_L \end{bmatrix}.$$

The first term on the right-hand side of equation 2.12 comes from the leakage impedances Z_{HT} , Z_{TL} and Z_{HL} and is identical to the first term on the right-hand side of equation 2.11. The second and third terms on the right-hand side of equation 2.12 come from the interwinding capacitances. Equation 2.12 will be identical to equation 2.11 only if the sum of these two terms is the same as the second term on the right-hand side of equation 2.11, which also comes from the interwinding capacitances. The sum of the second and third terms on the right-hand side of equation 2.12 is

$$[Y_C] = \begin{bmatrix} [Y'_D] + [Y_{C_1}] & -[Y'_D] + [Y_{C_2}] \\ -[Y'_D] + [Y_{C_2}] & [Y'_D] + [Y_{C_1}] \end{bmatrix} \quad (2.13)$$

There are only two distinct elements in the above matrix, i.e. the diagonal and off-diagonal blocks. By substitution, each of the matrices in the diagonal position of equation 2.13 becomes

$$\begin{bmatrix} -C'_H & -C_{HT} & -C_{HL} \\ -C_{HT} & -C'_T & -C_{TL} \\ -C_{HT} & -C_{TL} & -C'_L \end{bmatrix} + \begin{bmatrix} C'_H + C_{HL} + C_{HT} & 0 & 0 \\ 0 & C'_T + C_{TL} + C_{HT} & 0 \\ 0 & 0 & C'_L + C_{TL} + C_{HL} \end{bmatrix}$$

$$= \begin{bmatrix} C_{HL} + C_{HT} & -C_{HT} & -C_{HL} \\ -C_{HT} & C_{HT} + C_{TL} & -C_{TL} \\ -C_{HT} & -C_{TL} & C_{HL} + C_{TL} \end{bmatrix},$$

and each of the off-diagonal matrices is

$$-\begin{bmatrix} -C'_H & -C_{HT} & -C_{HL} \\ -C_{HT} & -C'_T & -C_{TL} \\ -C_{HT} & -C_{TL} & -C'_L \end{bmatrix} + \begin{bmatrix} -C'_H & -C_{HT} & -C_{HL} \\ -C_{HT} & C'_T & -C_{TL} \\ -C_{HL} & -C_{TL} & -C'_L \end{bmatrix} = \begin{bmatrix} 0 & 0 & 0 \\ 0 & 0 & 0 \\ 0 & 0 & 0 \end{bmatrix}.$$

Substituting the diagonal matrices and the off-diagonal matrices into $[Y_C]$ makes it exactly the same as the matrix in the right-hand side of equation 2.11. Therefore, it can be concluded that the representation in fig. 2.10 is also the valid model for a transformer when interwinding capacitances are included. The impedances in delta of fig. 2.10a are transformed back to the T-circuit and then back to the original circuit of fig. 2.9a. The only difference now is that the leakage impedance of each winding has a part of the interwinding capacitance in it. This makes it consistent to synthesise each of them with a number of RLC blocks, each block for each resonance to be matched.

5. Implementation of Interwinding Capacitance Modification

In the model, modification of interwinding capacitance connection is done in the nodal decoupled domain. The capacitance value in the decoupled mode is the same as that in the coupled mode because the interwinding capacitance exists only between

windings of the same phase. Only the part of the interwinding capacitance which is combined with the decoupled leakage impedance is modelled in the decoupled mode. All other capacitances resulting from the modification process will be additionally entered into equation 2.5 in the phase domain as other stray capacitances are treated. Therefore, there will be either four (two-winding) or nine (three-winding) more capacitances to be included in each phase. Eventually, equation 2.5 can be written symbolically as:

$$\frac{2}{\Delta t}[C_{stray}][v_{node}(t)] = [I_{hist-c}(t - \Delta t)] \quad (2.14)$$

Equation 2.14 describes the model for stray capacitances in phase co-ordinates and, along with the model built from the frequency dependent part, (to be explained next in chapter 4) constitute the complete frequency dependent model for the transformer.

Chapter Three

MODELLING OF FREQUENCY DEPENDENT COMPONENTS

It was mentioned briefly in the previous chapter that the frequency dependent components in the proposed transformer model consist of the leakage impedance in combination with part of the interwinding capacitances. Also included in the measured parameters are the hidden effects arising from the simplified modelling of the actual stray capacitances with constant capacitances. In this chapter, the detailed modelling of the frequency dependent part will be discussed at length. The objective in the modelling of the frequency dependent part is to find a representative network consisting of a combination of constant parameter components, which are basically resistances, inductances and capacitances. The parameters will be chosen such that the network produces frequency responses which closely match the actual data obtained from laboratory measurements.

1. Short-Circuit Responses of Transformers

The measurements required to determine the characteristics of the frequency dependent branch of the transformer model are short-circuit tests. These tests need to be performed with a device which is capable of generating a signal of variable frequency so that the measurements can be taken in a broad frequency range, extending from a few Hz

up to a few MHz. Most transformers will exhibit their frequency dependent behaviour clearly in this frequency range. Figure 3.1 shows a frequency response of a distribution transformer under a short-circuit test. This type of response is typical for most power transformers [16, 17]. This measurement was taken at the high voltage laboratory of the Electricity Generating Authority of Thailand (EGAT). The measuring device available at EGAT was a network analyser model HP4192A which has a working frequency range between 5 Hz and 13 MHz. The four-terminal pair measuring technique (known as "Kelvin connection") was used in order to achieve a wide range of impedance measurements (1 mΩ to 10 MΩ) and to minimise measuring errors due to parasitic coupling with the test

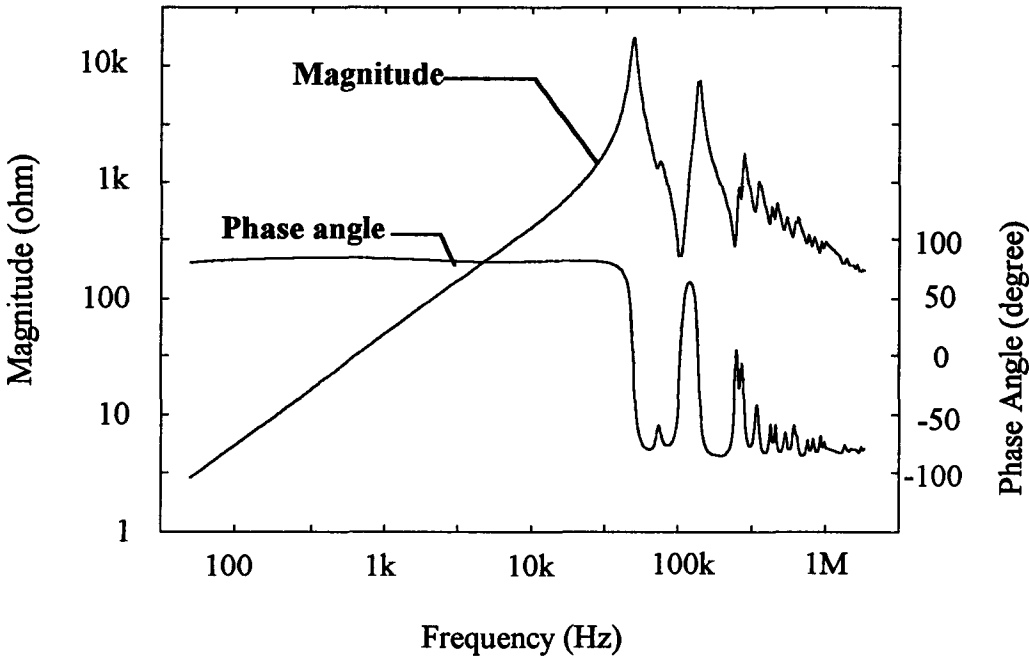


Fig. 3.1 Typical short-circuit frequency responses of a transformer. $Z_{\text{measured}} = \frac{V_{\text{source}}}{I_{\text{source}}}$

leads. The network analyser was connected to a personal computer (PC). Variation of frequency in discrete steps, either on a linear scale or a log scale, can be accomplished via a software installed in the personal computer. The network analyser measures the magnitude and phase angle of the device under test (DUT) at each discrete frequency and transmits the measured data to the PC to be stored. The data can then be retrieved for plotting or can be transferred to a diskette for later processing.

The short-circuit test data so obtained are not yet in a form useful for transformer modelling. In order to obtain the data for the frequency dependent branch of the model, the value of stray capacitances (known from prior measurements and/or calculations) must be deducted from the raw data. Under short-circuit condition, the measured impedance is

$$\frac{1}{Z_{short}(\omega)} = j\omega \cdot C_{ext} + \frac{1}{Z_{winding}(\omega)} \quad (3.1)$$

where,

- $Z_{short}(\omega)$ = Measured short-circuit impedance,
- C_{ext} = Sum of all capacitances except part of the interwinding capacitance which becomes combined with the leakage impedance.
- $Z_{winding}(\omega)$ = Impedance of the frequency dependent series branch, and
- ω = $2\pi f$.

Then, $Z_{winding}(\omega)$ can be computed as

$$Z_{winding}(\omega) = \frac{1}{\frac{1}{Z_{short}(\omega)} - j\omega \cdot C_{ext}} \quad (3.2)$$

The stray capacitances (C_{ext}) that is deducted must not include the part of the interwinding capacitance (C_{HL}/n in fig. 2.8b) which has been combined with the leakage impedance to make $Z_{winding}$.

2. Equivalent Network Representation for $Z_{winding}$

The magnitude of $Z_{winding}$ is similar in shape to the magnitude of the measured short-circuit response. It possesses many portions with sharp peaks, these portions are not symmetrical around their peak and there are many peaks clustering together,

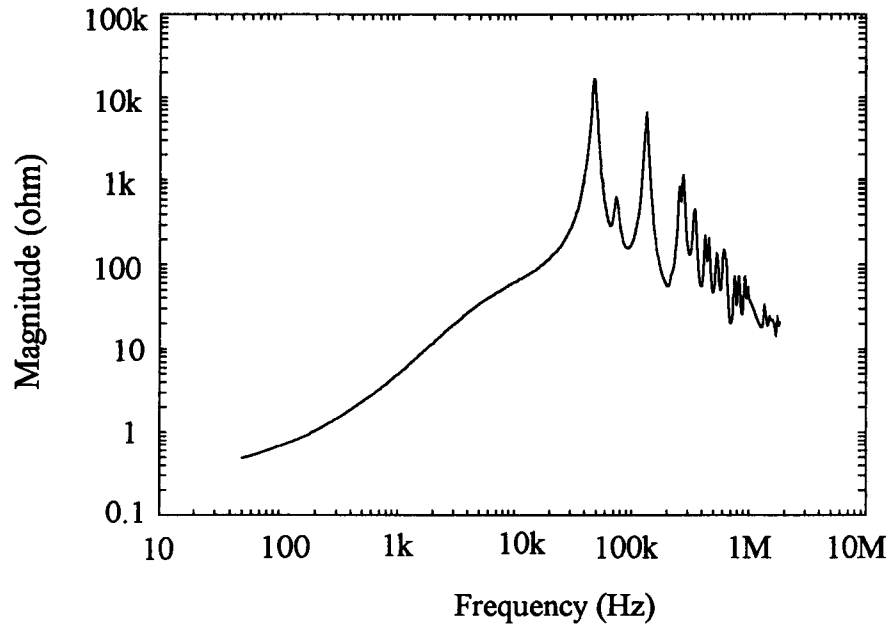


Fig. 3.2 Frequency dependent characteristics of the real part of the series impedance $Z_{winding}$.

especially in the high frequency region. Due to this nature, it is somewhat difficult to directly apply the pole-zero approximation method [10] to find a rational function representing $Z_{winding}$. However, it has been found that the real part of $Z_{winding}$ reveals more recognisable information. It displays more clearly the resonance characteristics which consist of several peaks superimposed on each other, similar to those shown in fig. 3.2. The peaks of the real parts are almost symmetrical around their resonance frequencies which are similar to the response of the real part of a parallel RLC network. This suggests a simple solution to the problem which otherwise could have been significantly hard to solve. As a first approximation, those peaks in the real part of $Z_{winding}$ to be duplicated are each fitted with a parallel RLC network. The resistance of this network can be viewed as representing ohmic losses in the windings and parasitic losses in the metallic parts caused by leakage fluxes. The inductance represents the leakage fluxes and the capacitance represents part of the interwinding capacitance. Therefore, all the circuit elements have associated physical meaning. The resonance frequency of the block is can be read off from the plot of $Z_{winding}$ at the peak it duplicates. For an RLC parallel block, its real part is

$$Re\{Z(\omega)\} = \frac{\omega^2 L^2 R}{R^2(1 - \omega^2 LC)^2 + \omega^2 L^2} \quad (3.3)$$

where,

- $Re\{Z(\omega)\}$ = Real part of the impedance of an RLC parallel block,
 ω = angular frequency in radian/second,

L, R and C = inductance, resistance and capacitance respectively of the RLC parallel block.

The product LC in equation 3.3 is known, it is the inverse of the square of the resonance frequency (angular frequency). Therefore, it is only necessary to estimate two more variables: R and L . If the real part of each resonance peak is expressed as in equation 3.3, the sum of all these functions will, approximately, represent the real part of the entire series branch. If there are n peaks, the expression for the desired function will be

$$Re\{Z_{winding}(\omega)\} = \sum_{i=1}^{i=n} \frac{\omega^2 L_i^2 R_i}{R_i^2 \left(1 - \frac{\omega^2}{\Omega_i^2}\right)^2 + \omega^2 L_i^2} \quad (3.4)$$

where,

- $Re\{Z_{winding}(\omega)\}$ = Function representing the real part of the frequency dependent impedance ($Z_{winding}$) of the transformer model,
- n = no. of peaks to be matched,
- R_i and L_i = R and L of the block representing peak i ,
- Ω_i = angular frequency corresponding to the resonant frequency of peak i .

In equation 3.4, there are $2 \times n$ unknown variables, namely, R_i and L_i . The variable Ω_i is known, and the capacitance for each block can be calculated from Ω_i after the inductance L_i has been found. The variables R_i and L_i are estimated by fitting the function $Re\{Z_{winding}(\omega)\}$ to the real part of $Z_{winding}$. Since $Re\{Z_{winding}(\omega)\}$ is a non-linear function, a

non-linear curve fitting method must be used to find the unknown variables. In this thesis, a non-linear least-squares fit with the Levenberg-Marquardt method [11] has been applied. Even though the effort is spent entirely on fitting the real part of the function, the imaginary part of the function will automatically be matched. As explained in [1], the imaginary part of any analytical function is uniquely determined by its real part.

The result from the first approximation technique described above will match the response of $Z_{winding}$ moderately well except in the neighbourhood of the "major peak". The major peak is the one with maximum amplitude, usually occurring as the first peak in the frequency response, and contains most of the information available from the short-circuit tests. Because only one RL block is used for the major peak in the first approximation, the fitting will not match this region properly and will need to be fine tuned. The asymptotic pole-zero approximation method of [1,10] is used to find more RL blocks (series Foster) for the major peak region. Capacitance of this section (known from the first approximation) is first removed from the frequency response (as in equation 3.2) leaving a non-resonant response which can be fitted with simple poles and zeroes. The rational function used to approximate the impedance after extracting the C is

$$F_{first}(\omega) = K \cdot \frac{(s+z_0)(s+z_1)(s+z_2)\dots(s+z_m)}{(s+p_0)(s+p_1)(s+p_3)\dots(s+p_n)} \quad (3.5)$$

where,

$F_{first}(\omega)$ = rational function to approximate the remaining magnitude of the first peak after its capacitance has been removed,

- K = a constant,
 s = $j\omega$,
 z_i and p_i = zeroes and poles of the function,
 m and n = no. of zeroes and poles, respectively, $m \leq n$.

The poles and zeroes in equation 3.5 can be taken from the plot of the magnitude function ($\sqrt{R^2(\omega) + \omega^2 \cdot L^2(\omega)}$) on a log-log scale. Applying partial fractions to equation 3.5 yields

$$F_{first}(\omega) = A + \frac{B \cdot s}{(s+p_1)} + \frac{C \cdot s}{(s+p_2)} + \frac{D \cdot s}{(s+p_3)} + \dots \quad (3.6)$$

or,

$$F_{first}(\omega) = R_{10} + \frac{s \cdot R_{11}}{\left(s + \frac{R_{11}}{L_{11}}\right)} + \frac{s \cdot R_{12}}{\left(s + \frac{R_{12}}{L_{12}}\right)} + \frac{s \cdot R_{13}}{\left(s + \frac{R_{13}}{L_{13}}\right)} \dots \quad (3.7)$$

Equation 3.7 gives all the desired parameters for the first peak. Using these RL blocks instead of a single RL block will improve the approximation a great deal especially in the region from dc to the first peak of the frequency response. However, due to the fact that parameters for the first peak and the remaining peaks are obtained at different stages in the optimisation process, the resulting combination will not be globally optimised. Further improvement is required to increase the quality of the fitting. The previous results from the first optimisation and the fine-tuning will be used as initial condition for another optimisation. This time, the model function is based on the real part of the circuit shown in fig

3.3. Resistances R_{10} , R_{20} ,..., representing dc resistances for each peak are inserted because in reality each coil section will have a small dc resistance. Insertion of those resistances makes it possible to satisfy the dc response of the network. Examples of how

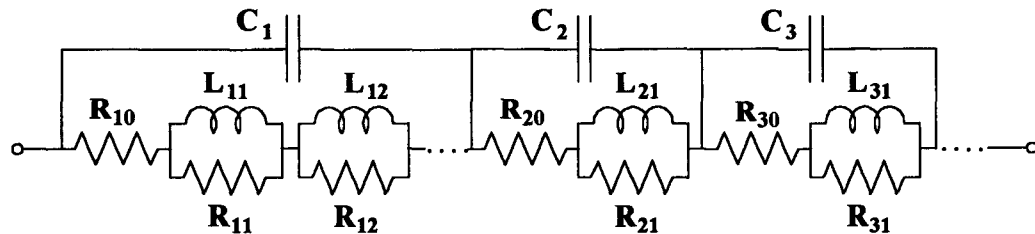


Fig. 3.3 RLC synthesis network to approximate $Z_{winding}$.

$Z_{winding}$ is realised from the test data will be given in chapter 6. Next, the parameters of the equivalent network for $Z_{winding}$ must be discretized. This can be done in the normal, straightforward manner.

3. Discretization of Equivalent Network for $Z_{winding}$

The equivalent network for $Z_{winding}$ consists of a number of constant R, L and C's. In spite of the fact that all the R, L and C's are constant, the overall characteristics of the network is frequency dependent and follows that of the impedance $Z_{winding}$ it represents. In the EMTP, as well as in other electromagnetic transient programs based on time domain simulation, all circuit elements must be represented in a discrete time form. The discrete-time representation of L and C depends on the integration rule used in performing the

discretization [10]. Table 3.1 summarises the discrete-time representations for a capacitance and an inductance with respect to trapezoidal and backward Euler rules.

Table 3.1--Summary of discrete-time models for inductances and capacitances using the trapezoidal and backward Euler integration rules.

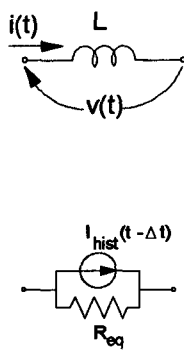
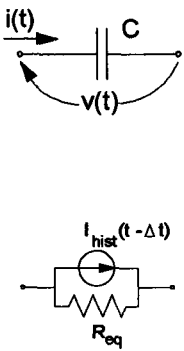
Circuit Element	Integration Rule	Difference Equation
	Trapezoidal	$i(t) = \frac{\Delta t}{2L} \cdot v(t) + \frac{\Delta t}{2L} \cdot v(t - \Delta t) + i(t - \Delta t)$ $R_{eq} = \frac{2L}{\Delta t}$ $I_{hist}(t - \Delta t) = \frac{\Delta t}{2L} \cdot v(t - \Delta t) + i(t - \Delta t)$
	Backward Euler	$i(t) = \frac{\Delta t}{L} \cdot v(t) + i(t - \Delta t)$ $R_{eq} = \frac{L}{\Delta t}$ $I_{hist}(t - \Delta t) = i(t - \Delta t)$
	Trapezoidal	$i(t) = \frac{2C}{\Delta t} \cdot v(t) - \frac{2C}{\Delta t} \cdot v(t - \Delta t) - i(t - \Delta t)$ $R_{eq} = \frac{\Delta t}{2C}$ $I_{hist}(t - \Delta t) = -\frac{2C}{\Delta t} \cdot v(t - \Delta t) - i(t - \Delta t)$
	Backward Euler	$i(t) = \frac{C}{\Delta t} \cdot [v(t) - v(t - \Delta t)]$ $R_{eq} = \frac{\Delta t}{C}$ $I_{hist}(t - \Delta t) = -\frac{C}{\Delta t} \cdot v(t - \Delta t)$

Figure 3.4 shows one of the blocks used to model the frequency dependent branch. This block has to be transformed into its corresponding discrete time

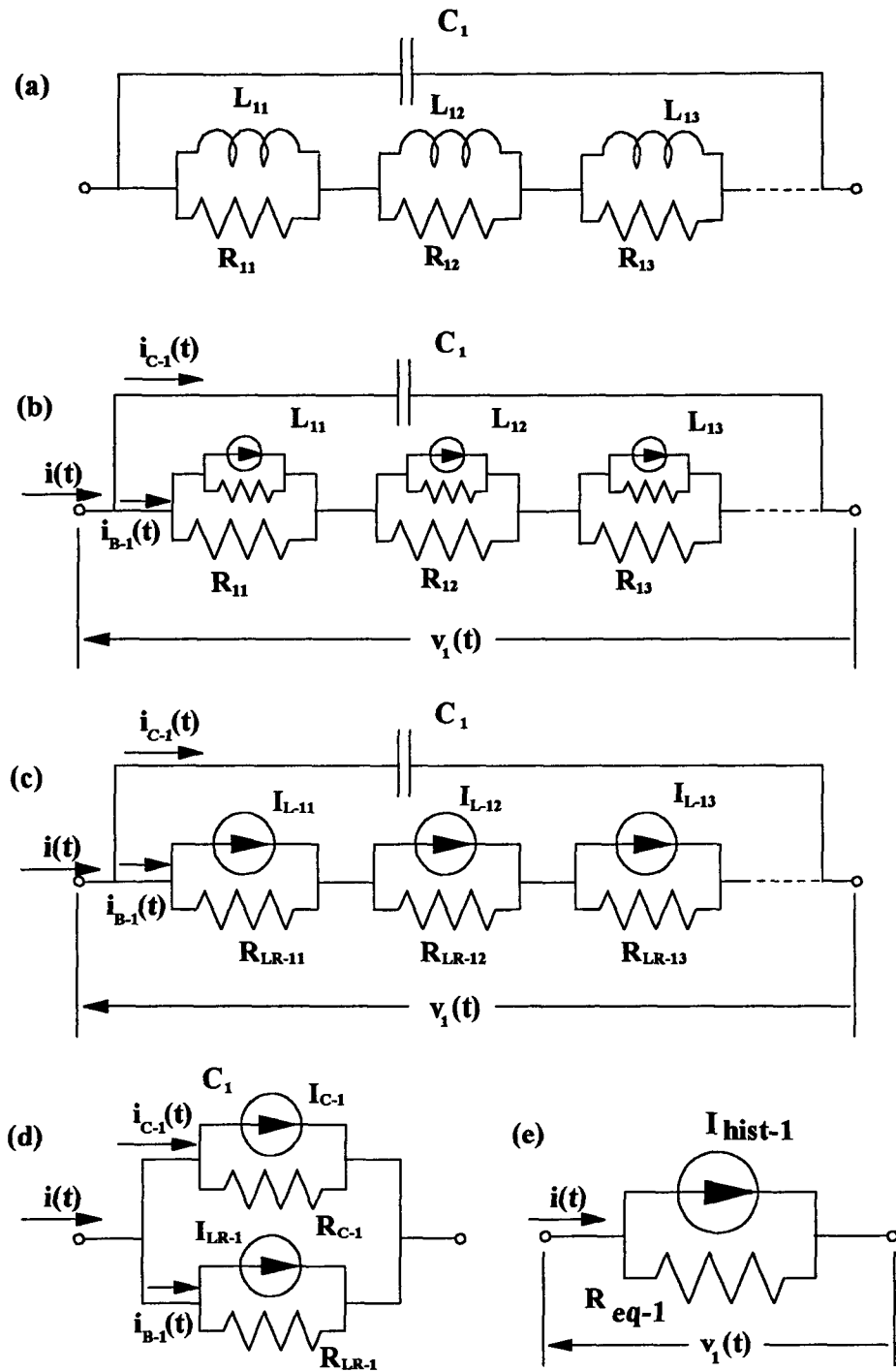


Fig. 3.4 Discretization of a section of the equivalent network for $Z_{winding}$. This section represents a general network used to duplicate a resonant peak.

representation. Each block of the approximating network has a single C regardless of how many RL parallel blocks the section contains. Parameters of the network in fig. 3.4a are found from non-linear fitting and/or from the pole-zero approximation described earlier in this chapter. This general network can also include the case of a section containing a dc resistance: an R can be regarded as an RL block without an L . The discretization process can be carried out as outlined in fig. 3.4. Initially, each inductance is replaced by its discrete time equivalent (fig. 3.4b). After that the equivalent resistance of the discrete-time inductance is combined with the physical resistance of the RL block (fig. 3.4c), resulting in a combined circuit which has the same form as that of a single C or L (table 3.1). Subsequently, all these circuits can be added mathematically leading to a final equivalent current source connected in parallel with its source resistance. At this point, the capacitance C_1 is replaced with its discretized form to produce the circuit of fig. 3.4d. After another combination, the network becomes again one dc current source with its internal resistance as shown in fig. 3.4e.

The sequence described above is repeated for all blocks of the approximating network. After the process has been completed, all the equivalent circuits (which are connected in series) are again combined into a single equivalent similar to the one shown in fig. 3.4e. If the equivalent resistance of L_{1j} is R_{L-1j} and its current source (or history term) is $I_{1j}(t-\Delta t)$, $j = 1, n$, where n is the number of RL parallel blocks, the following equations can be written (with reference to figs. 3.4b and 3.4c),

$$R_{LR-1j} = \frac{R_{1j} \cdot R_{L-1j}}{R_{1j} + R_{L-1j}}, \quad R_{1j} \neq 0, L_{1j} \neq 0, \quad (3.8)$$

$$= R_{1j}, \quad L_{1j} = 0, \quad (3.9)$$

$$= R_{L-1j}, \quad R_{1j} = 0, \quad (3.10)$$

and,

$$I_{L-1j} = I_{1j}, \quad L_{1j} \neq 0, \quad (3.11)$$

$$= 0, \quad L_{1j} = 0 \quad (3.12)$$

and with reference to fig. 3.4-c,

$$\begin{aligned} v_1(t) &= (i_{B-1}(t) - I_{L-11}) \cdot R_{LR-11} + (i_{B-1}(t) - I_{L-12}) \cdot R_{LR-12} \\ &\quad + (i_{B-1}(t) - I_{L-13}) \cdot R_{LR-13} + \dots \\ &= i_{B-1}(t) \cdot (R_{LR-11} + R_{LR-12} + R_{LR-13} + \dots) \\ &\quad - (I_{L-11} \cdot R_{LR-11} + I_{L-12} \cdot R_{LR-12} + I_{L-13} \cdot R_{LR-13} + \dots) \\ &= i_{B-1}(t) \cdot \sum_{j=1}^n R_{LR-1j} - \sum_{j=1}^n I_{L-1j} \cdot R_{LR-1j} \end{aligned}$$

or,

$$\begin{aligned} i_{B-1}(t) &= \frac{v_1(t)}{\sum_{j=1}^n R_{LR-1j}} + \frac{\sum_{j=1}^n I_{L-1j} \cdot R_{LR-1j}}{\sum_{j=1}^n R_{LR-1j}} \\ &= \frac{v_1(t)}{R_{LR-1}} + I_{LR-1} \end{aligned} \quad (3.13)$$

with reference to fig. 3.4d,

$$\begin{aligned}
i(t) &= i_{C-1}(t) + i_{B-1}(t) \\
&= I_{C-1} + \frac{v_1(t)}{R_{C-1}} + I_{LR-1} + \frac{v_1(t)}{R_{LR-1}} \\
&= v_1(t) \cdot \left(\frac{1}{R_{C-1}} + \frac{1}{R_{LR-1}} \right) + I_{C-1} + I_{LR-1} \\
&= \frac{v_1(t)}{R_{eq-1}} + I_{hist-1}(t - \Delta t)
\end{aligned} \tag{3.14}$$

In deriving equation 3.13 and equation 3.14, the term $(t - \Delta t)$ was omitted from the history terms for simplicity.

Equations 3.8 to 3.14 can be used to compute the equivalent resistance and the history term for peaks no. 2, 3, and so on. If R_{eq} and $I_{hist}(t - \Delta t)$ denote the equivalent resistance and history term of the discrete time representation of the entire frequency dependent branch, the computations needed for R_{eq} and $I_{hist}(t - \Delta t)$ will be the same as those needed for the corresponding terms in equation 3.14, which are as follows:

$$R_{eq} = \sum_{i=1}^m R_{eq-i} \quad , \quad i = 1, m \tag{3.15}$$

$$I_{hist}(t - \Delta t) = \frac{\sum_{i=1}^m I_{hist-i} \cdot R_{eq-i}}{R_{eq}} \quad , \quad i = 1, m \tag{3.16}$$

where,

$$m = \text{no. of peaks to be fitted.}$$

and,

$$\frac{1}{R_{eq-i}} = \frac{1}{R_{C-i}} + \frac{1}{R_{LR-i}}$$

The process described must be implemented three times - once for the zero-sequence network and repeated for the positive- and negative-sequence networks. Since the parameters of the positive-sequence network are identical to those of the negative-sequence network, R_{eq} are the same for both networks. The history terms, though, must be calculated independently.

The next and the last action to be taken in modelling $Z_{winding}$ is to update the history terms of its discrete time representation so that the simulation can proceed to the next time step ($t+\Delta t$).

4. Updating History Terms

To update the history terms for a capacitance or an inductance, the voltage across its terminals and the currents flowing through it must be known before any calculations can be performed. From the power network solution, the voltage at every node in the system in phase co-ordinates is known at each particular time step. Terminal voltages of the transformer are, therefore, known at the current time step in phase co-ordinates. These values have to be transformed into sequence co-ordinates in order to update the history currents of the model discrete-time circuits. The steps to update the history terms are as follows:

(1) Calculate $v_1(t)$ (fig. 3.4e),

$$v_1(t) = [i(t) - I_{hist-1}(t - \Delta t)] \cdot R_{eq-1} \quad (3.17)$$

(2) Compute $i_{C-1}(t)$ and $i_{B-1}(t)$ (fig. 3.4d),

$$i_{C-1}(t) = I_{C-1}(t - \Delta t) + \frac{v_1(t)}{R_{C-1}} \quad (3.18)$$

$$i_{B-1}(t) = I_{LR-1}(t - \Delta t) + \frac{v_1(t)}{R_{LR-1}} \quad (3.19)$$

(3) Evaluate the voltage of each RL block, $v_{RL-1j}(t)$ (fig. 3.4c),

$$v_{RL-1j}(t) = [i_{B-1}(t) - I_{L-1j}(t - \Delta t)] \cdot R_{LR-1j} \quad (3.20)$$

4) Find the current of the element L_{1j} (fig. 3.4-b),

$$i_{L-1j}(t) = i_{B-1}(t) - \frac{v_{RL-1j}(t)}{R_{1j}} \quad (3.21)$$

(5) Determine the history term of each individual L and C at the current time step, $I_{L-1j}(t)$ and $I_{C-1}(t)$, using the formulas given in table 3.1.

(6) Combine the history terms of all inductances ,

$$I_{LR-1}(t) = \frac{\sum_{j=1}^n I_{L-1j}(t) \cdot R_{LR-1j}}{R_{LR-1}} \quad (3.22)$$

where,

n = no. of RL parallel blocks in the section for peak no. 1.

(7) Finally, add $I_{C-1}(t)$ and $I_{LR-1}(t)$ together to obtain history terms associated with peak no. 1.

The history terms for the blocks associated with the other peaks are calculated in the same manner. In the end, all the history terms can be combined together to get the total equivalent history term which will be used along with R_{eq} to formulate the nodal admittance matrix at the next time step $t + \Delta t$,

$$I_{hist}(t) = \frac{\sum_{i=1}^m I_{hist-i}(t) \cdot R_{eq-i}}{R_{eq}} \quad (3.23)$$

where,

m = no. of peaks to be fitted,

$R_{eq} = \sum_{i=1}^m R_{eq-i}$.

The history term in equation 3.23 need to be computed three times for the three symmetrical component networks. Although the equivalent networks for $Z_{winding}$ in the positive and negative sequences are identical, the transformer voltages and currents are different in all the three sequences.

The discrete-time model for the frequency dependent part of the transformer described in this chapter will be used subsequently to construct the full transformer model. Details will be found in the next chapter.

Chapter Four

THE COMPLETE MODEL

All the component parts of the transformer model were discussed in the previous chapters. The equivalent circuits for these components were also developed for both the frequency domain and the discrete-time domain. In this chapter, all the pieces are put together to form the full transformer model. Equivalent networks for the leakage impedances and lumped terminal capacitances, together with ideal transformers, are the basic building blocks for the full transformer model. In the derivation of the full three-phase model, it will be assumed that the transformer is physically symmetrical so that symmetrical components can be applied. This eliminates the need to model directly the mutual coupling between phases, which may cause numerical stability problems [13]. The proposed approach not only does make the modelling simple but also reduces the number of elements to be mathematically synthesised. Although there are no transformers in existence which are truly symmetrical, tests performed on actual power transformers show that there are no significant errors in making such an assumption [1].

1. Discrete-Time Model in Sequence Domain

Following the discretization procedure described in section 3 of chapter 3, the discrete-time model for a three-winding three-phase transformer in either of the three se-

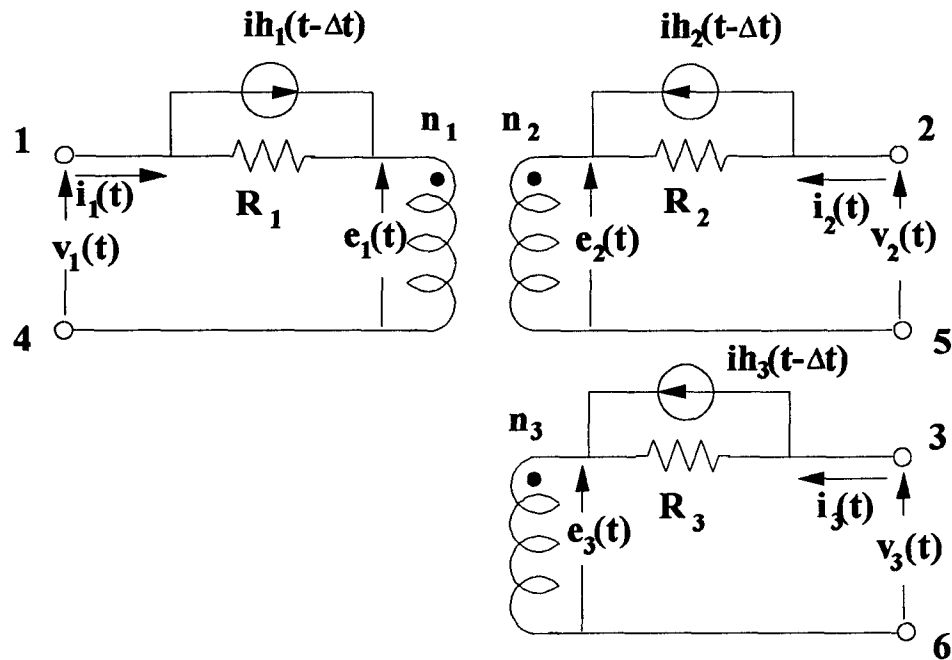


Fig. 4.1 Discrete-time equivalent circuit for a sequence model of a transformer.

quences [14] (positive, negative, or zero sequence) is depicted in fig. 4.1. The transformer is visualised as three coupled windings [15]. This representation is also known as a T-circuit [21]. The magnetising branch is not shown in the model of fig. 4. As an approximation, this branch can be added externally to the model. The exact placement of the magnetising branch is not critical in switching transient studies in which the frequencies

are beyond the kHz. At these frequencies, the transformer core behaves close to ideal since the core flux is inversely proportional to the frequency and the incremental values for these high frequency harmonics will be very small. However, if the magnetising branch model at the power frequency is available, it can be incorporated to the proposed model in the same way as it is implemented in the conventional model. (The particular modelling of the magnetising branch is beyond the scope of this thesis).

The models for the positive and negative sequence circuits will be exactly the same in the frequency domain but they will be different in the discrete time representation due to the history terms. Terminal capacitances are not shown in the network of fig. 4.1 because it is more convenient to model the capacitances directly in phase co-ordinates. Once the circuits of fig. 4.1 are transferred to the phase domain, the capacitance can be added to obtain the complete model. With reference to fig. 4.1, the following equations can be written:

$$i_1(t) \cdot R_1 + e_1(t) = v_1(t) + ih_1(t - \Delta t) \cdot R_1 \quad (4.1)$$

$$i_2(t) \cdot R_2 + e_2(t) = v_2(t) + ih_2(t - \Delta t) \cdot R_2 \quad (4.2)$$

$$i_3(t) \cdot R_3 + e_3(t) = v_3(t) + ih_3(t - \Delta t) \cdot R_3 \quad (4.3)$$

$$n_1 \cdot i_1(t) + n_2 \cdot i_2(t) + n_3 \cdot i_3(t) = 0 \quad (4.4)$$

$$n_2 \cdot e_1(t) - n_1 \cdot e_2(t) = 0 \quad (4.5)$$

$$n_3 \cdot e_1(t) - n_1 \cdot e_3(t) = 0 \quad (4.6)$$

where,

- $i_i(t)$ = current in winding i ,
- $ih_i(t - \Delta t)$ = history terms of frequency dependent part for winding i ,
- R_i = equivalent resistance of frequency dependent part for winding i ,
- n_i = no. of turns of winding i ,
- $e_i(t)$ = voltage at the ideal transformer terminal on the side of winding i ,
- $v_i(t)$ = terminal voltage of winding i .

The terminal voltage $v_i(t)$ in equations 4.1 to 4.3 becomes known after the system of equations has been solved at the time step t . Therefore, there are only two unknowns, $i_i(t)$ and $e_i(t)$, in equations 4.1 to 4.6. The unknown variables can be found systematically if equations 4.1 to 4.6 are rewritten as matrix equation as follows:

$$\begin{bmatrix} R_1 & 0 & 0 & 1 & 0 & 0 \\ 0 & R_2 & 0 & 0 & 1 & 0 \\ 0 & 0 & R_3 & 0 & 0 & 1 \\ n_1 & n_2 & n_3 & 0 & 0 & 0 \\ 0 & 0 & 0 & n_2 & -n_1 & 0 \\ 0 & 0 & 0 & n_3 & 0 & -n_1 \end{bmatrix} \begin{bmatrix} i_1(t) \\ i_2(t) \\ i_3(t) \\ e_1(t) \\ e_2(t) \\ e_3(t) \end{bmatrix} = \begin{bmatrix} 1 & 0 & 0 & R_1 & 0 & 0 \\ 0 & 1 & 0 & 0 & R_2 & 0 \\ 0 & 0 & 1 & 0 & 0 & R_3 \\ 0 & 0 & 0 & 0 & 0 & 0 \\ 0 & 0 & 0 & 0 & 0 & 0 \\ 0 & 0 & 0 & 0 & 0 & 0 \end{bmatrix} \begin{bmatrix} v_1(t) \\ v_2(t) \\ v_3(t) \\ ih_1(t - \Delta t) \\ ih_2(t - \Delta t) \\ ih_3(t - \Delta t) \end{bmatrix} \quad (4.7)$$

or, in a more compact form,

$$\begin{bmatrix} [R] & [I] \\ [N_1] & [N_2] \end{bmatrix} \begin{bmatrix} [i(t)] \\ [e(t)] \end{bmatrix} = \begin{bmatrix} [I] & [R] \\ [\Phi] & [\Phi] \end{bmatrix} \begin{bmatrix} [v(t)] \\ [ih(t-\Delta t)] \end{bmatrix} \quad (4.8)$$

where,

$$[R] = \begin{bmatrix} R_1 & 0 & 0 \\ 0 & R_2 & 0 \\ 0 & 0 & R_3 \end{bmatrix},$$

$$[N_1] = \begin{bmatrix} n_1 & n_2 & n_3 \\ 0 & 0 & 0 \\ 0 & 0 & 0 \end{bmatrix},$$

$$[N_2] = \begin{bmatrix} 0 & 0 & 0 \\ n_2 & -n_1 & 0 \\ n_3 & 0 & -n_1 \end{bmatrix},$$

$$[i(t)] = [i_1(t) \ i_2(t) \ i_3(t)]^T,$$

$$[e(t)] = [e_1(t) \ e_2(t) \ e_3(t)]^T,$$

$$[v(t)] = [v_1(t) \ v_2(t) \ v_3(t)]^T,$$

$$[ih(t-\Delta t)] = [ih_1(t-\Delta t) \ ih_2(t-\Delta t) \ ih_3(t-\Delta t)]^T,$$

and

$$[I] \text{ and } [\Phi] = \text{unity matrix and zero matrix, respectively.}$$

Equation 4.8 is also valid for the two winding transformer. In this case, submatrices $[R]$, $[N_1]$ and $[N_2]$ will be of order 2 and their elements will not contain the third row and third column of the submatrices for the three winding transformer. Also, $[i(t)]$, $[e(t)]$, $[v(t)]$ and $[ih(t-\Delta t)]$ will contain only the first and second elements. Expanding equation 4.8 gives the following two equations:

$$[R][i(t)] + [e(t)] = [v(t)] + [R][ih(t - \Delta t)] \quad (4.9)$$

and,

$$[N_1][i(t)] + [N_2][e(t)] = [0] \quad (4.10)$$

Multiplying equation 4.9 by $[N_2]$ and subtracting equation 4.10 yields

$$[N_2][R][i(t)] - [N_1][i(t)] = [N_2][v(t)] + [N_2][R][ih(t - \Delta t)] \quad (4.11)$$

or,

$$[i(t)] = [Y][v(t)] + [I_h(t - \Delta t)] \quad (4.12)$$

where,

$$\begin{aligned} [Y] &= [[N_2][R] - [N_1]]^{-1} [N_2], \\ [I_h(t - \Delta t)] &= [Y][R][ih(t - \Delta t)]. \end{aligned}$$

Equation 4.12 relates the currents of each transformer winding to the terminal voltages and the history terms of all three windings for any of the three sequences. Matrix $[Y]$ is the admittance matrix for the corresponding sequence and its order is equal to the number of transformer windings. Three equations similar to equation 4.12 will be required to construct the complete model in the sequence domain, for the zero, positive and negative sequences. The full model in symmetrical components representation is

$$\begin{bmatrix} [i_{zero}(t)] \\ [i_{pos}(t)] \\ [i_{neg}(t)] \end{bmatrix} = \begin{bmatrix} [Y_{zero}] & [0] & [0] \\ [0] & [Y_{pos}] & [0] \\ [0] & [0] & [Y_{neg}] \end{bmatrix} \begin{bmatrix} [v_{zero}(t)] \\ [v_{pos}(t)] \\ [v_{neg}(t)] \end{bmatrix} + \begin{bmatrix} [ih_{zero}(t-\Delta t)] \\ [ih_{pos}(t-\Delta t)] \\ [ih_{neg}(t-\Delta t)] \end{bmatrix} \quad (4.13)$$

where,

zero, pos and *neg* signify the variables for zero, positive and negative sequences, respectively, and

[0] = zero matrix (all elements are zeroes).

If $[i_{seq}(t)]$, $[Y_{seq}]$, $[v_{seq}(t)]$ and $[ih_{seq}(t-\Delta t)]$ denote the currents, the admittance matrix, the terminal voltages and the history terms in equation 4.13, then the transformer model in the sequence domain can be expressed as

$$[i_{seq}(t)] = [Y_{seq}] [v_{seq}(t)] + [ih_{seq}(t-\Delta t)] \quad (4.14)$$

2. Discrete-Time Model in Phase Co-ordinates

Equation 4.14 is not yet ready to be used in transient simulation programs, such as the EMTP, in which all the voltages and currents must be expressed in phase co-ordinates. Equation 4.14 can be transformed into phase co-ordinates by means of a transformation matrix. For a balanced systems, the transformation matrix is not unique. Due to the fact that the symmetrical components transformation involves complex numbers, other transformations with real matrix elements, such as the one given by Edith Clarke [12], will be used for the numerical transformation procedure. Clarke's transformation matrix for a three-phase system is

$$[T_{3 \times 3}] = \begin{bmatrix} \frac{1}{\sqrt{3}} & \frac{1}{\sqrt{2}} & \frac{1}{\sqrt{6}} \\ \frac{1}{\sqrt{3}} & \frac{-1}{\sqrt{2}} & \frac{1}{\sqrt{6}} \\ \frac{1}{\sqrt{3}} & 0 & \frac{-2}{\sqrt{6}} \end{bmatrix} \quad (4.15)$$

and,

$$[T_{3 \times 3}]^{-1} = [T_{3 \times 3}]^T \quad (4.16)$$

Matrix $[T_{3 \times 3}]$ given in equation 4.15 can be modified to fit the transformer problem by replacing each of its scalar elements with a diagonal submatrix. The order of the submatrix is determined by the number of windings of the transformer, i.e., two for a two-winding transformer and three for a three-winding transformer. All the diagonal elements in these submatrices are identical and equal to the corresponding scalar value of the original transformation matrix. For example, the transformation matrix for a three-phase, three-winding transformer is the following $[9 \times 9]$ matrix

$$[T] = \begin{bmatrix} \frac{1}{\sqrt{3}} & 0 & 0 & \frac{1}{\sqrt{2}} & 0 & 0 & \frac{1}{\sqrt{6}} & 0 & 0 \\ 0 & \frac{1}{\sqrt{3}} & 0 & 0 & \frac{1}{\sqrt{2}} & 0 & 0 & \frac{1}{\sqrt{6}} & 0 \\ 0 & 0 & \frac{1}{\sqrt{3}} & 0 & 0 & \frac{1}{\sqrt{2}} & 0 & 0 & \frac{1}{\sqrt{6}} \\ \frac{1}{\sqrt{3}} & 0 & 0 & \frac{-1}{\sqrt{2}} & 0 & 0 & \frac{1}{\sqrt{6}} & 0 & 0 \\ 0 & \frac{1}{\sqrt{3}} & 0 & 0 & \frac{-1}{\sqrt{2}} & 0 & 0 & \frac{1}{\sqrt{6}} & 0 \\ 0 & 0 & \frac{1}{\sqrt{3}} & 0 & 0 & \frac{-1}{\sqrt{2}} & 0 & 0 & \frac{1}{\sqrt{6}} \\ \frac{1}{\sqrt{3}} & 0 & 0 & 0 & 0 & 0 & \frac{-2}{\sqrt{6}} & 0 & 0 \\ 0 & \frac{1}{\sqrt{3}} & 0 & 0 & 0 & 0 & 0 & \frac{-2}{\sqrt{6}} & 0 \\ 0 & 0 & \frac{1}{\sqrt{3}} & 0 & 0 & 0 & 0 & 0 & \frac{-2}{\sqrt{6}} \end{bmatrix} \quad (4.17)$$

$$[T]^{-1} = [T]^T \quad (4.18)$$

The voltages and currents of each transformer winding in phase co-ordinates are related to the corresponding sequence voltages and currents by [14]

$$[v_{phase}(t)] = [T][v_{seq}(t)] \quad (4.19)$$

and,

$$[i_{phase}(t)] = [T][i_{seq}(t)] \quad (4.20)$$

where,

$[v_{phase}(t)]$ and $[i_{phase}(t)]$ = voltages and currents in phase co-ordinates,

$[v_{seq}(t)]$ and $[i_{seq}(t)]$ = voltages and currents in sequence co-ordinates.

Applying equations 4.19 and 4.20 to equation 4.14 yields

$$[i_{phase}(t)] = [T][Y_{seq}][T]^{-1}[v_{phase}(t)] + [T][ih_{seq}(t - \Delta t)] \quad (4.21)$$

or,

$$[i_{phase}(t)] = [Y_{phase}][v_{phase}(t)] + [ih_{phase}(t - \Delta t)] \quad (4.22)$$

where,

$$[Y_{phase}] = [T][Y_{seq}][T]^{-1},$$

and

$$[ih_{phase}(t - \Delta t)] = [T][ih_{seq}(t - \Delta t)].$$

In full matrix form, equation 4.22 for a three-winding transformer is

$$\begin{bmatrix} i_{11}(t) \\ i_{12}(t) \\ i_{13}(t) \\ i_{21}(t) \\ i_{22}(t) \\ i_{23}(t) \\ i_{31}(t) \\ i_{32}(t) \\ i_{33}(t) \end{bmatrix} = \begin{bmatrix} [Y_s] & [Y_m] & [Y_m] \\ [Y_m] & [Y_s] & [Y_m] \\ [Y_m] & [Y_m] & [Y_s] \end{bmatrix} \begin{bmatrix} v_{11}(t) \\ v_{12}(t) \\ v_{13}(t) \\ v_{21}(t) \\ v_{22}(t) \\ v_{23}(t) \\ v_{31}(t) \\ v_{32}(t) \\ v_{33}(t) \end{bmatrix} + \begin{bmatrix} Ih_{11}(t - \Delta t) \\ Ih_{12}(t - \Delta t) \\ Ih_{13}(t - \Delta t) \\ Ih_{21}(t - \Delta t) \\ Ih_{22}(t - \Delta t) \\ Ih_{23}(t - \Delta t) \\ Ih_{31}(t - \Delta t) \\ Ih_{32}(t - \Delta t) \\ Ih_{33}(t - \Delta t) \end{bmatrix} \quad (4.23)$$

where,

$i_{ij}(t)$ = current of phase i , winding j ,

$v_{ij}(t)$ = terminal voltage of phase i , winding j ,

$[Y_s]$ and $[Y_m]$ = $[3 \times 3]$ submatrices (or $[2 \times 2]$ for a two-winding transformer) for the self and mutual terms of the admittance matrix $[Y_{phase}]$ in equation 4.22,

$Ih_{ij}(t - \Delta t)$ = element of history vector associated with phase i , winding j .

In the actual implementation of the model, there are only two transformations involved. Phase voltages need to be transformed into sequence voltages in order to calculate and update the history terms. After that, the history terms are transformed from sequence co-ordinates back into phase co-ordinates and are entered into the right hand side of the system equations. There is no need to calculate $[Y_{phase}]$ in equation 4.23 directly from $[T][Y_{seq}][T]^{-1}$ because it is already known that

$$[Y_s] = \frac{1}{3} \cdot ([Y_{zero}] + 2[Y_{pos}])$$

and,

$$[Y_m] = \frac{1}{3} \cdot ([Y_{zero}] - [Y_{pos}])$$

Also, from equation 4.19, $[v_{seq}(t)] = [T]^{-1}[v_{phase}(t)]$, or in a full matrix form

$$\begin{bmatrix} v_{zero-1}(t) \\ v_{zero-2}(t) \\ v_{zero-3}(t) \\ v_{pos-1}(t) \\ v_{pos-2}(t) \\ v_{pos-3}(t) \\ v_{neg-1}(t) \\ v_{neg-2}(t) \\ v_{neg-3}(t) \end{bmatrix} = \begin{bmatrix} \frac{1}{\sqrt{3}} & 0 & 0 & \frac{1}{\sqrt{3}} & 0 & 0 & \frac{1}{\sqrt{3}} & 0 & 0 \\ 0 & \frac{1}{\sqrt{3}} & 0 & 0 & \frac{1}{\sqrt{3}} & 0 & 0 & \frac{1}{\sqrt{3}} & 0 \\ 0 & 0 & \frac{1}{\sqrt{3}} & 0 & 0 & \frac{1}{\sqrt{3}} & 0 & 0 & \frac{1}{\sqrt{3}} \\ \frac{1}{\sqrt{2}} & 0 & 0 & \frac{-1}{\sqrt{2}} & 0 & 0 & 0 & 0 & 0 \\ 0 & \frac{1}{\sqrt{2}} & 0 & 0 & \frac{-1}{\sqrt{2}} & 0 & 0 & 0 & 0 \\ 0 & 0 & \frac{1}{\sqrt{2}} & 0 & 0 & \frac{-1}{\sqrt{2}} & 0 & 0 & 0 \\ \frac{1}{\sqrt{6}} & 0 & 0 & \frac{1}{\sqrt{6}} & 0 & 0 & \frac{-2}{\sqrt{6}} & 0 & 0 \\ 0 & \frac{1}{\sqrt{6}} & 0 & 0 & \frac{1}{\sqrt{6}} & 0 & 0 & \frac{-2}{\sqrt{6}} & 0 \\ 0 & 0 & \frac{1}{\sqrt{6}} & 0 & 0 & \frac{1}{\sqrt{6}} & 0 & 0 & \frac{-2}{\sqrt{6}} \end{bmatrix} \begin{bmatrix} v_{11}(t) \\ v_{12}(t) \\ v_{13}(t) \\ v_{21}(t) \\ v_{22}(t) \\ v_{23}(t) \\ v_{31}(t) \\ v_{32}(t) \\ v_{33}(t) \end{bmatrix} \quad (4.24)$$

If the elements of the sequence voltage vector $[v_{seq}(t)]$ in equation 4.24 are arranged in the order of *windings*, instead of *sequences*, equation 4.24 becomes

$$\begin{bmatrix} v_{zero-1}(t) \\ v_{pos-1}(t) \\ v_{neg-1}(t) \\ v_{zero-2}(t) \\ v_{pos-2}(t) \\ v_{neg-2}(t) \\ v_{zero-3}(t) \\ v_{pos-3}(t) \\ v_{neg-3}(t) \end{bmatrix} = \begin{bmatrix} \frac{1}{\sqrt{3}} & \frac{1}{\sqrt{3}} & \frac{1}{\sqrt{3}} & 0 & 0 & 0 & 0 & 0 & 0 \\ \frac{1}{\sqrt{2}} & \frac{-1}{\sqrt{2}} & 0 & 0 & 0 & 0 & 0 & 0 & 0 \\ \frac{1}{\sqrt{6}} & \frac{1}{\sqrt{6}} & \frac{-2}{\sqrt{6}} & 0 & 0 & 0 & 0 & 0 & 0 \\ 0 & 0 & 0 & \frac{1}{\sqrt{3}} & \frac{1}{\sqrt{3}} & \frac{1}{\sqrt{3}} & 0 & 0 & 0 \\ 0 & 0 & 0 & \frac{1}{\sqrt{2}} & \frac{-1}{\sqrt{2}} & 0 & 0 & 0 & 0 \\ 0 & 0 & 0 & \frac{1}{\sqrt{6}} & \frac{1}{\sqrt{6}} & \frac{-2}{\sqrt{6}} & 0 & 0 & 0 \\ 0 & 0 & 0 & 0 & 0 & 0 & \frac{1}{\sqrt{3}} & \frac{1}{\sqrt{3}} & \frac{1}{\sqrt{3}} \\ 0 & 0 & 0 & 0 & 0 & 0 & \frac{1}{\sqrt{2}} & \frac{-1}{\sqrt{2}} & 0 \\ 0 & 0 & 0 & 0 & 0 & 0 & \frac{1}{\sqrt{6}} & \frac{1}{\sqrt{6}} & \frac{-2}{\sqrt{6}} \end{bmatrix} \begin{bmatrix} v_{11}(t) \\ v_{21}(t) \\ v_{31}(t) \\ v_{12}(t) \\ v_{22}(t) \\ v_{32}(t) \\ v_{13}(t) \\ v_{23}(t) \\ v_{33}(t) \end{bmatrix} \quad (4.25)$$

where,

$v_{zero-i}(t)$, $v_{pos-i}(t)$, $v_{neg-i}(t)$ = Zero-, positive- and negative-sequence voltages for winding i respectively.

Equation 4.25 can be further simplified, if the voltages are rearranged into matrices instead of vectors. Now, the sequence voltages can be computed with a single matrix multiplication, which is more efficient, as follows:

$$\begin{bmatrix} v_{zero-1}(t) & v_{zero-2}(t) & v_{zero-3}(t) \\ v_{pos-1}(t) & v_{pos-2}(t) & v_{pos-3}(t) \\ v_{neg-1}(t) & v_{neg-2}(t) & v_{neg-3}(t) \end{bmatrix} = \begin{bmatrix} \frac{1}{\sqrt{3}} & \frac{1}{\sqrt{3}} & \frac{1}{\sqrt{3}} \\ \frac{1}{\sqrt{2}} & \frac{-1}{\sqrt{2}} & 0 \\ \frac{1}{\sqrt{6}} & \frac{1}{\sqrt{6}} & \frac{-2}{\sqrt{6}} \end{bmatrix} \begin{bmatrix} v_{11}(t) & v_{12}(t) & v_{13}(t) \\ v_{21}(t) & v_{22}(t) & v_{23}(t) \\ v_{31}(t) & v_{32}(t) & v_{33}(t) \end{bmatrix} \quad (4.26)$$

The sequence voltages in equation 4.26 can be reshuffled into a vector as in equation 4.24, which is in the desired order in sequence co-ordinates. The sequence currents can be calculated likewise. For the history terms, transformation from sequence variables to phase variables are also required. A similar implementation to that used to derive equation 4.26 can be applied to obtain the history terms in phase co-ordinates. But the transformation matrix $[T_{3 \times 3}]$ is used in this case.

3. Nodal Admittance Matrix

Equation 4.22, however, is not yet of the right form for an electromagnetic transient program solution because the variables are associated with voltages and currents in the transformer windings. It must be further modified so that voltages and currents are

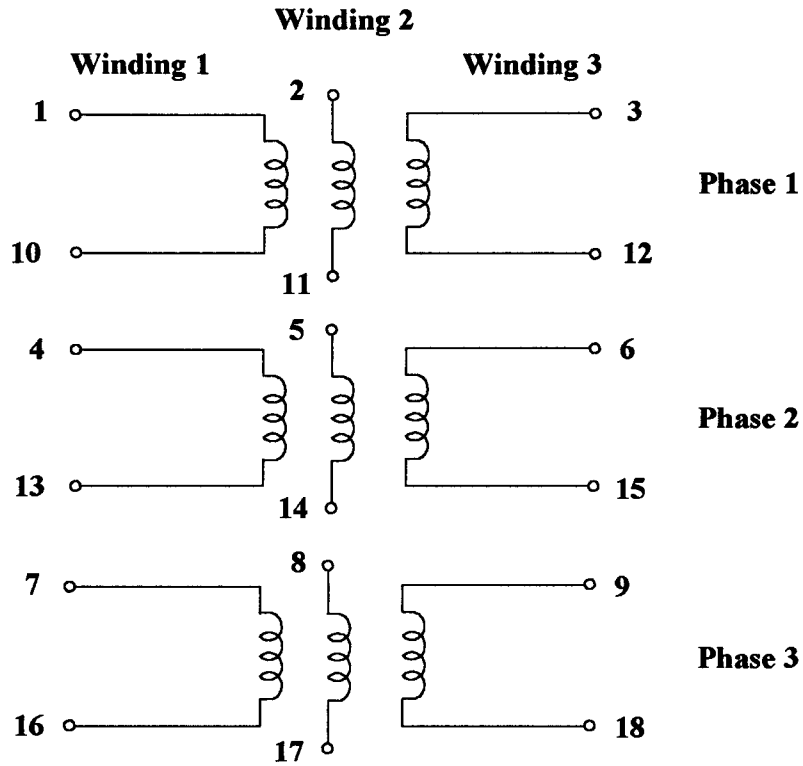


Fig. 4.2 Transformer node labelling for external network connection.

the node voltages and the currents flowing into the node of the transformer. This involves labelling of the nodes in a certain way, as shown in fig. 4.2. Since the terminal voltage is the difference of the voltages of the two nodes at both ends of the winding, it follows that

$$v_{11}(t) = v_1(t) - v_{10}(t) \quad (4.27)$$

$$v_{12}(t) = v_2(t) - v_{11}(t) \quad (4.28)$$

$$v_{13}(t) = v_3(t) - v_{12}(t) \quad (4.29)$$

$$v_{21}(t) = v_4(t) - v_{13}(t) \quad (4.30)$$

$$v_{22}(t) = v_5(t) - v_{14}(t) \quad (4.31)$$

$$v_{23}(t) = v_6(t) - v_{15}(t) \quad (4.32)$$

$$v_{31}(t) = v_7(t) - v_{16}(t) \quad (4.33)$$

$$v_{32}(t) = v_8(t) - v_{17}(t) \quad (4.34)$$

$$v_{33}(t) = v_9(t) - v_{18}(t) \quad (4.35)$$

where,

$$v_i(t) = \text{node voltage with respect to fig. 4.2.}$$

In addition, it is also true that $i_{10}(t), i_{11}(t), i_{12}(t), \dots, i_{18}(t)$, are equal to the negative of $i_1(t), i_2(t), i_3(t), \dots, i_9(t)$, respectively. Arranging the node voltages and currents in this manner makes it possible to construct the final equation in phase co-ordinates without much work. It is just an extension of equation 4.22, which is as follows,

$$[i_{node}(t)] = \begin{bmatrix} Y_{phase} & -Y_{phase} \\ -Y_{phase} & Y_{phase} \end{bmatrix} [v_{node}(t)] + \begin{bmatrix} ih_{phase}(t - \Delta t) \\ -ih_{phase}(t - \Delta t) \end{bmatrix} \quad (4.36)$$

where,

$$[i_{node}(t)] = \text{vector of currents flowing into node 1, node 2, node 3, \dots, node 18,}$$

- $[v_{node}(t)]$ = vector of voltages of node 1, node 2, node3,..., node 18,
- $[Y_{phase}]$ = admittance matrix in equation 4.22,
- $[ih_{phase}(t - \Delta t)]$ = history terms in equation 4.22.

Equation 4.36 is the nodal equation without terminal capacitances. The complete frequency dependent model for the three-phase transformer comprises equations 4.36 and 2.14 combined. Elements of the admittance matrices from both models can be added algebraically to the corresponding elements of the system admittance matrix. The history terms in equation 4.36, though, must be subtracted from the right hand side of the system nodal equation because the history terms are considered known and must, therefore, be on the opposite side of the equation.

Chapter Five

MEASUREMENT OF THE MODEL PARAMETERS

This chapter describes the techniques used to measure the transformer parameters and to calculate the circuit parameters from these measurements. As explained earlier, there are two types of parameters in the model - stray capacitances, represented by constant capacitances, and the leakage impedances represented by branches of constant RLC sections. Numerical examples on the network synthesis realization of the model parameters will be presented in chapter 6.

1. Measurement of the Frequency Dependent Leakage Impedance

The measurements required to obtain the leakage impedances are the short-circuit frequency response tests. Measurements must be conducted such that both the zero-sequence and the positive-sequence impedances can be determined. The measuring device used in the present research work for impedance measurements was an "Impedance Analyzer", which produces a low voltage signal with variable frequencies. The signal voltage energizes the transformer under test. At the same time the Analyzer senses the current that flows into the transformer. Voltages and currents are then used by the device to calculate the magnitude and phase angle of the transformer impedance within a band of

frequencies specified by the users. The results are both displayed and stored in a diskette. The "single-phase" Impedance Analyzer can be used to measure both the zero-sequence and the positive sequence impedances. Details of the measurement technique are explained next, with special note on transformers with delta-connected windings.

1.1 Transformer without Delta Windings

The zero-sequence tests can be performed as usual. However, since the Impedance Analyzer is a single phase source, the positive-sequence tests cannot be conducted directly. In this case, the positive-sequence information will be calculated from the zero-sequence data and some additional data obtained from separated measurements.

A three-phase, three-winding transformer (without terminal capacitances) can be described by the following matrix equation [14]:

$$\begin{bmatrix} I_{A-1} \\ I_{A-2} \\ I_{A-3} \\ I_{B-1} \\ I_{B-2} \\ I_{B-3} \\ I_{C-1} \\ I_{C-2} \\ I_{C-3} \end{bmatrix} = \begin{bmatrix} [Y_s] & [Y_m] & [Y_m] \\ [Y_m] & [Y_s] & [Y_m] \\ [Y_m] & [Y_m] & [Y_s] \end{bmatrix} \begin{bmatrix} V_{A-1} \\ V_{A-2} \\ V_{A-3} \\ V_{B-1} \\ V_{B-2} \\ V_{B-3} \\ V_{C-1} \\ V_{C-2} \\ V_{C-3} \end{bmatrix} \quad (5.1)$$

where,

I_{A-j} , I_{B-j} and I_{C-j} = transformer currents in winding j of phases A, B and C respectively, at a particular frequency.

V_{A-j} , V_{B-j} and V_{C-j} = terminal voltages of winding j of phases A, B and C respectively, at a particular frequency.

$[Y_s]$ and $[Y_m]$ = $[3 \times 3]$ self and mutual submatrices of the transformer admittance matrix. Both $[Y_s]$ and $[Y_m]$ are symmetric.

From the zero-sequence short-circuit test, a zero-sequence admittance matrix is obtained.

This matrix is related to $[Y_s]$ and $[Y_m]$ by

$$[Y_{zero}] = [Y_s] + 2 \cdot [Y_m] \quad (5.2)$$

If either $[Y_s]$ or $[Y_m]$ is available, it can also be used to compute the positive-sequence admittance matrix. Suppose that $[Y_s]$ is available from the measurement. The positive-sequence admittance matrix can then be calculated from the zero-sequence admittance as

$$[Y_{pos}] = \frac{1}{2} \cdot (3 \cdot [Y_s] - [Y_{zero}]) \quad (5.3)$$

In fact, it is not necessary to know all the elements of the matrix $[Y_s]$. Only the diagonal elements are sufficient for the calculation of $[Y_{pos}]$. The diagonal elements of $[Y_s]$ can be measured easily with the impedance analyzer. The readings will be taken at one coil while all the other coils are short-circuited at their terminals. The measured admittance can be expressed, for example for phase A, as:

$$y_{s-ij} = \frac{I_{A-j}}{V_{A-j}}, V_{A-i, i \neq j} = 0, V_{B-i} = 0, V_{C-i} = 0; i = 1, 3. \quad (5.4)$$

where,

I_{A-j} and V_{A-j} = current and voltage measured at the terminals of coil j ,
 $j = 1, 3$.

Measurement of y_{s-jj} should be taken for phases A, B and C and the averaged values of the three measurements should be used. The diagonal elements of $[Y_{pos}]$ can be computed now with equation 5.3. If the actual measurements could be performed, these values would correspond to the positive-sequence impedances obtained from the short-circuit tests measured on one winding while the other two windings are shorted. If all stray capacitances are not taken into account (modelled seperately), the positive-sequence short circuit admittances can be related to the winding impedances as follows (circuit representation similar to fig. 2.9b) :

$$\frac{1}{Y_H} = Z_H + \frac{Z'_T \cdot Z'_L}{Z'_T + Z'_L} \quad (5.5)$$

$$\frac{1}{Y_T} \cdot \left(\frac{n_H}{n_T}\right)^2 = Z'_T + \frac{Z_H \cdot Z'_L}{Z_H + Z'_L} = \frac{1}{Y'_T} \quad (5.6)$$

$$\frac{1}{Y_L} \cdot \left(\frac{n_H}{n_L}\right)^2 = Z'_L + \frac{Z_H \cdot Z'_T}{Z_H + Z'_T} = \frac{1}{Y'_L} \quad (5.7)$$

where,

Y_H, Y_T and Y_L = diagonal elements of the positive-sequence admittance matrix when measurements are taken on the high, low and tertiary voltage windings, respectively. The windings where measurements are not taken are all shorted,

Z'_T and Z'_L = $\left(\frac{n_H}{n_T}\right)^2 Z_T$ and $\left(\frac{n_H}{n_L}\right)^2 Z_L$

Z_H = positive-sequence frequency dependent impedance for high-, tertiary- and low-voltage windings, respectively,

n_H, n_T and n_L = no. of turns for high-, tertiary- and low-voltage windings, respectively.

Since Y_H, Y_T and Y_L can be taken from the corresponding diagonal elements of $[Y_{pos}]$, Z_H, Z'_T and Z'_L , or, alternatively, $Z_H+Z'_T, Z'_T+Z'_L$ and $Z_H+Z'_L$ can be found by solving equations 5.5, 5.6 and 5.7. Rearranging terms in equation 5.5 gives

$$Z'_T + Z'_L = Y_H \cdot (Z_H \cdot Z'_L + Z_H \cdot Z'_T + Z'_L \cdot Z'_T) \quad (5.8)$$

Similarly, from equation 5.6 and equation 5.7,

$$Z_H + Z'_L = Y'_T \cdot (Z_H \cdot Z'_L + Z_H \cdot Z'_T + Z'_L \cdot Z'_T) \quad (5.9)$$

$$Z'_T + Z_H = Y'_L \cdot (Z_H \cdot Z'_L + Z_H \cdot Z'_T + Z'_L \cdot Z'_T) \quad (5.10)$$

If $Z_H Z'_T + Z_H Z'_L + Z'_L Z'_T$ is denoted by Z_π , then Equations 5.8, 5.9 and 5.10 can be solved for Z_H, Z'_T and Z'_L , which are given by

$$Z_H = \frac{1}{2}(-Y_H + Y'_T + Y'_L) \cdot Z_\pi \quad (5.11)$$

$$Z'_T = \frac{1}{2}(Y_H - Y'_T + Y'_L) \cdot Z_\pi \quad (5.12)$$

$$Z'_L = \frac{1}{2}(Y_H + Y'_T - Y'_L) \cdot Z_\pi \quad (5.13)$$

However, Z_π is still unknown. From direct multiplication, the following equations follows:

$$Z_H \cdot Z'_T = \frac{1}{4} Z_\pi^2 \cdot (-Y_H^2 - Y_T^2 + Y_L^2 + 2Y_H \cdot Y_T) \quad (5.14)$$

$$Z'_T \cdot Z'_L = \frac{1}{4} Z_\pi^2 \cdot (Y_H^2 - Y_T^2 - Y_L^2 + 2Y_L \cdot Y_T) \quad (5.15)$$

$$Z_H \cdot Z'_L = \frac{1}{4} Z_\pi^2 \cdot (-Y_H^2 + Y_T^2 - Y_L^2 + 2Y_H \cdot Y_L) \quad (5.16)$$

Adding equations 5.14, 5.15 and 5.16 together yields

$$Z_\pi = \frac{1}{4} Z_\pi^2 \cdot [-Y_H^2 - Y_T^2 - Y_L^2 + 2(Y_H \cdot Y_T + Y_T \cdot Y_L + Y_H \cdot Y_L)] \quad (5.17)$$

Dividing equation 5.17 by $Z_\pi \neq 0$ and rearranging terms results in

$$Z_\pi = \frac{4}{-Y_H^2 - Y_T^2 - Y_L^2 + 2(Y_H \cdot Y_T + Y_T \cdot Y_L + Y_H \cdot Y_L)} \quad (5.18)$$

In conclusion, the positive-sequence impedances for the transformer without delta windings can be obtained in the following manner:

- 1) Find the zero-sequence impedance in the usual way from the short-circuit tests.
- 2) Measure the diagonal elements of the admittance matrix in phase coordinates for the three phases.

- 3) Average the corresponding measurements from the three phases to obtain the diagonal element of the self-admittance sub-matrix.
- 4) Calculate the diagonal elements of the positive-sequence admittance matrix with equation 5.3.
- 5) Compute Z_{π} with equation 5.18.
- 6) Substitute Z_{π} back into Equations 5.8, 5.9 and 5.10 to obtain the short-circuit impedances for the positive sequence. In this case, the short-circuit impedances are those which would be obtained if the short-circuit tests were conducted between pairs of windings at a time. Equations 5.11, 5.12 and 5.13 can also be used to calculate the impedances of the individual windings of the "T" circuit. If this was done, however, one or more of the individual impedances might not be minimum-phase-shift. This problem can be avoided if the combined impedance of every two windings is fitted instead.

By applying the above outlined steps, it is only necessary to measure nine functions for a three-winding transformer and six functions for a two-winding transformer in order to get the positive-sequence data for a transformer without delta windings. The total number of measurements to obtain both the positive and zero-sequence data for the three and two-winding transformers comes, therefore, to a total of twelve and eight, respectively. This indicates a dramatic reduction in the number of tests which would normally amount to ninety-one for a three-winding transformer and to thirty-six for a two-winding transformer if all the elements of the admittance matrix were to be

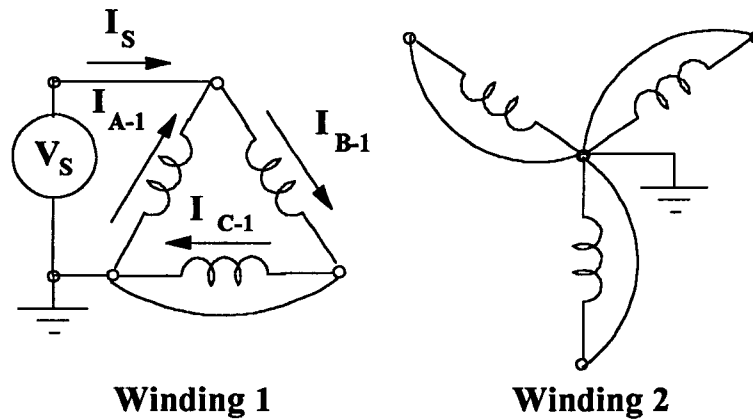


Fig. 5.1 Measurement of positive-sequence impedance in a Yd transformer.

measured. This latter case is, for instance, where the transformer is modeled directly from the $[Y]$ matrix.

1.2 Transformer with Delta Winding

If one of the windings of a three-phase transformer is connected in delta and all the delta terminals are accessible from the outside, the positive-sequence test can be conducted with a short-cut. It is very common for a power transformer to have one of the windings connected in delta, but the delta winding might have just one accessible terminal to be grounded. If all the delta winding terminals are accessible, measurements can be taken on one winding while the other windings are either shorted or open.

1.2.1 Two-Winding Transformer

A two-winding transformer (without terminal capacitances) can be described by the following matrix equation:

$$\begin{bmatrix} I_{A-1} \\ I_{A-2} \\ I_{B-1} \\ I_{B-2} \\ I_{C-1} \\ I_{C-1} \end{bmatrix} = \begin{bmatrix} y_{s11} & y_{s12} & y_{m11} & y_{m12} & y_{m11} & y_{m12} \\ y_{s21} & y_{s22} & y_{m21} & y_{m22} & y_{s21} & y_{m22} \\ y_{m11} & y_{m12} & y_{s11} & y_{s12} & y_{m11} & y_{m12} \\ y_{s21} & y_{m22} & y_{s21} & y_{s22} & y_{s21} & y_{m22} \\ y_{m11} & y_{m12} & y_{m11} & y_{m12} & y_{s11} & y_{s12} \\ y_{s21} & y_{m22} & y_{s21} & y_{m22} & y_{s21} & y_{s22} \end{bmatrix} \begin{bmatrix} V_{A-1} \\ V_{A-2} \\ V_{B-1} \\ V_{B-2} \\ V_{C-1} \\ V_{C-2} \end{bmatrix} \quad (5.19)$$

where,

I_{A-i} , I_{B-i} and I_{C-i} = Currents entering terminals i , $i = 1,2$ of phase A, phase B and phase C, respectively,

V_{A-i} , V_{B-i} and V_{C-i} = Terminal voltages of terminals i , $i = 1,2$ of phase A, phase B and phase C, respectively,

Assume a short-circuit test is performed on this transformer and that the measurement is taken on winding 1, which is delta-connected, while winding 2 is shorted. Under this condition, $V_{A-2} = V_{B-2} = V_{C-2} = 0$. Consequently, the measured currents in winding 1 are

$$\begin{bmatrix} I_{A-1} \\ I_{B-1} \\ I_{C-1} \end{bmatrix} = \begin{bmatrix} y_{s11} & y_{m11} & y_{m11} \\ y_{m11} & y_{s11} & y_{m11} \\ y_{m11} & y_{m11} & y_{s11} \end{bmatrix} \begin{bmatrix} V_{A-1} \\ V_{B-1} \\ V_{C-1} \end{bmatrix} \quad (5.20)$$

If V_{A-1} , V_{B-1} and V_{C-1} are in positive sequence, i.e., having equal magnitude and 120 degrees apart in phase angles, the ratio of I_{A-1} to V_{A-1} would give the positive-sequence admittance of the transformer. This could be accomplished if a variable frequency, three-phase source were available. However, a single-phase source with variable frequency such as an impedance analyzer can be used also to obtain the same result. Suppose phase C of winding 1 is shorted to ground, as shown in the arrangement of fig. 5.1. Because phase C is shorted, V_{C-1} is zero. V_{B-1} is connected to the source in its normal polarity while V_{A-1} is in the reverse polarity. We then have that $V_{A-1} = -V_s$, $V_{B-1} = +V_s$, $I_{A-1} = (-y_{s11} + y_{m11})$ and $I_{B-1} = (+y_{s11} - y_{m11})$. The measured current I_s flowing from the source is

$$\begin{aligned} I_s &= I_{B-1} - I_{A-1} \\ &= 2 \cdot (y_{s11} - y_{m11}) \cdot V_s \end{aligned}$$

or,

$$\frac{I_s}{V_s} = 2 \cdot (y_{s11} - y_{m11}) \quad (5.21)$$

Equation 5.21 is, in fact, an admittance which is twice as much the short-circuit admittance of a two-winding transformer in the positive sequence mode. The model's series impedance is then twice the impedance measured in the way described. The measured impedance contains both the leakage impedance and stray capacitances. The stray capacitances can be obtained from short-circuit measurements in the high frequency spectrum where they become the dominant factor. What remains after removing these capacitances

can be combined with part of the interwinding capacitance to become the frequency dependent series impedance of the model, as explained in chapter 4.

1.2.2 Three-Winding Transformer

The measurement technique explained in the previous section for the two-winding transformer can be applied to the three-winding transformer as well, but the measurements will involve two or three winding at a time. For example, if a transformer is connected in YYd (high-voltage, low-voltage and tertiary-windings are connected in wye, wye, and delta, respectively), the zero-sequence measurements can be performed on the wye-connected windings while the other two windings are either both shorted or only one of them is shorted. Two tests can be conducted to measure the short-circuit impedances between each of the two wye-connected windings with the delta winding shorted while the other wye-connected winding is left open. The third measurement will be taken on either of the wye-connected winding while the two other windings are shorted.

A positive-sequence measurement can be taken on the delta winding by first shorting one of the wye-connected windings. A second measurement may then be conducted with the previously open winding short-circuited and the previously short-circuited winding open. The third measurement should be taken on the delta winding while the other two wye-connected windings are short-circuited.

From these measurements, the leakage impedances for each individual winding or the sum of two of them can be computed as follows (assuming that the tertiary winding is connected in delta and the equivalent circuit is similar to that of fig. 2.9b):

1.2.2.1 Zero-Sequence Tests

There are a few possible combinations of ways to perform short-circuit tests for the three-winding transformer. The following combination involves two complete short-circuit tests and one partial short-circuit test:

(a) Perform a short-circuit test by shorting the high-voltage and low-voltage windings to ground. The impedance Z_A seen from the low-voltage side (after the terminal capacitances have been removed) is:

$$Z_A = \left(\frac{n_L}{n_H}\right)^2 \left(Z'_L + \frac{Z_H \cdot Z'_T}{Z_H + Z'_T} \right)$$

or,

$$\left(\frac{n_H}{n_L}\right)^2 Z_A = Z'_L + \frac{Z_H \cdot Z'_T}{Z_H + Z'_T} \quad (5.22)$$

(b) Perform short-circuit test with high-voltage winding open. The measured impedance Z_B on the low-voltage side (after removing the terminal capacitances) is

$$Z_B = \left(\frac{n_L}{n_H}\right)^2 (Z'_T + Z'_L)$$

or,

$$\left(\frac{n_H}{n_L}\right)^2 Z_B = Z'_T + Z'_L \quad (5.23)$$

(c) Perform a short-circuit test with both tertiary and low-voltage windings shorted. The measured impedance Z_C on the high-voltage side (after removing terminal capacitances) is

$$Z_C = Z_H + \frac{Z'_T \cdot Z'_L}{Z'_T + Z'_L} \quad (5.24)$$

All the symbols used in equations 5.22, 5.23 and 5.24 have the same meanings as those in equations 5.5, 5.6 and 5.7. Equations 5.22, 5.23 and 5.24 can be solved for Z'_T as follows:

(1) Multiply equation 5.22 and 5.24 by $(Z_H + Z'_T)$ and $(Z'_L + Z'_T)$ respectively,

$$Z'_T Z_H + Z'_T Z'_L + Z_H Z'_L = (Z_H + Z'_T) Z_A \cdot \left(\frac{n_H}{n_L}\right)^2$$

and

$$Z'_T Z_H + Z'_T Z'_L + Z_H Z'_L = (Z'_T + Z'_L) Z_C$$

which, together with equation 5.23, results in

$$(Z_H + Z'_T) Z_A \cdot \left(\frac{n_H}{n_L}\right)^2 = (Z'_T + Z'_L) Z_C = \left(\frac{n_H}{n_L}\right)^2 Z_B Z_C$$

or

$$Z_H + Z'_T = \frac{Z_B Z_C}{Z_A} \quad (5.25)$$

(2) Subtract equation 5.22 from equation 5.23,

$$\left(\frac{n_H}{n_L}\right)^2 (Z_B - Z_A) = Z'_T - \frac{Z_H Z'_T}{Z_H + Z'_T} = \frac{(Z'_T)^2}{Z_H + Z'_T} \quad (5.26)$$

(3) Solve equation 5.25 with equation 5.26,

$$Z'_T = \pm \left(\frac{n_H}{n_L}\right) \sqrt{\frac{Z_B Z_C (Z_B - Z_A)}{Z_A}} \quad (5.27)$$

Then, Z_H and Z'_L can be solved by substituting Z'_T into equations 5.23 and 5.25 which are,

$$Z'_L = \left(\frac{n_H}{n_L}\right)^2 Z_B - Z'_T \quad (5.28)$$

and,

$$Z_H = \frac{Z_B Z_C}{Z_A} - Z'_T \quad (5.29)$$

1.2.2.2 Positive-Sequence Tests

For the positive-sequence tests, all measurements are taken on the delta winding.

The tests may be carried out as follows:

(a) Perform a the short-circuit test with the low-voltage winding shorted. The measured impedance (after the terminal capacitances have been removed) is:

$$\begin{aligned} Z_a &= \left(\frac{n_T}{n_H}\right)^2 \left[\left(\frac{n_H}{n_T}\right)^2 Z_T + \left(\frac{n_H}{n_L}\right)^2 Z_L \right] = Z_T + \left(\frac{n_T}{n_L}\right)^2 Z_L \\ &= Z_T + Z'_L \end{aligned} \quad (5.30)$$

(b) Perform a short-circuit test with both high-voltage and low-voltage windings shorted. The measured impedance (after removing the terminal capacitances) is

$$\begin{aligned}
 Z_b &= \left(\frac{n_T}{n_H}\right)^2 \left[\left(\frac{n_H}{n_T}\right)^2 Z_T + \frac{Z_H \cdot \left(\frac{n_H}{n_L}\right)^2 Z_L}{Z_H + \left(\frac{n_H}{n_L}\right)^2 Z_L} \right] \\
 &= Z_T + \frac{Z_H \cdot \left(\frac{n_T}{n_L}\right)^2 Z_L}{Z_H + \left(\frac{n_H}{n_L}\right)^2 Z_L} \\
 &= Z_T + \frac{\left(\frac{n_T}{n_H}\right)^2 Z_H \cdot \left(\frac{n_T}{n_L}\right)^2 Z_L}{\left(\frac{n_T}{n_H}\right)^2 Z_H + \left(\frac{n_T}{n_L}\right)^2 Z_L} = Z_T + \frac{Z'_H \cdot Z'_L}{Z'_H + Z'_L} \quad (5.31)
 \end{aligned}$$

(c) Perform a short-circuit test with only the high-voltage windings shorted. The measured impedance (after removing the terminal capacitances) is

$$Z_c = \left(\frac{n_T}{n_H}\right)^2 \left[\left(\frac{n_H}{n_T}\right)^2 Z_T + Z_H \right] = Z_T + Z'_H \quad (5.32)$$

Equations 5.30, 5.31 and 5.32 can be solved simultaneously for Z_T . By subtracting equation 5.30 from equation 5.3, and equation 5.32 from equation 5.31, the following two equations are obtained:

$$Z_b - Z_a = \frac{-(Z'_L)^2}{Z'_H + Z'_L} \quad (5.33)$$

and

$$Z_b - Z_c = \frac{-(Z'_H)^2}{Z'_H + Z'_L} \quad (5.34)$$

Multiplying equation 5.33 with equation 5.34 one obtains:

$$(Z_b - Z_a)(Z_b - Z_c) = \left[\frac{Z'_H Z'_L}{Z'_H + Z'_L} \right]^2 \quad (5.35)$$

From equation 5.31, it follows that

$$\left[\frac{Z'_H Z'_L}{Z'_H + Z'_L} \right]^2 = (Z_b - Z_T)^2 \quad (5.36)$$

or

$$(Z_b - Z_T) = \pm \sqrt{(Z_b - Z_a)(Z_b - Z_c)} \quad (5.37)$$

which gives

$$Z_T = Z_b \pm \sqrt{(Z_b - Z_a)(Z_b - Z_c)} \quad (5.38)$$

The leakage impedances for both zero and positive-sequences for the three-winding transformer are next converted into delta, as shown in fig 2.9c. The interwinding

capacitances are then added (fig. 2.10a) so that in the network synthesis procedure they form part of the RLC equivalent networks.

2. Measurement of Stray Capacitances

Some of the stray capacitances of the model can be directly measured but some of them must be calculated from the short-circuit test data. The method on how these stray capacitances are obtained is described next.

2.1 Direct Measurement

Stray capacitances which can be directly measured with a capacitance measuring device are the capacitance-to-ground and the interwinding capacitances. The device used at the high voltage lab of EGAT is the "Capacitance and D.F Bridge", model CB100. The device has three connection leads marked C_L , C_H and G which should be connected to the high-voltage, low-voltage windings of the transformer and ground respectively to ensure correct measurements. When the device is adjusted until a balanced condition is achieved, the values of capacitances can be read off the meter dial. Fig. 5.2 depicts a connection of the device to the transformer under test for a standard measurement of capacitances between the high-voltage and low voltage windings (C_{HL}) and capacitances between the high-voltage winding and ground (C_{HG}) of a two-winding, three-phase transformer. In the measurements, all six terminals of the high voltage winding are connected together (terminal H in fig. 5.2) and so are all terminals of the low-voltage winding (terminal L in

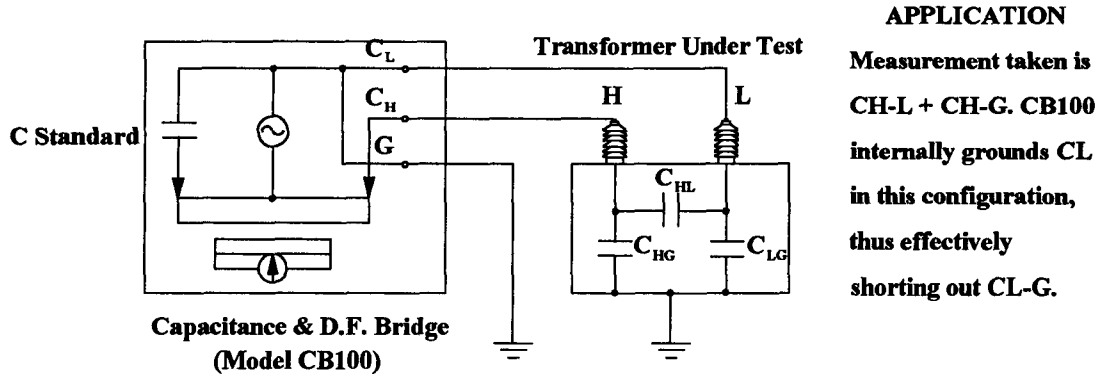


Fig. 5.2 Application of the Capacitance & D.F. Bridge to measure stray capacitances in a transformer. The configuration shown is for the measurement of C_{HL} plus C_{HG} .

fig. 5.2). Two more standard measurements are required to get C_{HL} and C_{HG} . From these measurements, the capacitances to ground and the interwinding capacitances of the transformer can be found. For a three winding transformer, the interwinding and winding-to-ground capacitances present in the transformer are as shown in fig 2.3, chapter 2. In this case, the measuring device CB100 is connected to a pair of the windings at a time while the third winding is grounded. An illustrative arrangement for measuring stray capacitances associated with the high-voltage and low-voltage windings of a three-winding transformer is shown in fig. 5.3.

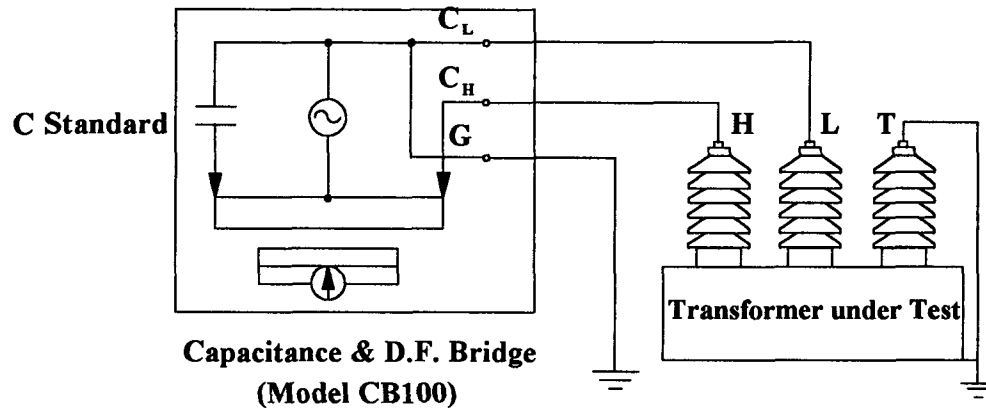


Fig. 5.3 Measurement of the sum of interwinding and winding-to-ground capacitances in a three-winding, three-phase transformer with CB100.

2.2 Stray Capacitances Calculated from Short-Circuit Tests

Stray capacitances for the model which are not available from direct measurements can be calculated from the short-circuit frequency responses. At the high end of the frequency range, the behavior of the short-circuit impedance becomes close to that of a capacitance. In this frequency range, all the inductive elements have very high impedances and can be considered open-circuited. The stray capacitances that can be obtained from the short-circuit tests data are the turn-to-turn and the phase-to-phase capacitances. The turn-to-turn capacitance are always present in the short-circuit tests but the phase-to-phase capacitance will be present only when the measurements are taken from the outermost winding on each transformer limb.

2.2.1 Turn-To-Turn Capacitances

In the proposed transformer model, the turn-to-turn capacitance is lumped as a single element and is connected across the two terminals of each transformer coil. Firstly, suppose that the winding where the short-circuit test is conducted is not the outermost winding so that the phase-to-phase capacitance is not present (the case in which the measurement is made on the outermost winding will be addressed next in the *Phase-to-Phase Capacitance* section).

In practice, the zero-sequence measurement is taken on the wye-connected winding because it is not possible to conduct the test on the delta winding with a single power source. In making the measurement, all three terminals of the wye are joined together. As a result, the measured turn-to-turn capacitance is three times that of a single coil. At the high end of the frequency response, a value of capacitance can be calculated from the magnitude of the impedance. By subtracting the known values of winding-to-ground capacitances and interwinding capacitances, which were previously obtained from the direct measurements, the value of the turn-to-turn capacitance of the winding under test can be determined.

The turn-to-turn capacitance of a delta winding, on the other hand, can be obtained from a positive-sequence test conducted on the delta winding, as explained earlier. The turn-to-turn capacitance obtained in the measurement is two times that of a single winding because two coils are connected in parallel while the third coil is shorted. With

simple subtraction, as in the case of the wye winding, the turn-to-turn capacitance for the model can be determined.

For a three winding transformer, the measurements should be taken while the other two windings are simultaneously short-circuited. This simplifies the calculation of the turn-to-turn capacitance because all apacitances in the model that are not shorted become connected in parallel.

2.2.2 Phase-To-Phase Capacitance

The phase-to-phase capacitance which exists between the outermost windings of the transformer legs are schematically shown in fig. 2.5. Figure 2.5a shows the case in which the windings are not connected, fig. 2.5b corresponds to the case in which the windings are connected in delta, and fig. 2.5c corresponds to the case in which the windings are connected in wye. Phase-to-phase capacitances of full value are present across each coil in the delta configuration, while only halves are effectively present between the wye terminals. In the positive-sequence tests (which are conducted on the delta windings), the phase-to-phase capacitances are combined with the turn-to-turn capacitances. For the delta connection, the phase-to-phase capacitance has to be modeled together with the turn-to-turn capacitance with both connected across the winding terminals, as shown in fig. 2.5b, because there is not enough information from the tests to separate them. For the wye connection, on the contrary, the phase-to-phase capacitance will not be present in the zero-sequence test even though the winding is the outermost one. This has the

advantage that it makes it possible to isolate the turn-to-turn capacitances from the test results. With reference to fig. 2.5g, if a short-circuit test is carried out with all the other coils short-circuited, the phase-to-phase capacitance will be the only unknown capacitance present in the test. The phase-to-phase capacitance can then be isolated and modeled as in fig. 2.5a.

Chapter Six

NUMERICAL EXAMPLES

The proposed method to calculate all the parameters required for the proposed frequency dependent transformer model was presented in chapter 5. This chapter is aimed at putting the method into practice. It covers some examples on how the model parameters are realised from the information gathered from the various short-circuit tests. The frequency responses calculated from the model are compared to those obtained from the tests. In addition, time-domain simulations with the model using the estimated parameters are verified by comparison with the results recorded in the laboratory. Examples are given for both two- and three-winding transformers.

1. Two-Winding Transformer

The numerical data for a two-winding transformer is based on measurements taken on a power transformer rated 30/40/50 MVA. The transformer is a two-winding transformer with the high-voltage winding connected in delta and the low-voltage winding connected in wye. The voltage rating is 115 Δ /23Y kV. The transformer was manufactured by Asia Brown Boveri (ABB).

1.1 Capacitances

The capacitances which can be directly measured with the Capacitance & D. F. Bridge for the tested transformer are listed in table 6.1.

Table 6.1--Measured values of capacitances for the tested transformer

Type of capacitance	Capacitance for 3 phases (pF)
Winding-to-ground	
-High-voltage (C_{HG})	3,418
-Low-voltage (C_{LG})	12,395
Winding-to-winding	
-High-voltage to low-voltage (C_{HL})	6,441

To reassure that stray capacitances can be assumed to be constant within a specific range of frequencies, a frequency response test was carried out by shorting all the high-voltage terminals (delta) to ground and connecting the three terminals of the low-voltage terminals (wye) to the wye neutral. The measurement was taken between the low-voltage terminals and ground from which the sum of C_{HL} and C_{LG} was obtained. The result of this test is shown in fig. 6.1 together with the equation $Z = 8.10 \times 10^6 f^{-0.994}$ which resulted from fitting the straight line portion of the capacitance curve to a function $Z = af^b$. As expected, the power of the frequency (f) is close to -1.0 because the

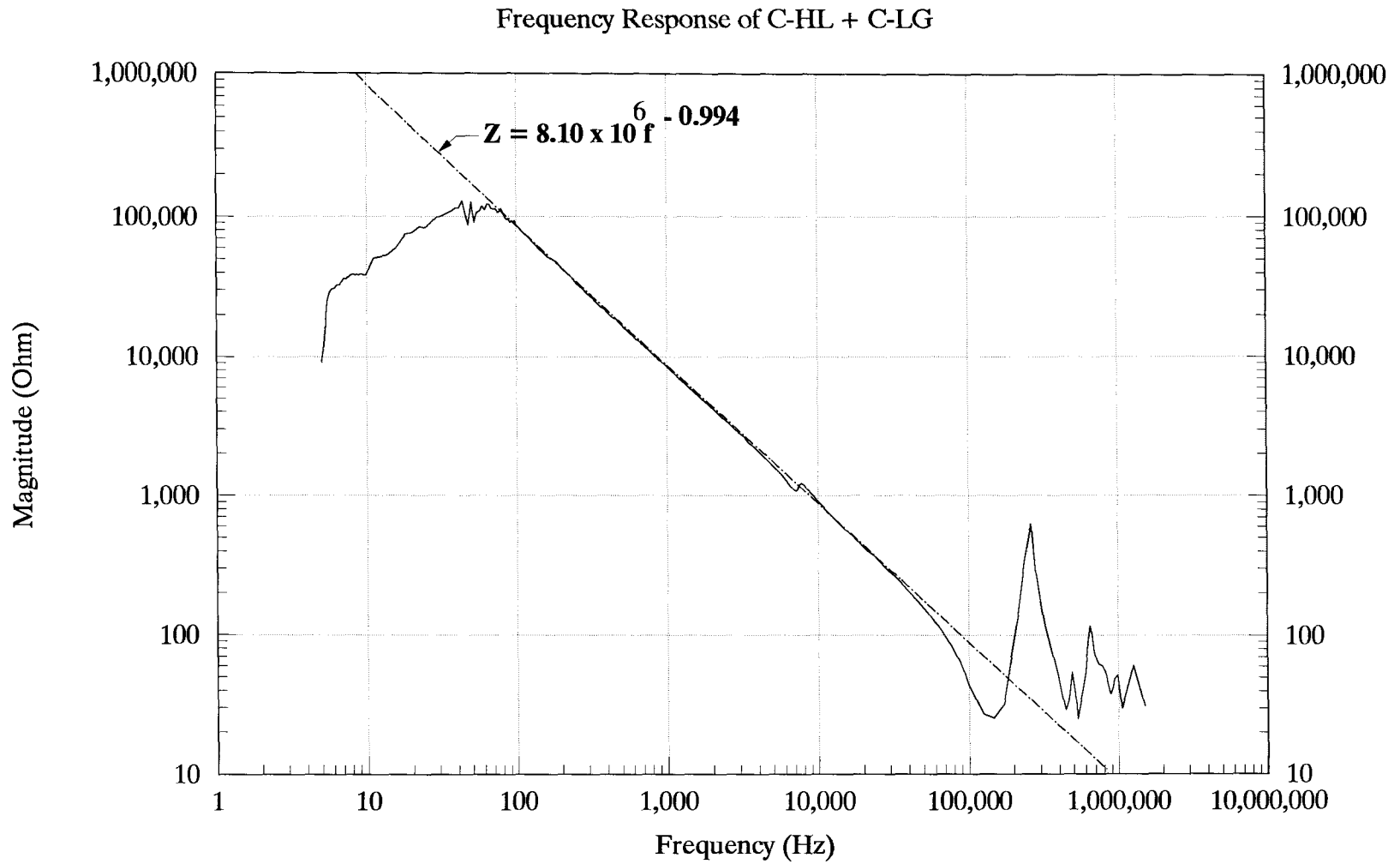


Fig. 6.1 Transformer capacitance impedance measured with the impedance analyser

magnitude of the impedance of a capacitance is inversely proportional to the frequency. The coefficient of f gives an estimate of $(2\pi C)^{-1}$ and C is found to be $19.644e-09$ farad. The sum of C_{HL} and C_{LG} taken from table 6.1 is $18.836e-09$ farad which is relatively close to C . Therefore, the values of the stray capacitances taken from the two different measurements agree with each other.

Other capacitances which must be calculated from the short-circuit frequency responses will be given later.

1.1.1 Capacitances Determined from Zero-Sequence Test

A zero-sequence short-circuit test was carried out with the circuit configuration shown in fig. 6.2a. Only one test is sufficient to get the zero-sequence data of a two-winding transformer. The test result was fitted with the network of fig. 3.3. The graphs in fig. 6.4 show the measured and fitted responses. The circuit parameters for the equivalent network are given in table 6.2. Numbers in table 6.2, and in other similar tables, are shown to five significance digits since sufficient accuracy in these values is needed for the correct placement of poles and zeroes of the fitting function. For the tested transformer, the capacitances which are present in the zero-sequence test are the turn-to-turn capacitance of the low-voltage winding, the interwinding capacitance, and the capacitance of the low-voltage winding to ground. The purpose of fitting the test results is to find out how much capacitance is included in the measured impedance. The measured short-circuit impedance was fitted up to the frequency at which the data are believed to

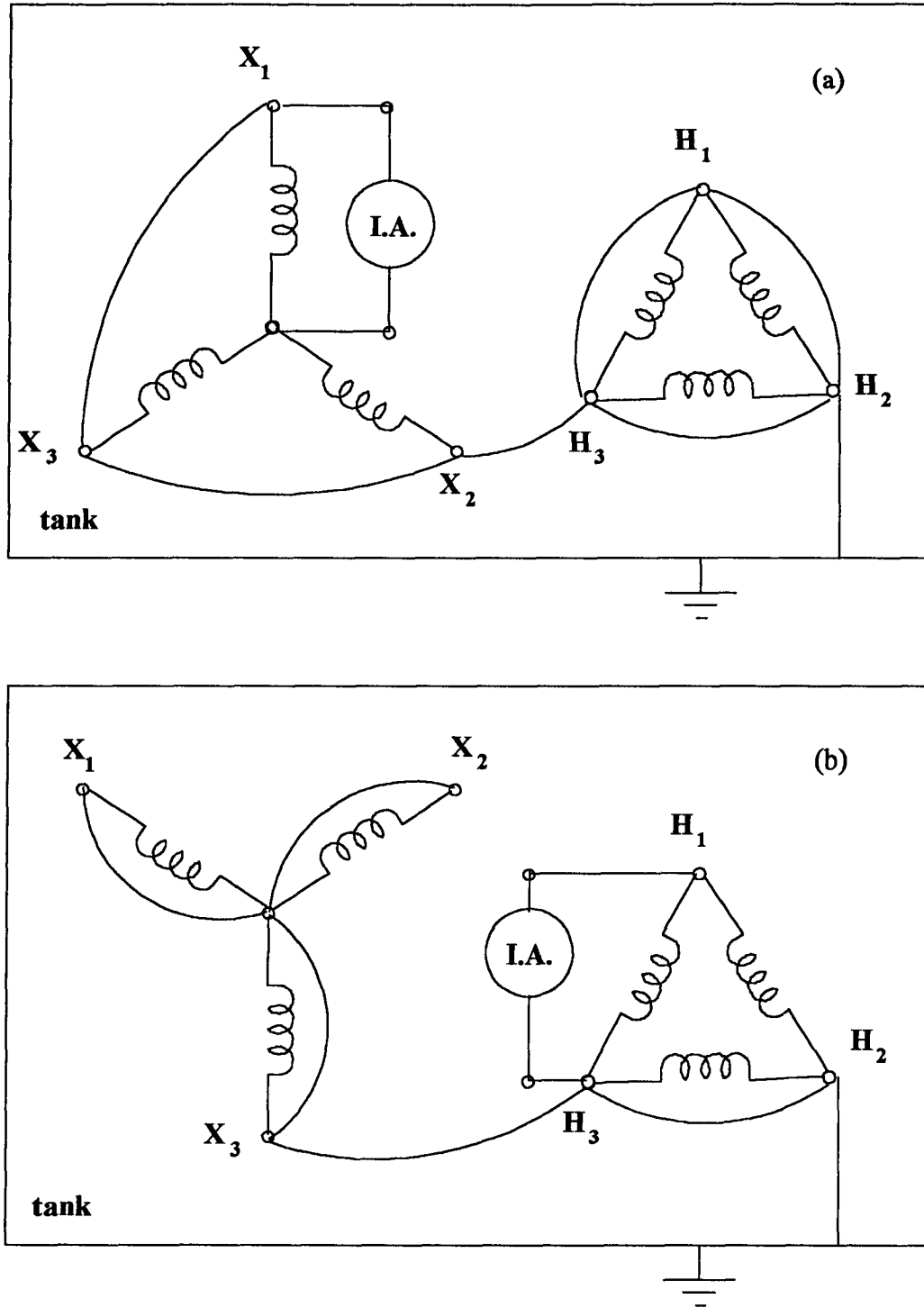


Fig. 6.2 Schematic of short-circuit frequency response tests: (a) Zero-sequence test; (b) Positive-sequence test.

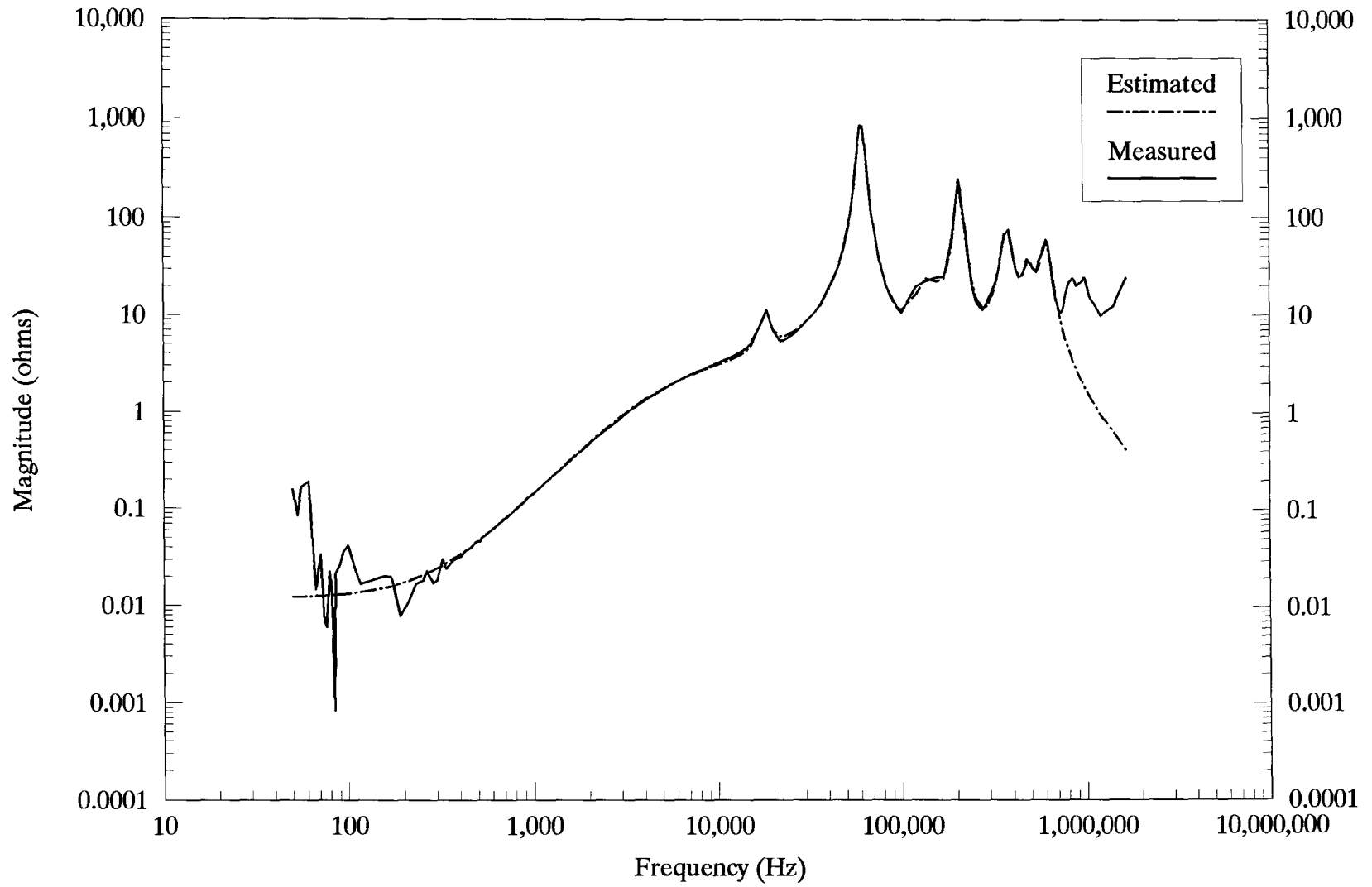


Fig. 6.3 Real part of short-circuit impedance (zero-sequence) for the two-winding transformer.

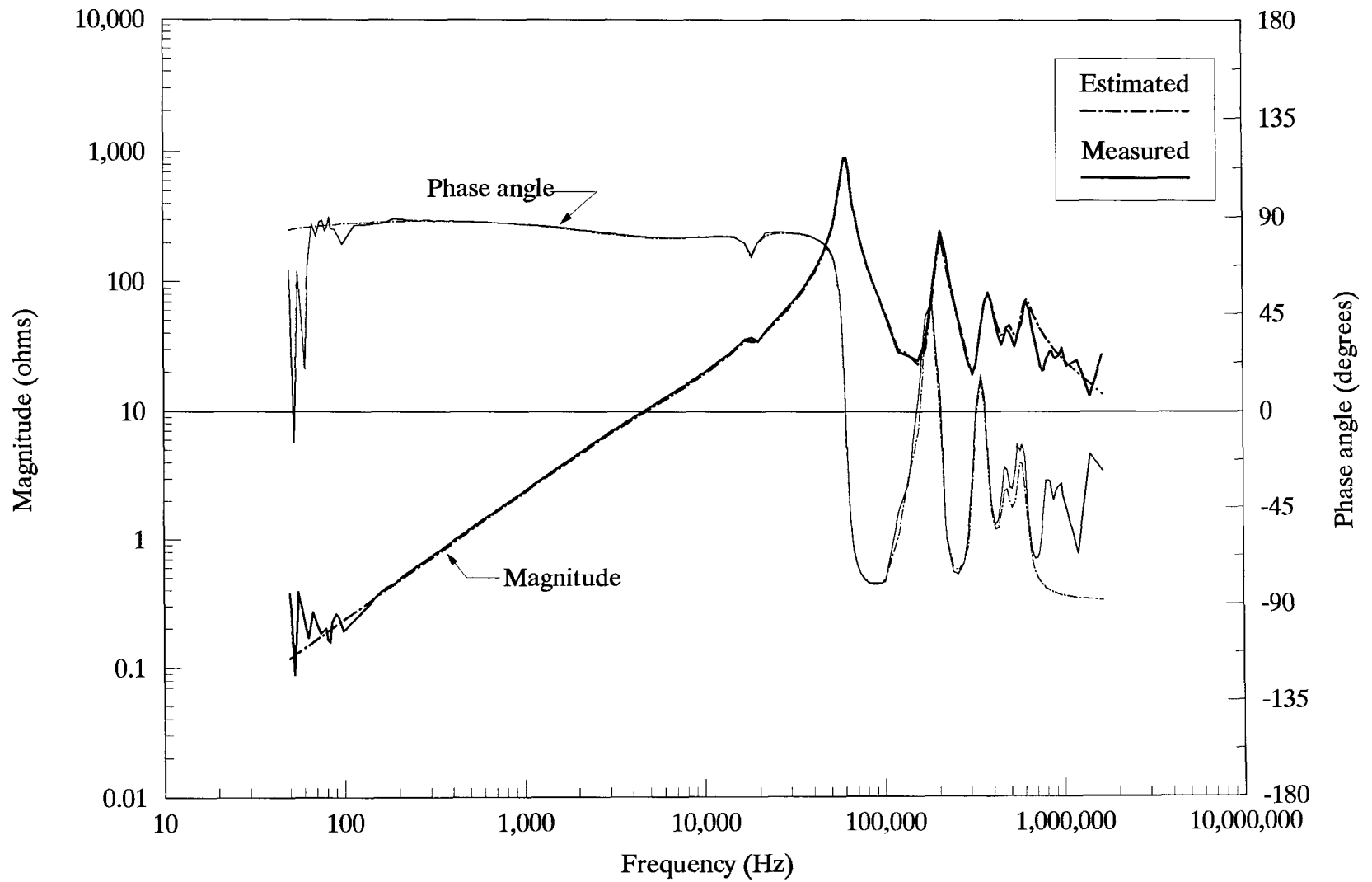


Fig. 6.4 Short-circuit impedance (zero-sequence) for the two-winding transformer.

Table 6.2-- Parameters of the zero-sequence short-circuit equivalent network for the tested two-winding transformer

Peak No.	Capacitance (farad)	RL parallel block	
		Resistance (ohms)	Inductance (henry)
1	2.96201e-08	4.69634e-05	-
		1.02500e+04	6.52899e-05
		2.21436e-01	6.46047e-06
		1.66978e+00	6.36733e-05
		1.61492e+00	3.80926e-05
		7.79935e+02	1.63820e-04
2	9.54346e-06	1.18106e-02	-
		7.54854e+00	7.97444e-06
3	1.59905e-07	2.10021e-07	-
		1.94427e+01	8.13311e-06
4	3.64525e-08	2.00860e-05	-
		2.22654e+02	1.65258e-05
5	3.90087e-08	9.79614e-05	-
		7.46147e+01	4.72049e-06
6	7.71330e-08	3.86791e-05	-
		2.47888e+01	1.38830e-06
7	3.52545e-08	4.31114e-05	-
		5.09657e+01	1.97948e-06
High-frequency equivalent capacitance = 7.43398e-09 farad			

be reliable, which is about 1 MHz. This capacitance is subtracted from the short-circuit impedance to obtain the leakage impedance of the transformer. This impedance is later combined with part of the interwinding capacitance ($\frac{1}{2n} C_{HL}$) to form the frequency dependent series branch of the transformer model ($Z_{winding}$). The combined impedance is then fitted once more to obtain the RLC network of fig. 3.3.

From the previous procedure, the turn-to-turn capacitance of the low-voltage winding can be calculated as follows:

Total capacitance from table 6.2	=	7.434e-09	farad
$\frac{1}{2} C_{H-L}$	=	3.220e-09	farad
$\frac{1}{3} C_{L-G}$	=	4.132e-09	farad
Turn-to-turn capacitance	=	0.082e-09	farad

The factor 1/3 is used instead of 1/2 for C_{L-G} is because the low-voltage winding was grounded while the measurement was carried out. When the winding is grounded, the effective winding-to-ground capacitance of the winding is reduced to 1/3, as suggested by Allan Greenwood [9].

1.1.2 Capacitance Determined from Positive-Sequence Tests

Three tests were conducted to determine the positive-sequence short-circuit impedance of the transformer. Each test is performed with one of the coils of the delta winding shorted, as shown in fig. 2b. Results of the tests are shown in fig. 6.5 in which all the three tests are superimposed. It can be seen in fig. 6.5 that there is no significant difference between results of the three tests. The average of the three tests is used as input data

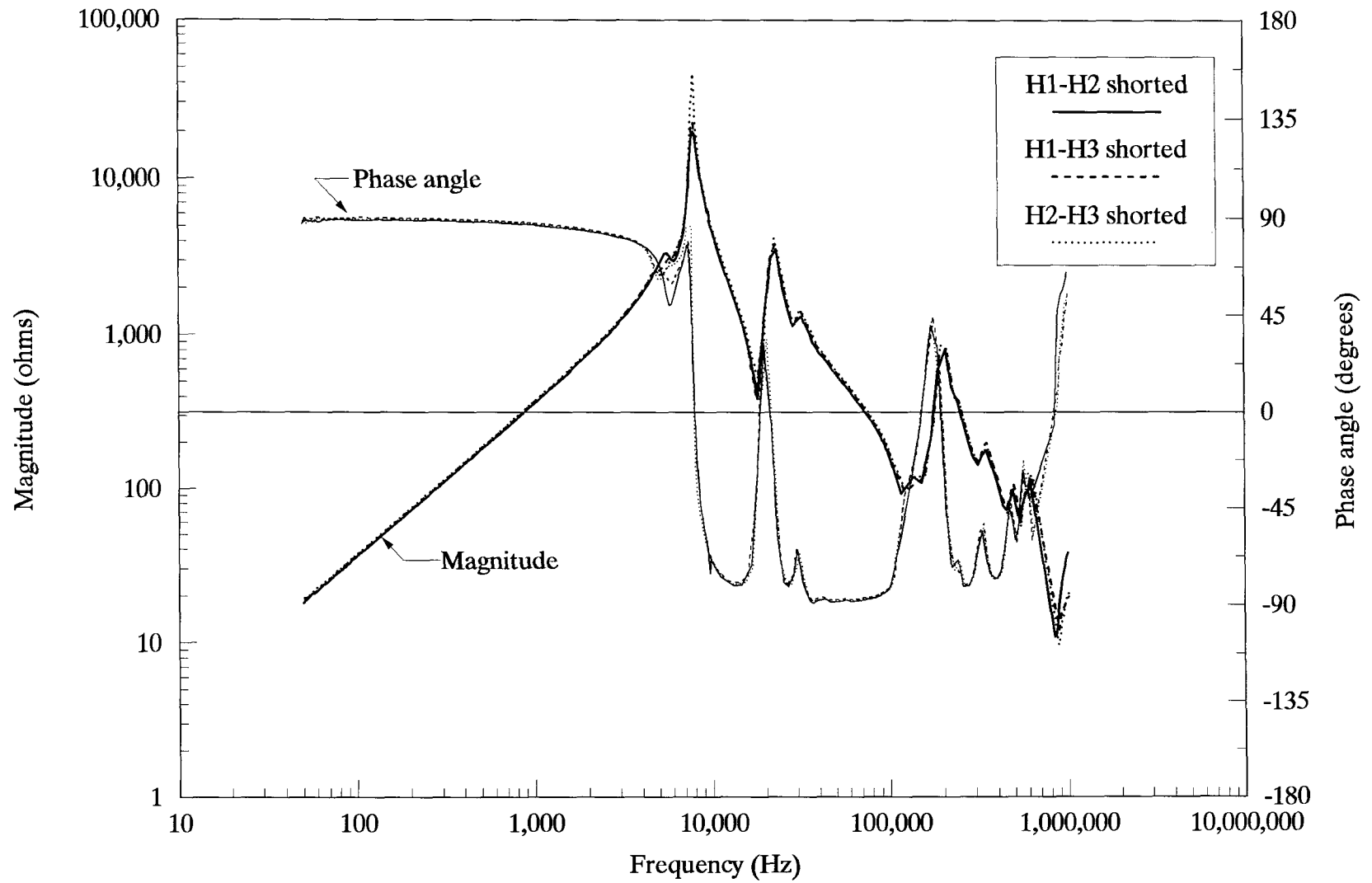


Fig. 6.5 Short-circuit impedances (positive-sequence) of the two-winding transformer measured on different windings.

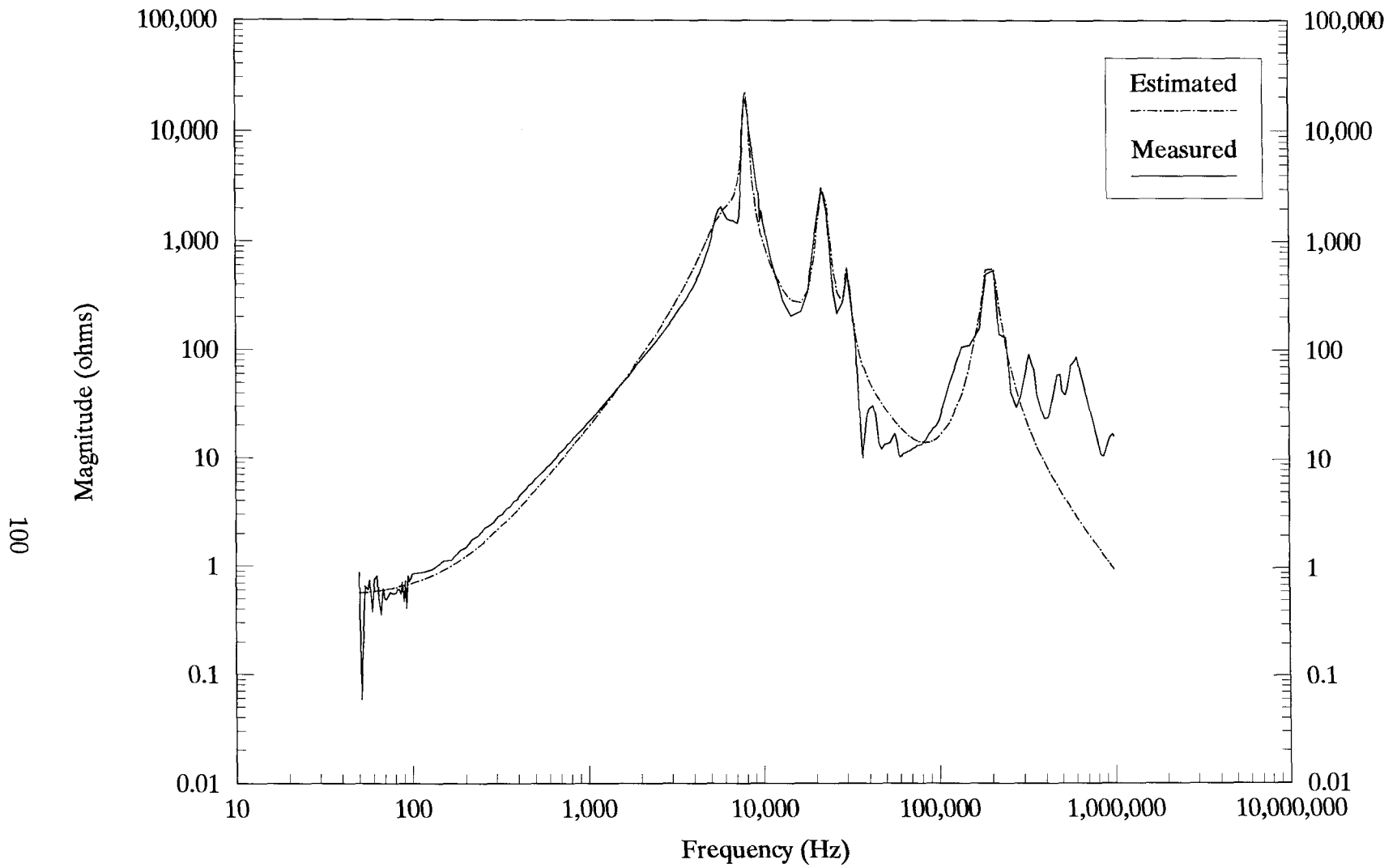


Fig. 6.6 Real part of the short-circuit impedance (positive-sequence) for the two-winding transformer.

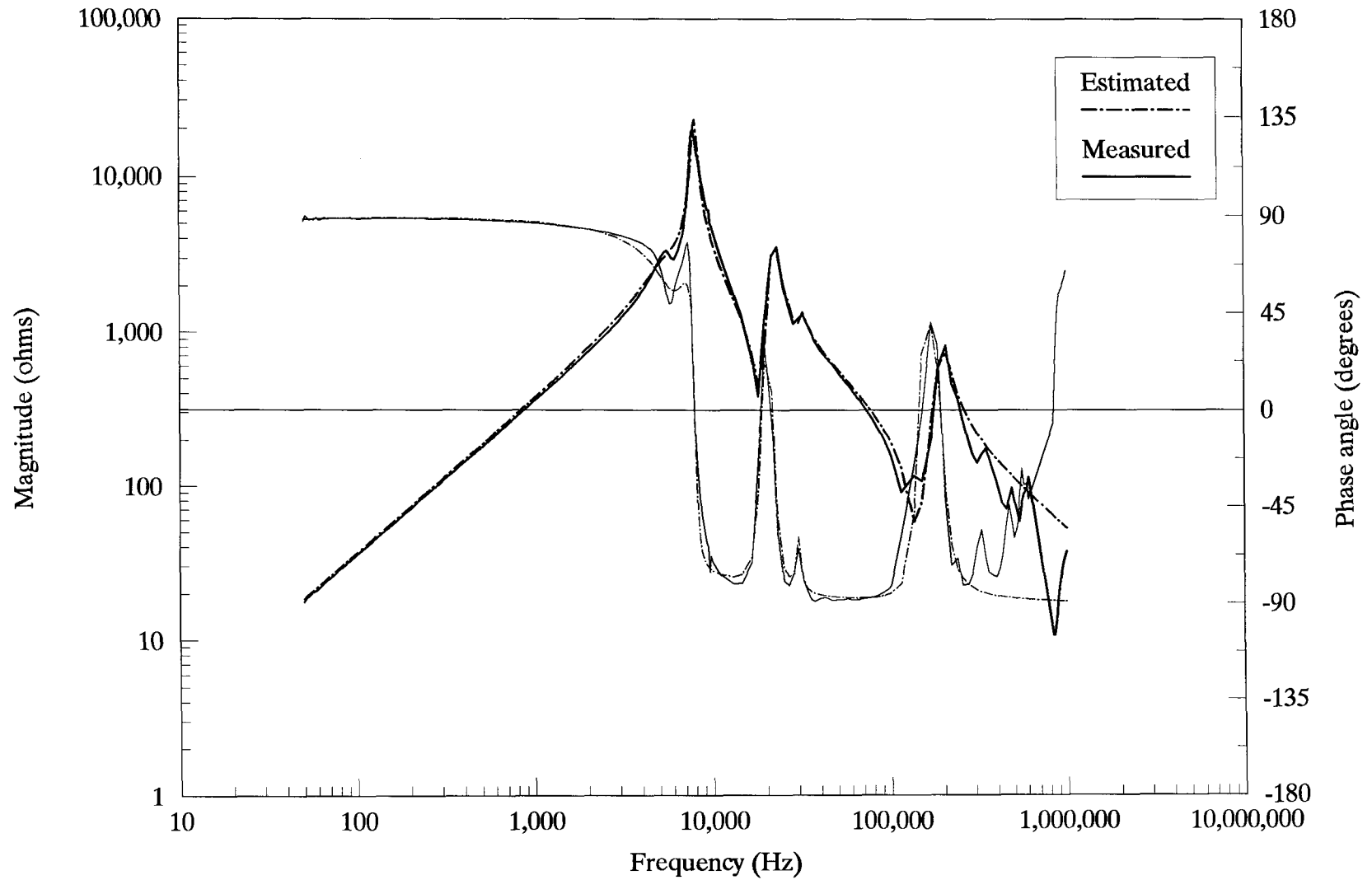


Fig. 6.7 Transformer short-circuit impedance (positive-sequence) for the two-winding transformer.

Table 6.3--Parameters of the positive-sequence short-circuit equivalent network for the tested two-winding transformer

Peak No.	Capacitance (farad)	RL parallel block	
		Resistance (ohms)	Inductance (henry)
1	2.34919e-08	5.21162e-01	-
		1.74892e+03	2.70085e-02
2	1.36025e-08	0.0	-
		2.17093e+04	2.94064e-02
3	1.91069e-08	0.0	-
		3.63068e+03	2.73908e-03
4	6.27161e-09	0.0	-
		7.71918e+02	1.06217e-04
5	1.48156e-07	0.0	-
		5.72532e+02	1.83790e-04
6	1.27424e-07	0.0	-
		7.35160e+01	1.17626e-05
High frequency equivalent capacitance = 2.91999e-09 farad			

to find the circuit parameters. The same process implemented for the zero-sequence test described earlier is applied to the positive-sequence test to obtain the capacitances to be subtracted from the short-circuit branch. In this case these capacitances are the phase-to-phase capacitances and the turn-to-turn capacitance of the high-voltage winding. The

result of the RLC synthesis procedure are shown in fig. 6.6 and fig. 6.7, while the circuit parameters are listed in table 6.3. Since, for the positive-sequence test, only two phases are involved, the capacitance values shown in table 6.1 must be multiplied by a factor of two thirds. The calculation of the unknown capacitances is as follows:

Total capacitance from table 6.3	=	2.920e-09	farad
$\frac{1}{2} \left(\frac{2}{3} C_{H-L} \right)$	=	2.147e-09	farad
$\frac{1}{3} \left(\frac{2}{3} C_{H-G} \right)$	=	0.760e-09	farad
Turn-to-turn plus phase-to-phase capacitances	=	0.013e-09	farad
	=	0.020e-09 (3 phases)	

1.2 The Series Branch Impedance ($Z_{winding}$)

Each short-circuit impedance is composed of two components of the transformer model, i.e., the leakage impedance and the short-circuit capacitance. The short-circuit capacitance can be obtained from the test result with the procedure described earlier in sections 1.1.1 and 1.1.2. The short-circuit capacitance will be subtracted from the measured impedance to obtain the leakage impedance. The leakage impedance is combined with part of the interwinding capacitance which is transferred to the side of the leakage impedance to become the series branch impedance used in the model.

For the zero-sequence, this capacitance is

$$\frac{115}{23} \times 0.5 \times \frac{6.441 \times 10^{-9}}{3} = 5.367 \times 10^{-9} \text{ farad/phase.}$$

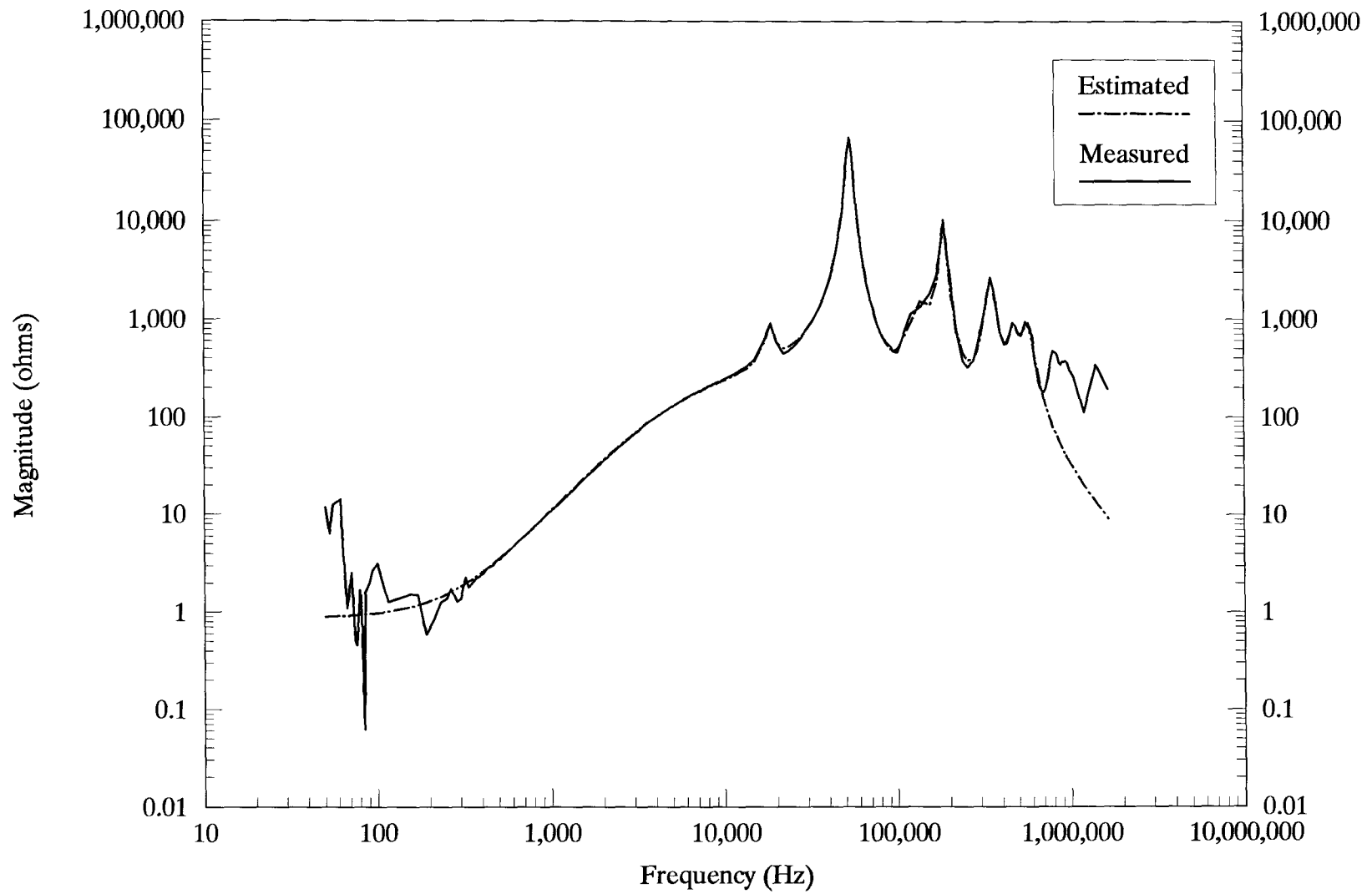


Fig. 6.8 Fitting of the real part of the $Z_{winding}$ impedance for the zero-sequence circuit of the two-winding transformer.

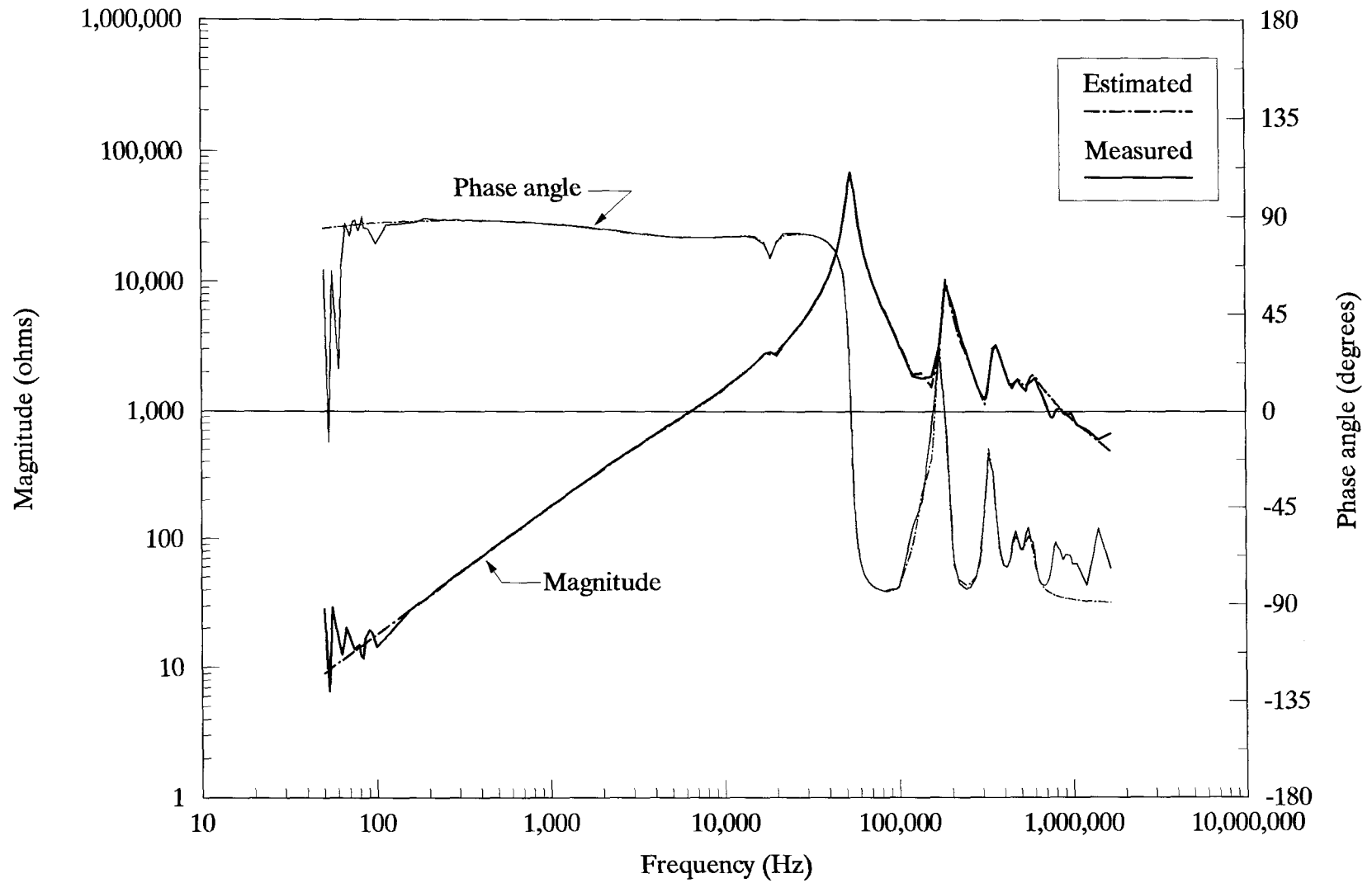


Fig. 6.9 Fitting of the magnitude and phase angle of the frequency dependent Z_{winding} impedance for the zero-sequence circuit of the two-winding transformer.

Table 6.4--Parameters of the zero-sequence $Z_{winding}$ impedance for the tested two-winding transformer (per phase values referred to high-voltage side)

Peak No.	Capacitance (farad)	RL parallel block	
		Resistance (ohms)	Inductance (henry)
1	4.76059e-10	9.02003e-03	-
		2.81494e+04	8.64570e-03
		3.44792e+01	1.91425e-03
		2.36751e+02	6.28649e-03
		5.59907e+05	1.00467e-02
2	1.27529e-07	7.78905e-01	-
		6.12763e+02	5.96037e-04
3	2.92333e-09	7.50465e-02	-
		1.30156e+03	4.54154e-04
4	1.00064e-09	1.04837e-03	-
		1.00262e+04	7.35136e-04
5	1.34472e-09	1.50116e-04	-
		2.56361e+03	1.57439e-04
6	3.60143e-09	7.55318e-04	-
		6.08895e+02	3.18966e-05
7	9.50437e-09	2.80912e-03	-
		2.57767e+02	8.18850e-06
8	2.67993e-09	3.21350e-03	-
		5.25896e+02	2.98555e-05
High-frequency equivalent capacitance = 2.02039e-10 farad			

And for the positive-sequence, the capacitance is

$$\frac{23}{115} \times 0.5 \times \frac{6.441 \times 10^{-9}}{3} = 0.215 \times 10^{-9} \text{ farad/phase.}$$

After the calculated amount of capacitances have been added to the leakage impedances, they are fitted with the synthesis RLC network. Figures 6.8 and 6.9 show the fitting results for the zero-sequence winding impedance. It is seen from these results that the calculated winding impedance of the tested transformer can be matched very well to 1MHz. The circuit parameters that resulted from the fitting are given in table 6.4. Five sections are used to simulate the response for the first peak and a total of eight peaks are matched all together. The parameters given in table 6.4 were converted to per phase values and transferred to the high-voltage side so that they can be used in the transients program directly.

The positive-sequence winding impedance is treated the same way as the zero-sequence winding impedance. The fitting results for the real part are shown in fig. 6.10. Five sections were used to fit the five dominant peaks of the real part and two RL parallel blocks were used to refine the fitting for the principal peak which occurred in the vicinity of 10 kHz. The calculated results for the magnitude and phase angle of the positive-sequence Z_{winding} are plotted in fig. 6.11. The fitted and measured results agree very well from 50 Hz to about 0.5 MHz. Even though the fitting results over 0.5 MHz are not as good as in the case of the zero-sequence impedance, the overall outcome can be considered sufficiently good. The circuit parameters for the network producing the response

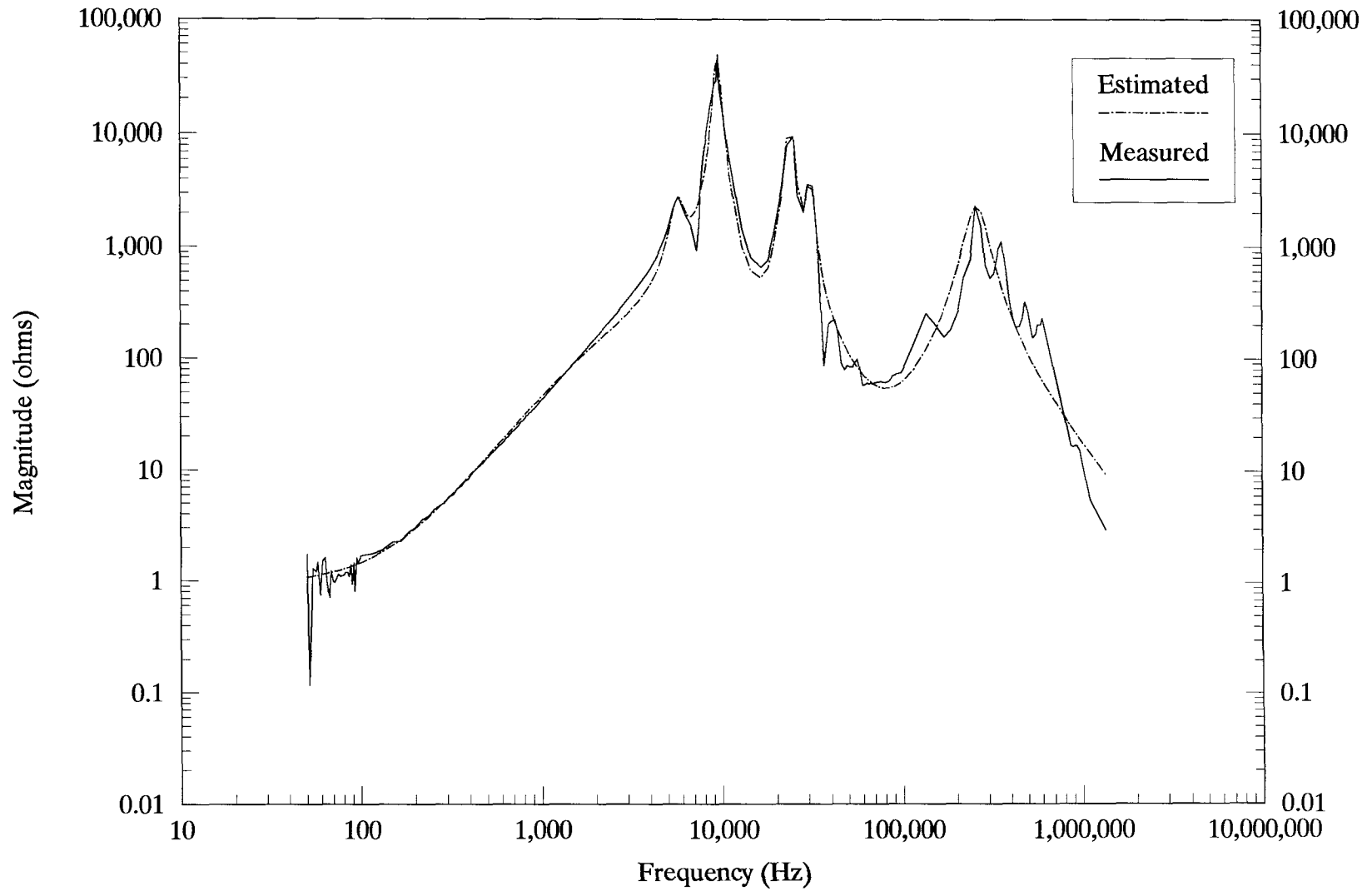


Fig. 6.10 Fitting of the real part of the Z_{winding} impedance for the positive sequence circuit of the two winding transformer.

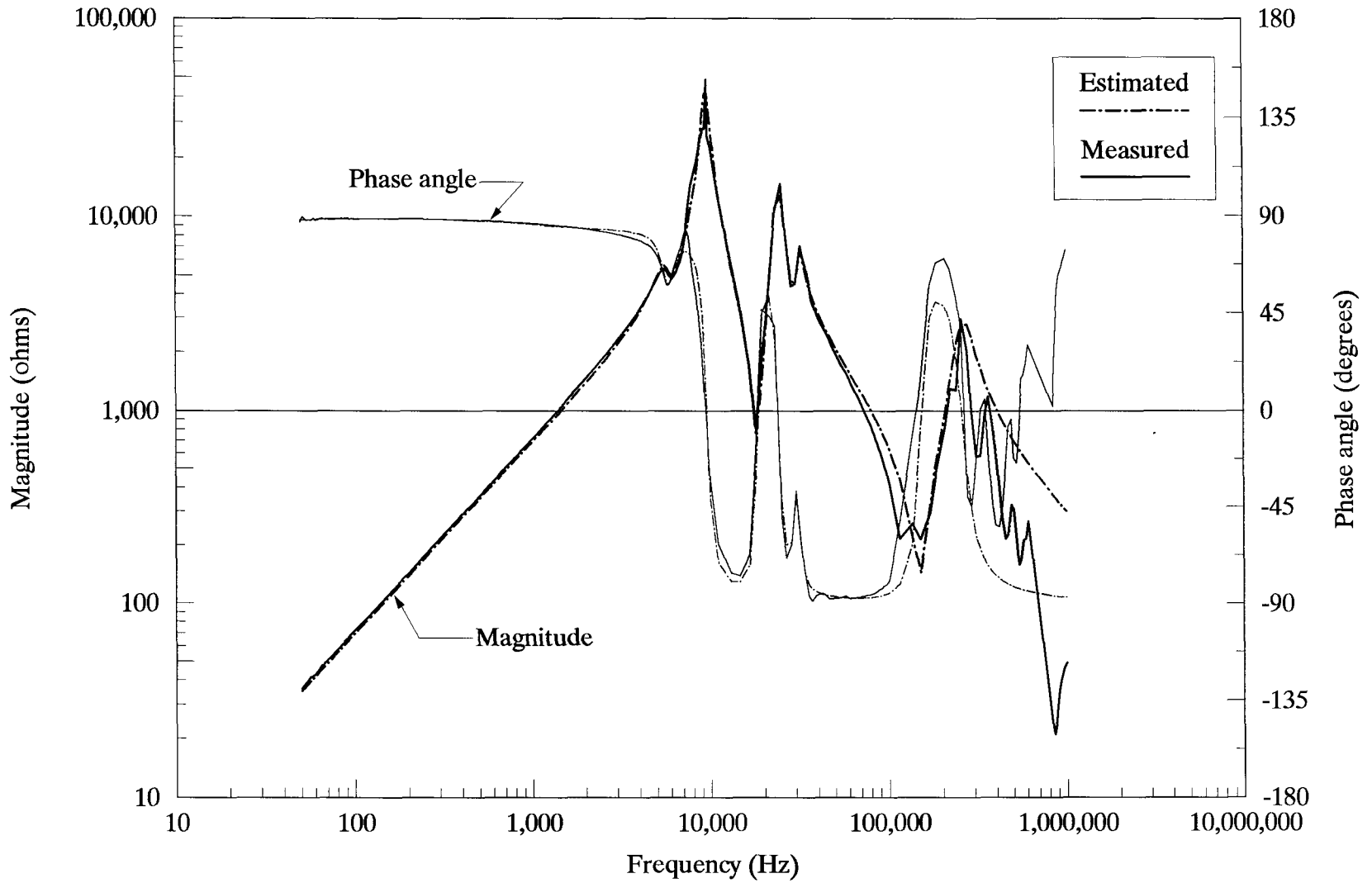


Fig. 6.11 Fitting of the magnitude and phase angle of the frequency dependent Z_{winding} impedance for the positive-sequence circuit of the two-winding transformer.

Table 6.5--Parameters of the positive-sequence $Z_{winding}$ impedance for the tested two-winding transformer (per phase values referred to high-voltage side)

Peak No.	Capacitance (farad)	RL parallel block	
		Resistance (ohms)	Inductance (henry)
1	3.83689e-09	9.66480e-01	-
		2.14788e+02	1.58297e-02
		7.79506e+04	7.16340e-02
2	6.63480e-08	0.0	-
		2.08566e+03	1.15472e-02
3	4.24785e-09	0.0	-
		1.50852e+04	1.03526e-02
4	1.38289e-08	0.0	-
		4.09054e+03	1.90603e-03
5	8.29235e-10	0.0	-
		1.01916e+03	4.51872e-04
High-frequency equivalent capacitance = 5.58860e-10 farad			

shown in fig. 6.11 are given in table 6.5. The numbers in the table are the per phase values which are ready to be used in the transformer model software.

1.3 Time-Domain Simulation

An impulse response test was also performed on the 50 MVA, 115/23 kV transformer from which the two-winding model data are derived. A standard 1.2/50 μ s voltage

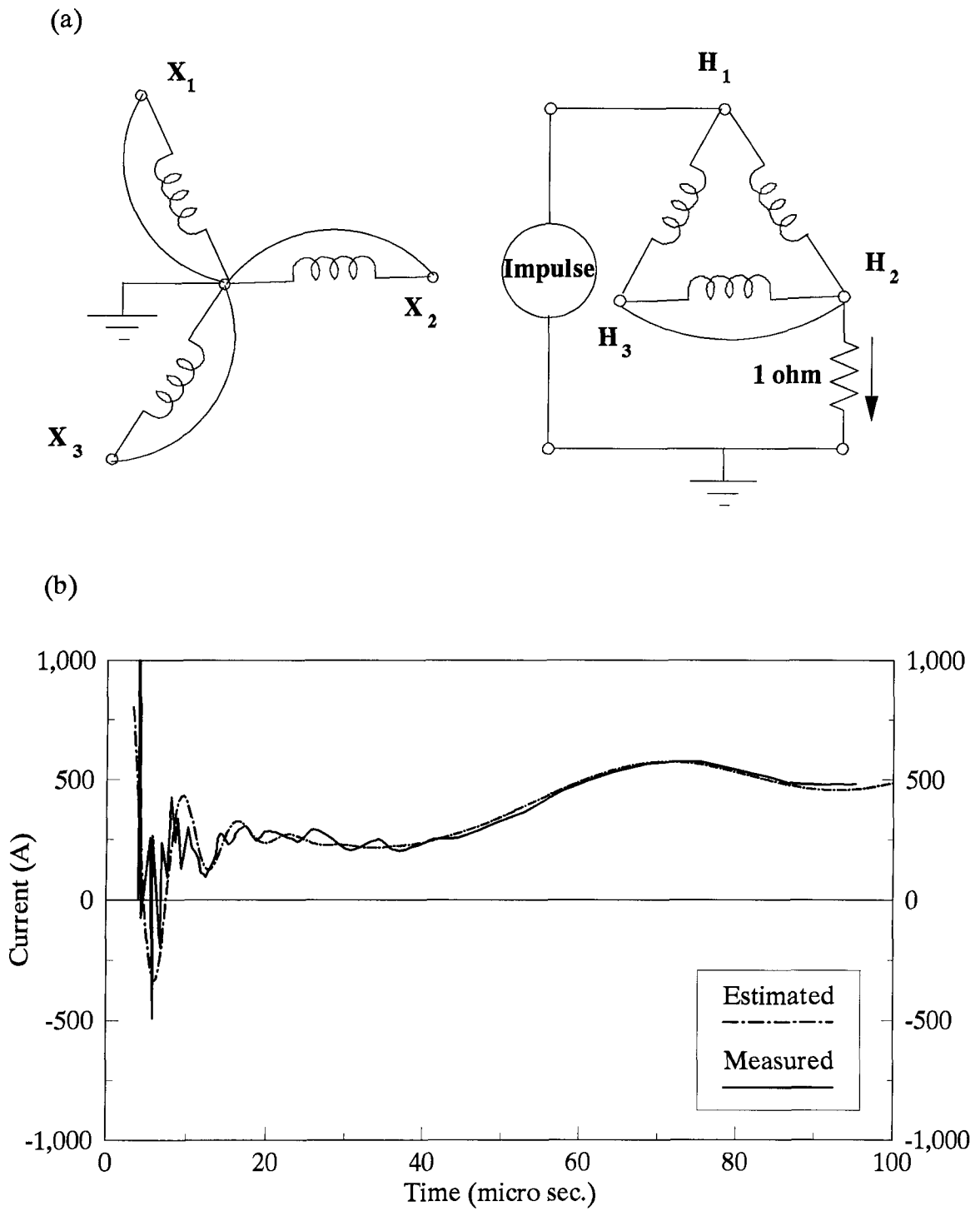


Fig. 6.12 Impulse response test. (a) Circuit diagram; (b) Simulation result.

impulse with a magnitude of 550 kV was applied to the delta winding while the wye winding was shorted. The schematic of the impulse test is shown in fig. 6.12a. The current in the 1 Ω -resistor was recorded. Figure 6.12b shows the measured current response of the tested transformer against the model response using the parameters given in tables 6.4 and 6.5. The agreement between measured and computed results is reasonably good.

2. Three-Winding Transformer

The three-winding transformer which was available for short-circuit tests was rated 25 MVA and 115/22/11 kV. The tertiary winding was connected in delta and the high and low-voltage windings were connected in wye. The transformer was manufactured by "Volta-Werke". The high-voltage winding is the outermost winding and the tertiary winding is located next to the core. Zero and positive-sequence tests were conducted on this transformer as explained in chapter 5.

2.1 Stray Capacitances

Similar to the two-winding transformer case, the stray capacitances that can be directly measured with the capacitance meter are the winding-to-winding capacitances and the capacitances from windings to ground. The terminals of the windings belonging to the same phase are connected together, therefore, the capacitance values obtained are the sum of the three phases. The measured capacitances are as shown in table 6.6 below.

Table 6.6--Measured values of capacitances for the three-winding transformer

Type of capacitance	Capacitance for 3 phases (pF)
Winding-to-ground	
-High-voltage (C_{HG})	531.5
-Low-voltage (C_{LG})	394.4
-Tertiary-voltage (C_{TG})	3.7
Winding-to-winding	
-High-voltage to low-voltage (C_{HL})	5,400.0
-High-voltage to tertiary-voltage (C_{HT})	87.5
-Low-voltage to tertiary-voltage (C_{LT})	7,900.0

In performing the short-circuit tests, one of the terminals of each winding is grounded. Therefore, half of the winding-to-winding capacitance and one-third of the stray capacitance to ground will appear in the tests. The capacitances that correspond to the short-circuit condition are shown in fig. 6.13. The turn-to-turn capacitances included in fig. 6.13 can be calculated from the measured short-circuit impedances.

Since the tertiary-winding, which is connected in delta, is not the outermost winding, the phase-to-phase capacitances will not be present in the positive-sequence tests. Therefore, the phase-to-phase capacitances cannot be calculated from the positive-sequence results and the identification of those capacitances requires some additional tests. Due to the fact that these tests were not carried out for the tested transformer, calculation

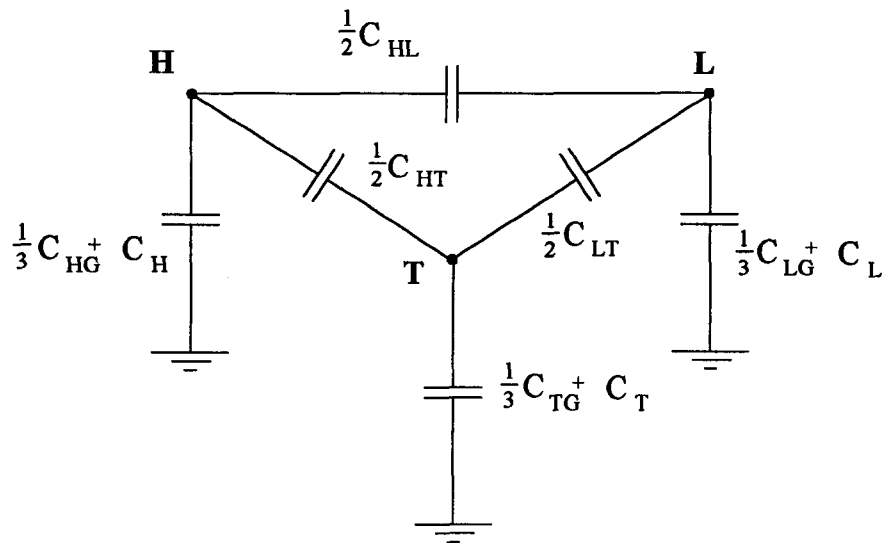


Fig. 6.13 Effective stray capacitances of a three-winding transformer during the short-circuit tests.

of the phase-to-phase capacitance will not be demonstrated here (an explanation on how to obtain the phase-to-phase capacitance is given in section 2.2.2 of chapter 5).

The turn-to-turn capacitances C_H , C_L and C_T in fig. 6.13 for the high-voltage, low-voltage and tertiary-voltage windings of the three-winding transformer can be calculated from the short-circuit tests. Six tests were conducted as follows:

Zero-sequence

- Z_{oL_HT} : impedance measured on the low-voltage winding with both high-voltage and tertiary-voltage windings short-circuited.
- Z_{oH_LT} : impedance measured on the high-voltage winding with both low-voltage and tertiary-voltage windings short-circuited.
- Z_{oL_T} : impedance measured on the low-voltage winding with only the tertiary-voltage winding short-circuited.

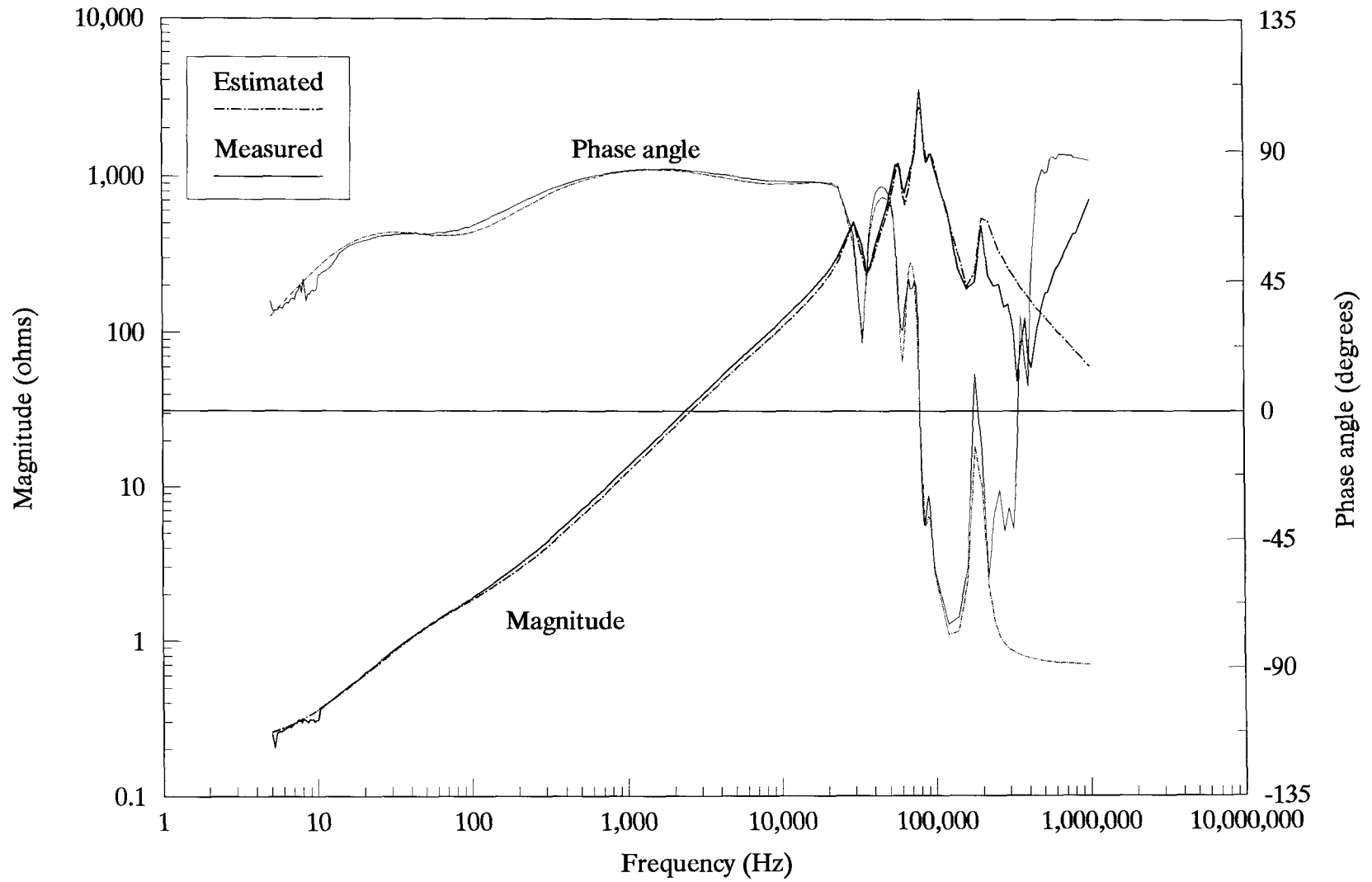


Fig. 6.14 Fitting of the short-circuit impedance measured on the low-voltage side with the high and tertiary-voltage windings short-circuited (zero-sequence).

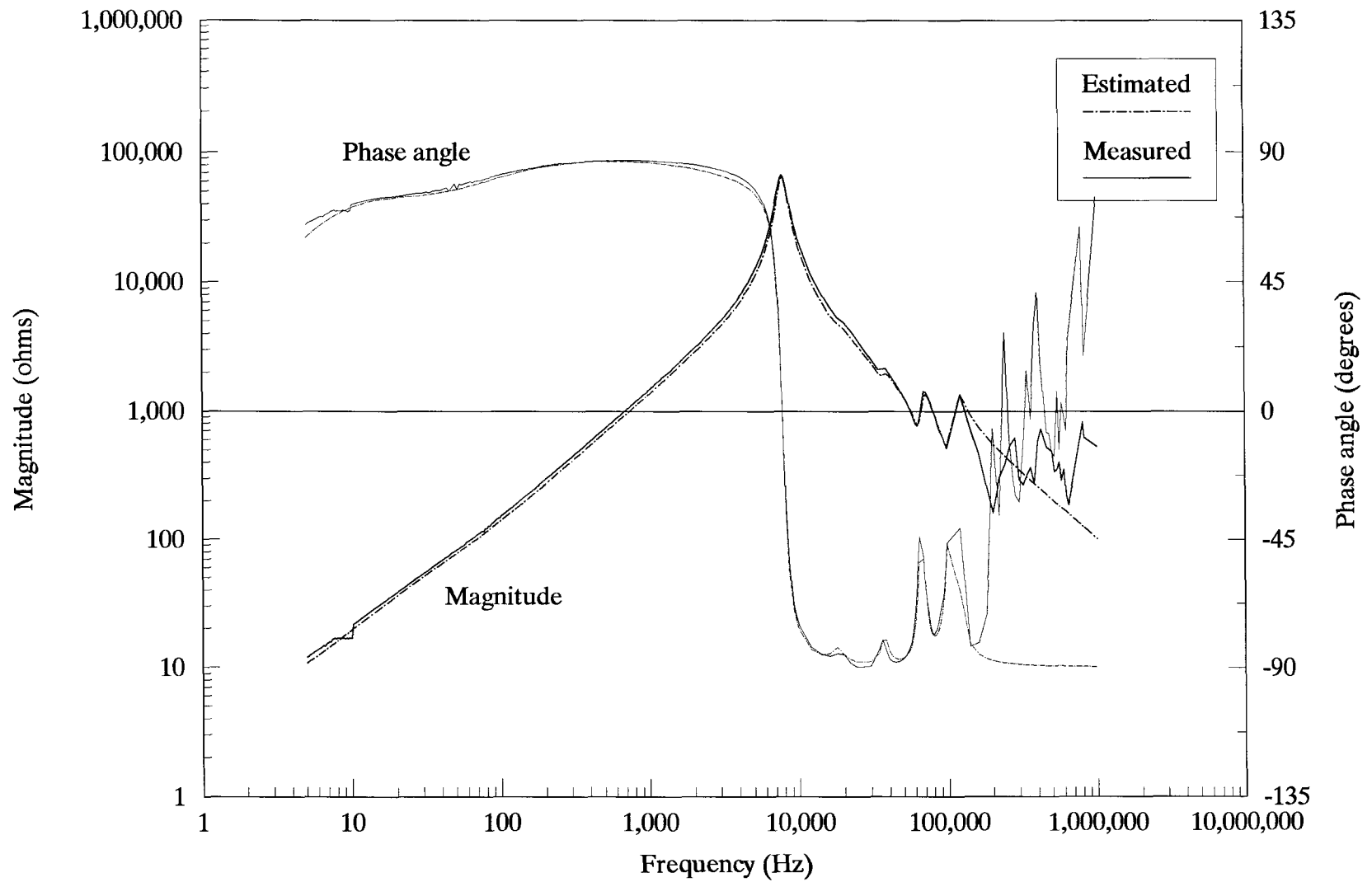


Fig. 6.15 Fitting of the short-circuit impedance measured on the high-voltage side with the low and tertiary-voltage windings short-circuited (zero-sequence).

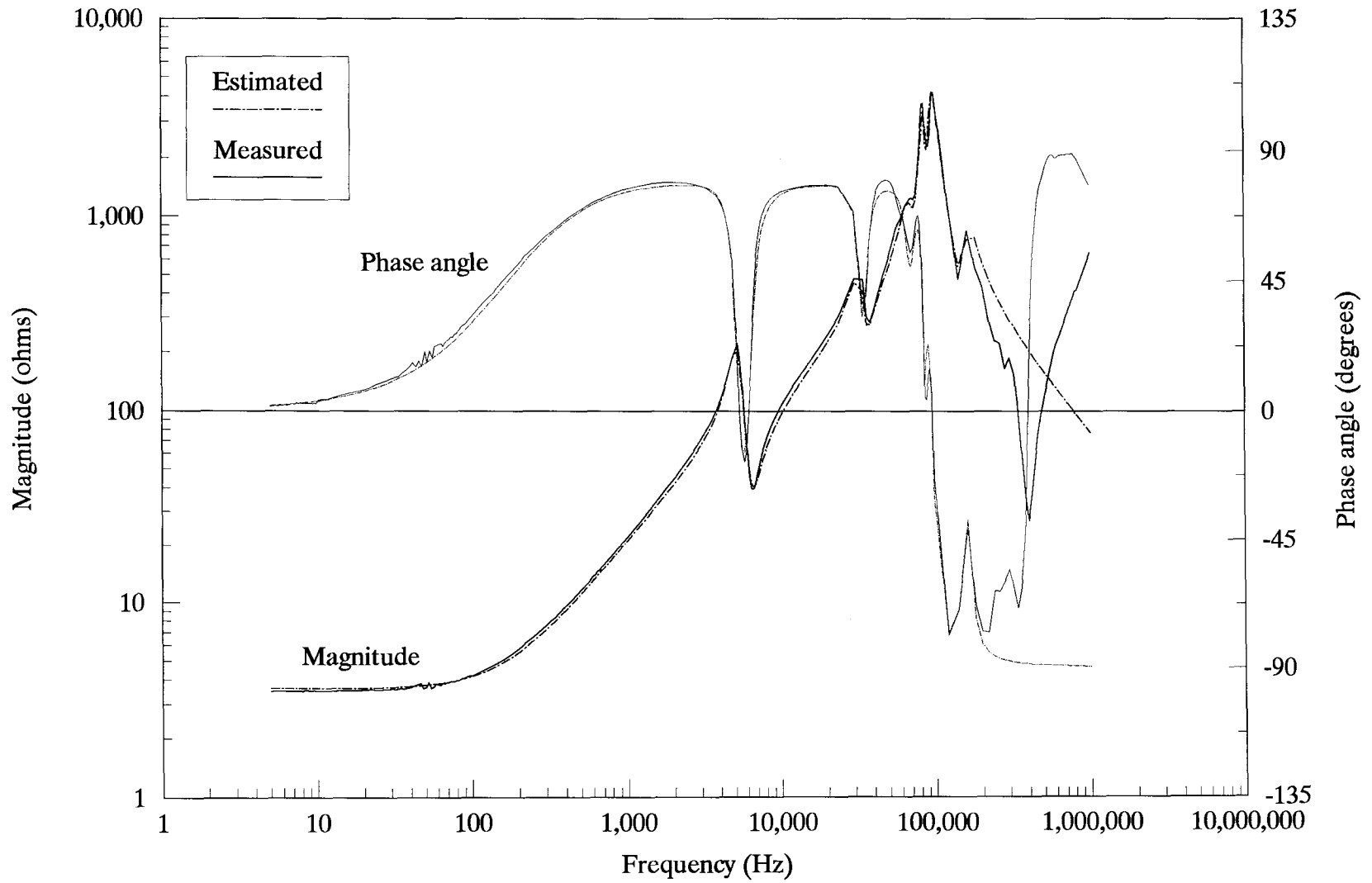


Fig. 6.16 Fitting of the short-circuit impedance measured on the low-voltage side with only the tertiary-voltage winding short-circuited (zero-sequence).

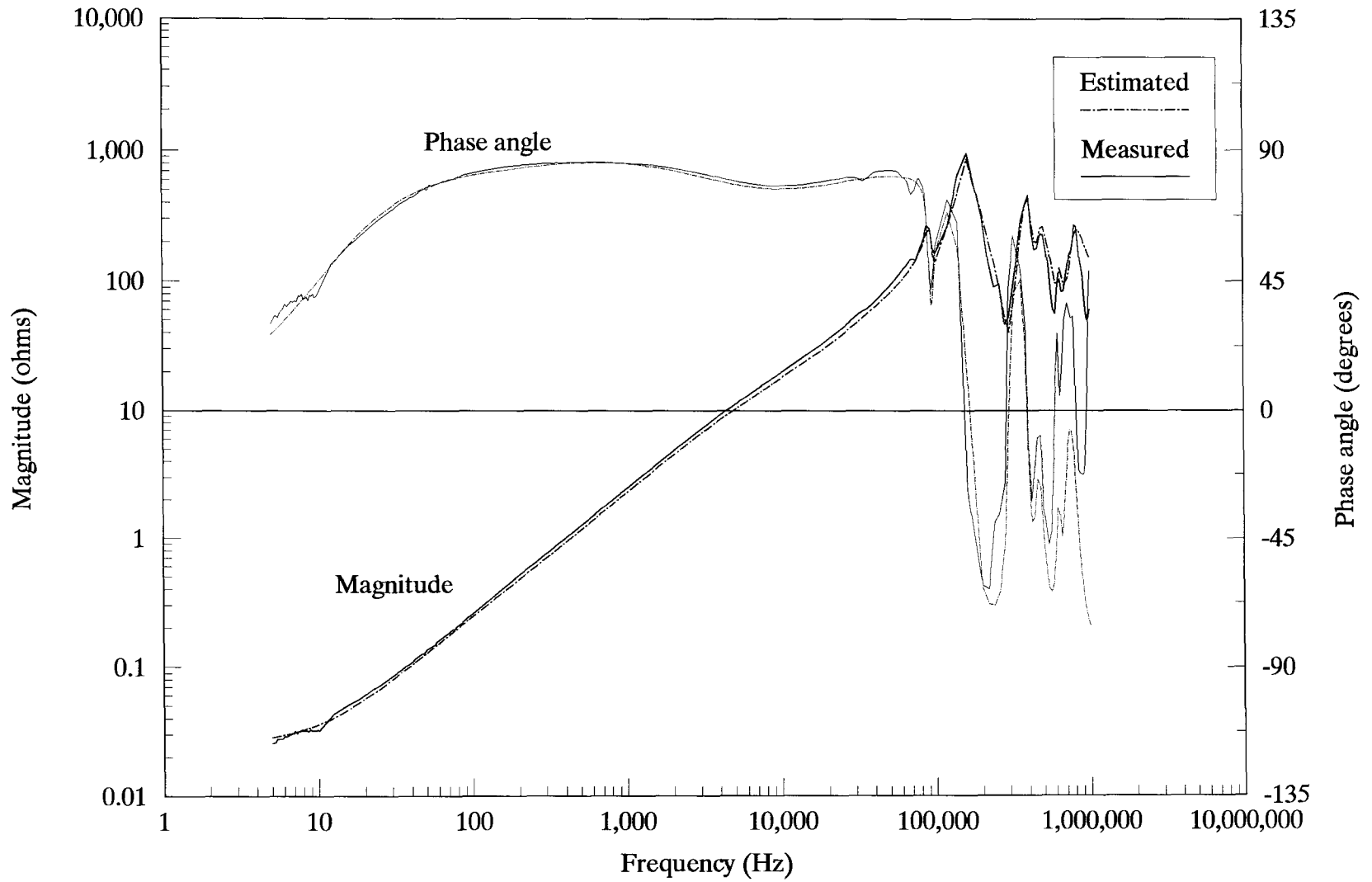


Fig. 6.17 Fitting of the short-circuit impedance measured on the tertiary-voltage side with the high and low-voltage windings short-circuited (positive-sequence).

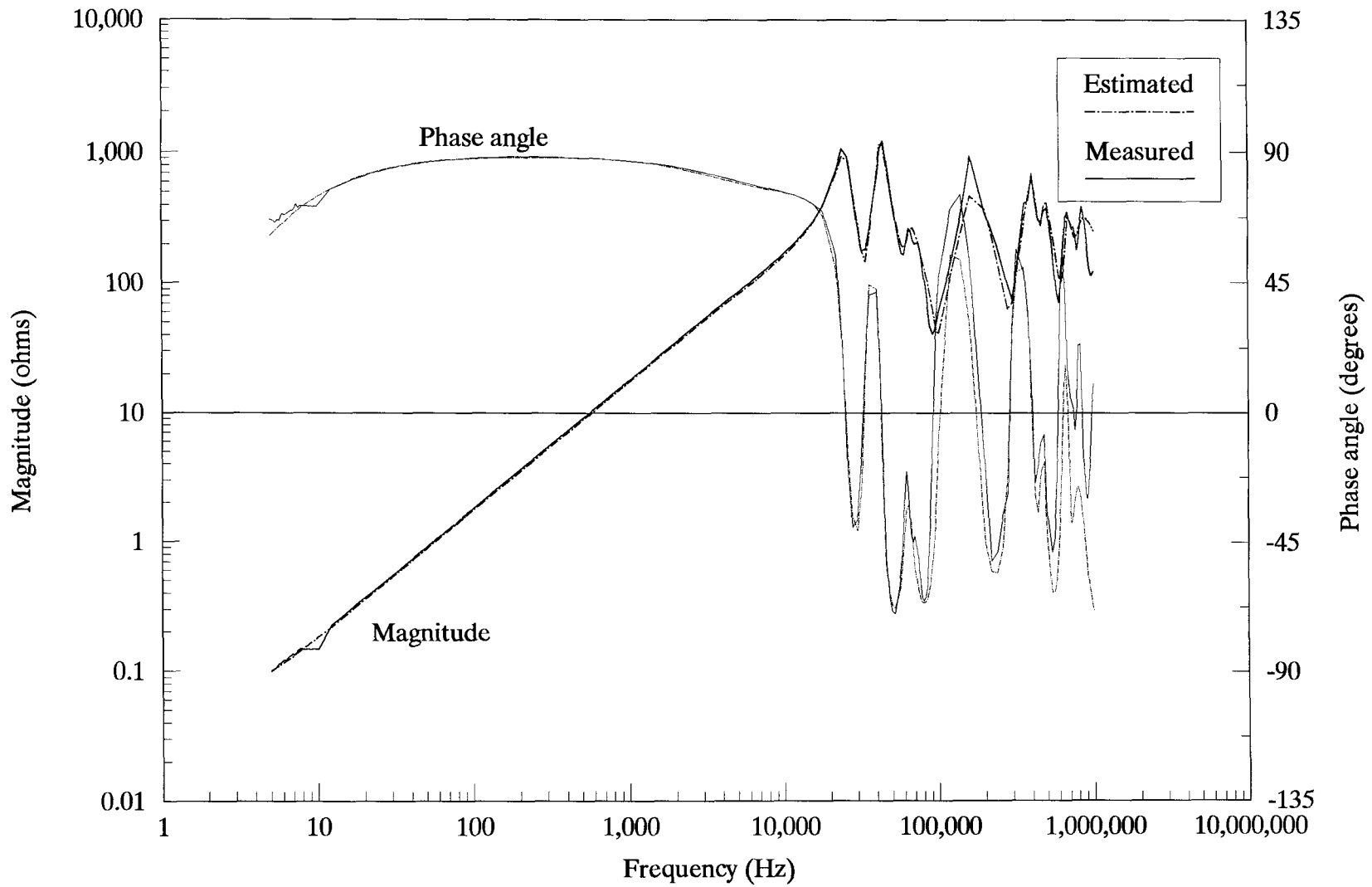


Fig. 6.18 Fitting of the short-circuit impedance measured on the tertiary-voltage side with only the high-voltage winding short-circuited (positive-sequence).

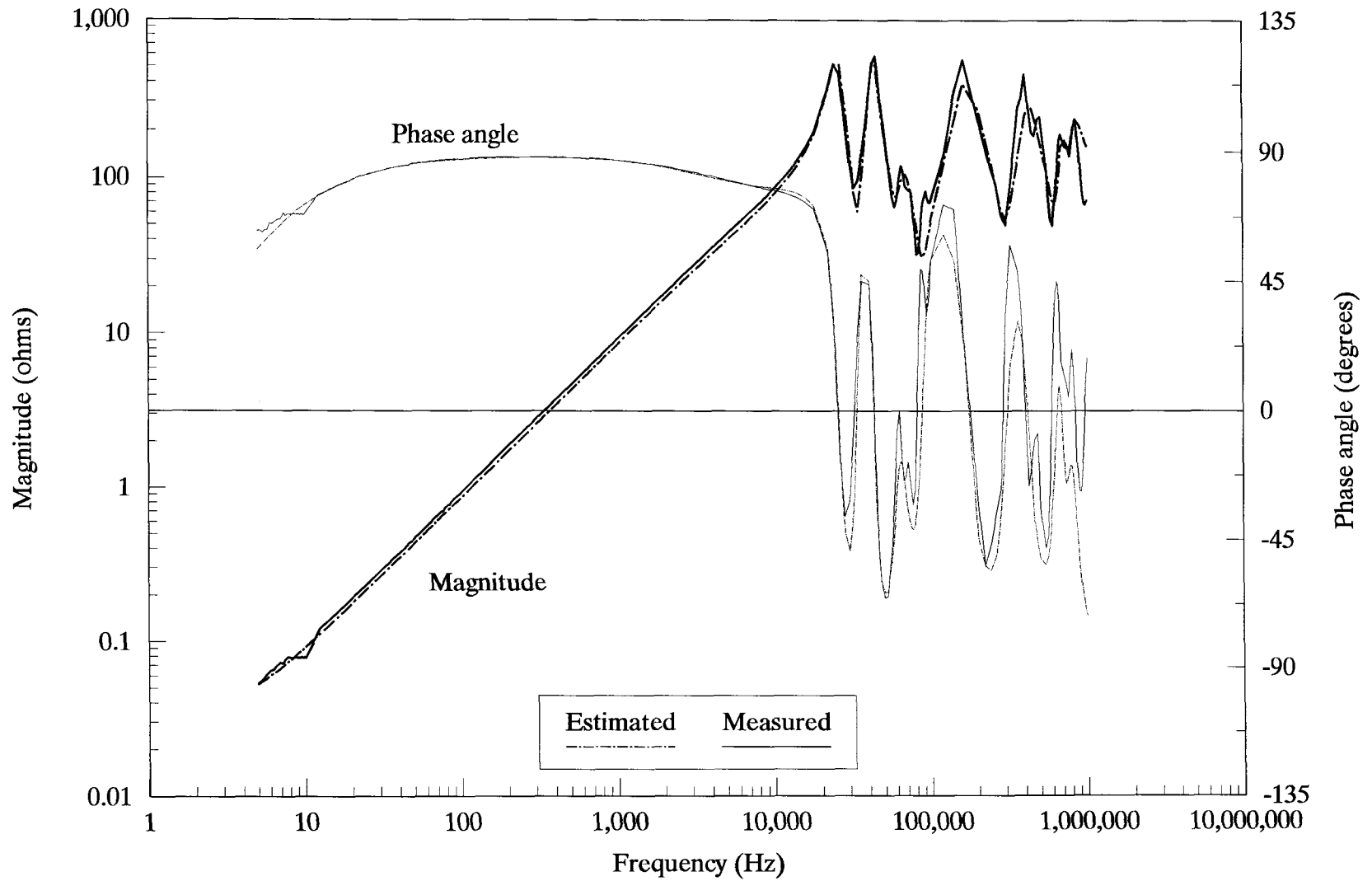


Fig. 6.19 Fitting of the short-circuit impedance measured on the tertiary-voltage side with only the low-voltage winding short-circuited (positive-sequence).

Table 6.7 -- Parameters of the zero-sequence short-circuit equivalent network for the tested three-winding transformer
(per phase values)

Case : ZoL_HT					Case : ZoH_LT					Case : ZoL_T				
Peak no.	C (farad)	R _z (Ω)	R _l (Ω)	L _l (Ω)	Peak no.	C (farad)	R _z (Ω)	R _l (Ω)	L _l (henry)	Peak no.	C (farad)	R _z (Ω)	R _l (Ω)	L _l (henry)
1	7.0913e-9	6.7400e-5	9.0443e-1	2.4790e-3	1	2.2592e-9	2.1720e+0	1.7950e+1	8.7832e-2	1	3.5442e-9	2.9224e-1	3.8500e+1	3.8599e-4
			2.8359e+1	5.8812e-4				1.2652e+3	4.4174e-2				7.1257e+0	5.1101e-4
			4.2490e+4	5.5459e-4				2.4716e+5	1.6921e-1				2.1473e+4	7.6706e-4
2	8.4926e-8	1.3492e-1	3.7518e+2	2.9200e-4	2	9.6098e-8	1.4946e+0	4.6004e+2	8.1353e-4	2	9.7392e-7	5.8695e-1	2.0642e+2	9.6540e-4
3	2.6750e-8	1.8318e-4	8.6748e+2	2.6851e-4	3	9.5892e-8	0.0000e+0	3.1787e+2	1.9087e-4	3	1.0361e-7	2.1972e+0	4.7329e+2	2.2034e-4
4	1.3775e-8	3.5086e-2	8.0248e+2	2.1116e-4	4	2.2672e-8	1.8869e-2	7.5099e+2	2.4447e-4	4	2.8894e-8	5.4405e-1	5.3471e+2	1.8971e-4
5	8.3690e-9	4.2042e-2	4.7543e+2	7.5667e-5	5	7.6848e-9	1.2863e+0	1.0750e+3	2.6704e-4	5	1.7176e-8	1.9244e-3	2.2344e+3	2.0885e-4
										6	1.0580e-8	2.4801e-4	5.8732e+2	9.0962e-5
High-frequency equivalent capacitance = 2.61602e-9 farad					High-frequency equivalent capacitance = 1.56810e-9 farad					High-frequency equivalent capacitance = 2.08256e-9 farad				

Table 6.8 -- Parameters of the positive-sequence short-circuit equivalent network for the tested three-winding transformer (per phase values)

Case : ZpT_HL					Case : ZpT_H					Case : ZpT_L				
Peak no.	C (farad)	R _{sc} (Ω)	R _i (Ω)	L ₁ (Ω)	Peak no.	C (farad)	R _{sc} (Ω)	R _i (Ω)	L ₁ (henry)	Peak no.	C (farad)	R _{sc} (Ω)	R _i (Ω)	L ₁ (henry)
1	5.8024e-9	2.3667e-3	3.4367e-2	3.7188e-5	1	3.2324e-8	4.8274e-3	1.4251e+4	2.2247e-13	1	6.7837e-8	1.0602e-2	1.0058e-1	6.8052e-6
			4.4709e+0	5.7350e-5				1.2728e+4	5.1797e-4				4.2487e+0	1.0914e-4
			2.7302e+0	8.4852e-5				8.7523e-2	6.3950e-5				2.9290e-2	3.5993e-5
			3.3721e+0	4.6749e-6				3.2372e+1	8.0960e-4				1.0878e+1	2.7954e-4
			1.2007e+3	1.5906e-4				1.0783e+3	6.5569e-4				6.6783e+3	5.5477e-4
2	1.2704e-7	4.0226e-3	1.4424e+2	2.3170e-5	2	2.7388e-8	1.0324e-2	1.2219e+3	5.0313e-4	2	6.1203e-8	3.0982e-3	5.5532e+2	2.2484e-4
3	8.0675e-9	5.4044e-3	4.1702e+2	2.0476e-5	3	7.1427e-8	2.2936e-5	1.7731e+2	8.2175e-5	3	1.2609e-7	3.0937e-3	8.0822e+1	4.5678e-5
4	1.2732e-8	5.4202e-3	1.8349e+2	8.4803e-6	4	6.3884e-9	7.4689e-3	5.6647e+2	1.3138e-4	4	7.9259e-9	3.4538e-3	4.2665e+2	1.0958e-4
5	7.1573e-8	3.1479e-3	5.7049e+1	8.7374e-7	5	5.0629e-9	1.1541e-2	5.9023e+2	3.1310e-5	5	5.7841e-9	3.2588e-3	2.6653e+2	2.4716e-5
6	4.8523e-9	5.3440e-3	2.0570e+2	8.0285e-6	6	1.0616e-8	1.4553e-2	3.0960e+2	1.0052e-5	6	1.6511e-8	2.9264e-3	1.2482e+2	3.1629e-6
					7	1.2366e-8	8.2188e-6	2.8295e+2	4.3123e-6	7	5.3568e-9	3.2541e-3	1.7151e+2	6.7650e-6
					8	3.0125e-9	8.8793e-7	2.4023e+2	1.1952e-5					
High-frequency equivalent capacitance = 1.65901e-9 farad					High-frequency equivalent capacitance = 1.06100e-9 farad					High-frequency equivalent capacitance = 1.70849e-9 farad				

Positive-sequence

ZpT_HL:	impedance measured on the tertiary-voltage winding with both high-voltage and low-voltage windings short-circuited.
ZpT_H:	impedance measured on the tertiary-voltage winding with only high-voltage winding short-circuited.
ZpT_L:	impedance measured on the tertiary-voltage winding with only low-voltage winding short-circuited.

To determine the capacitances included in the measured short-circuit impedances, the impedances are fitted by an RLC synthesis network. The results of this fitting for the six measured cases are shown in figs. 6.14 to 6.19. The parameters of the RLC networks are indicated in tables 6.7 and 6.8. All quantities in fig. 6.14 through fig. 6.19 and in tables 6.7 and 6.8 has been converted to per phase values.

To determine the turn-to-turn capacitances from the short-circuit tests, it preferable to use those tests in which the remaining two windings are both shorted. These correspond to cases:ZoL_HT, ZoH_LT and ZpT_HL. Using the total capacitances given in figs. 6.20, 6.21 and 6.24, together with the measured capacitances from table 6.6 and the capacitance diagram of fig. 6.13, C_H , C_L and C_T are found to be:

$$\begin{aligned} C_H \text{ (from case:ZoH_LT)} &= 1.56810e-09 - \frac{1}{3} \left(\frac{1}{2} C_{HL} + \frac{1}{2} C_{HT} + \frac{1}{3} C_{HG} \right) \\ &= 5.94461e-10 \text{ farad (per phase)} \end{aligned}$$

$$\begin{aligned} C_L \text{ (from case:ZoL_HT)} &= 2.61602e-09 - \frac{1}{3} \left(\frac{1}{2} C_{HL} + \frac{1}{2} C_{LT} + \frac{1}{3} C_{LG} \right) \\ &= 3.55531e-10 \text{ farad (per phase).} \end{aligned}$$

$$\begin{aligned} C_T \text{ (from case:ZpT_HL)} &= 1.65901e-09 - \frac{1}{3} \left(\frac{1}{2} C_{HT} + \frac{1}{2} C_{LT} + \frac{1}{3} C_{TG} \right) \\ &= 3.27349e-10 \text{ farad (per phase).} \end{aligned}$$

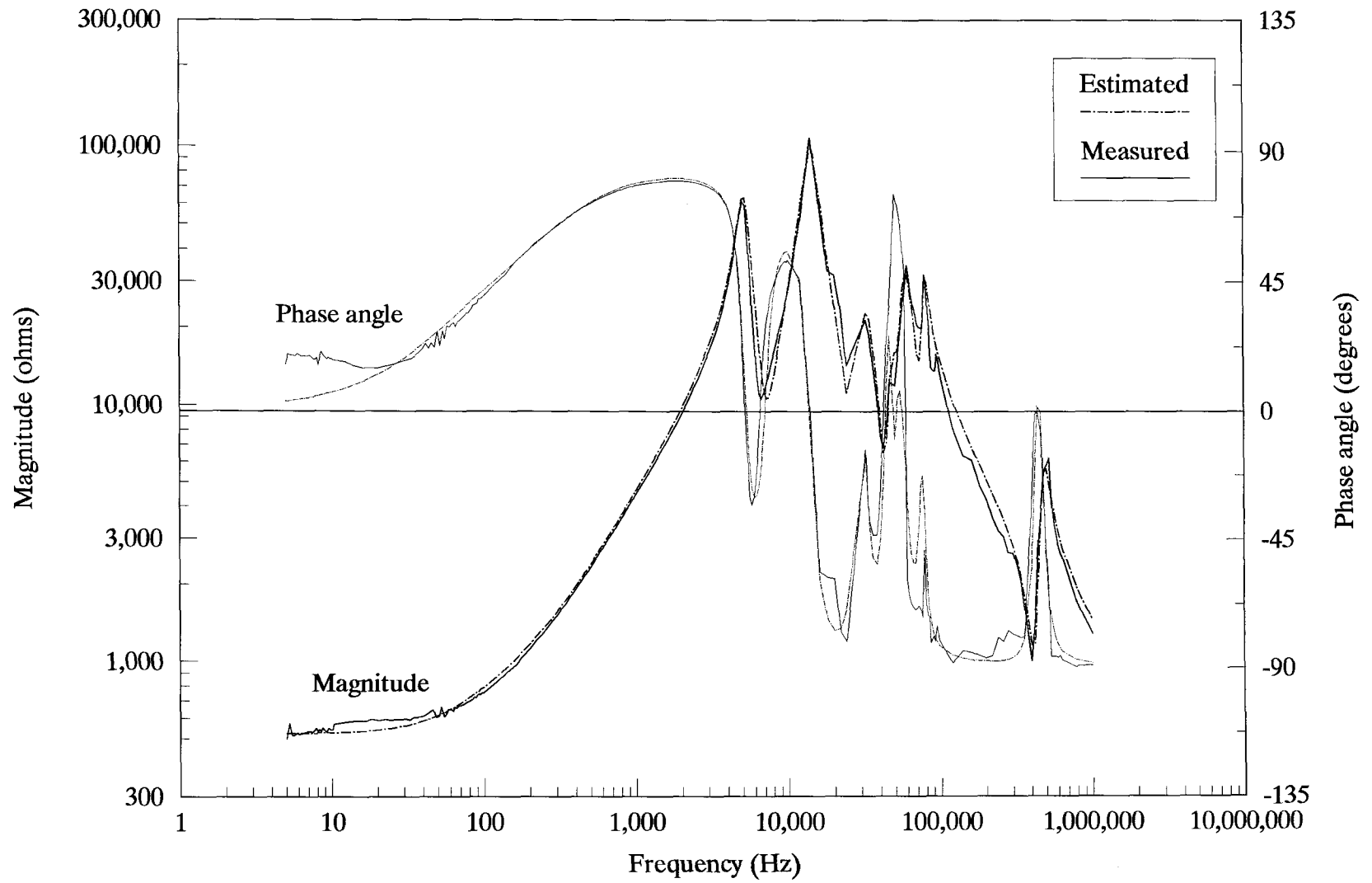


Fig. 6.20 Fitting of the sum of the high and low-voltage winding impedances (zero-sequence).

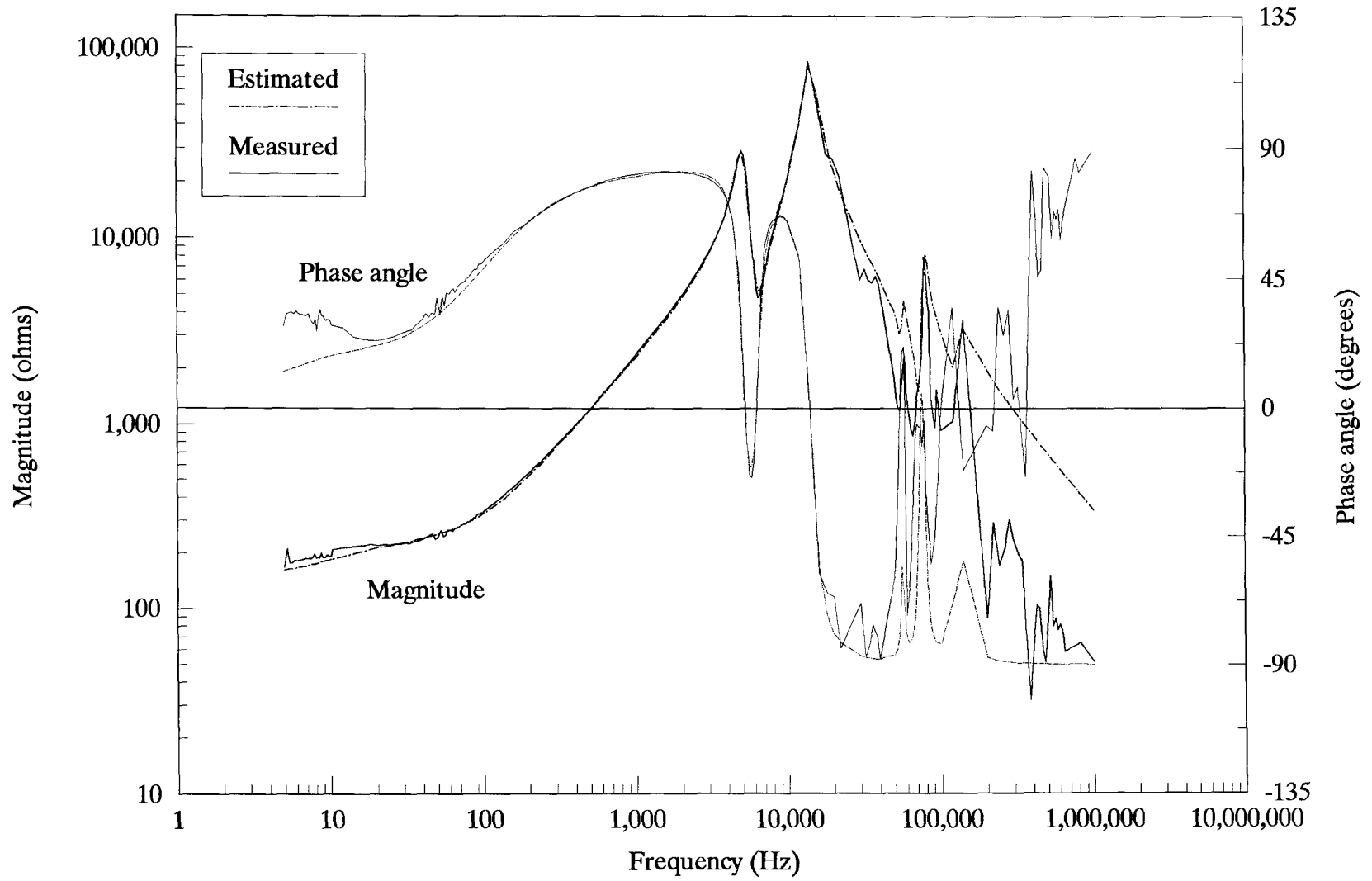


Fig. 6.21 Fitting of the sum of the high and tertiary-voltage winding impedances (zero-sequence).

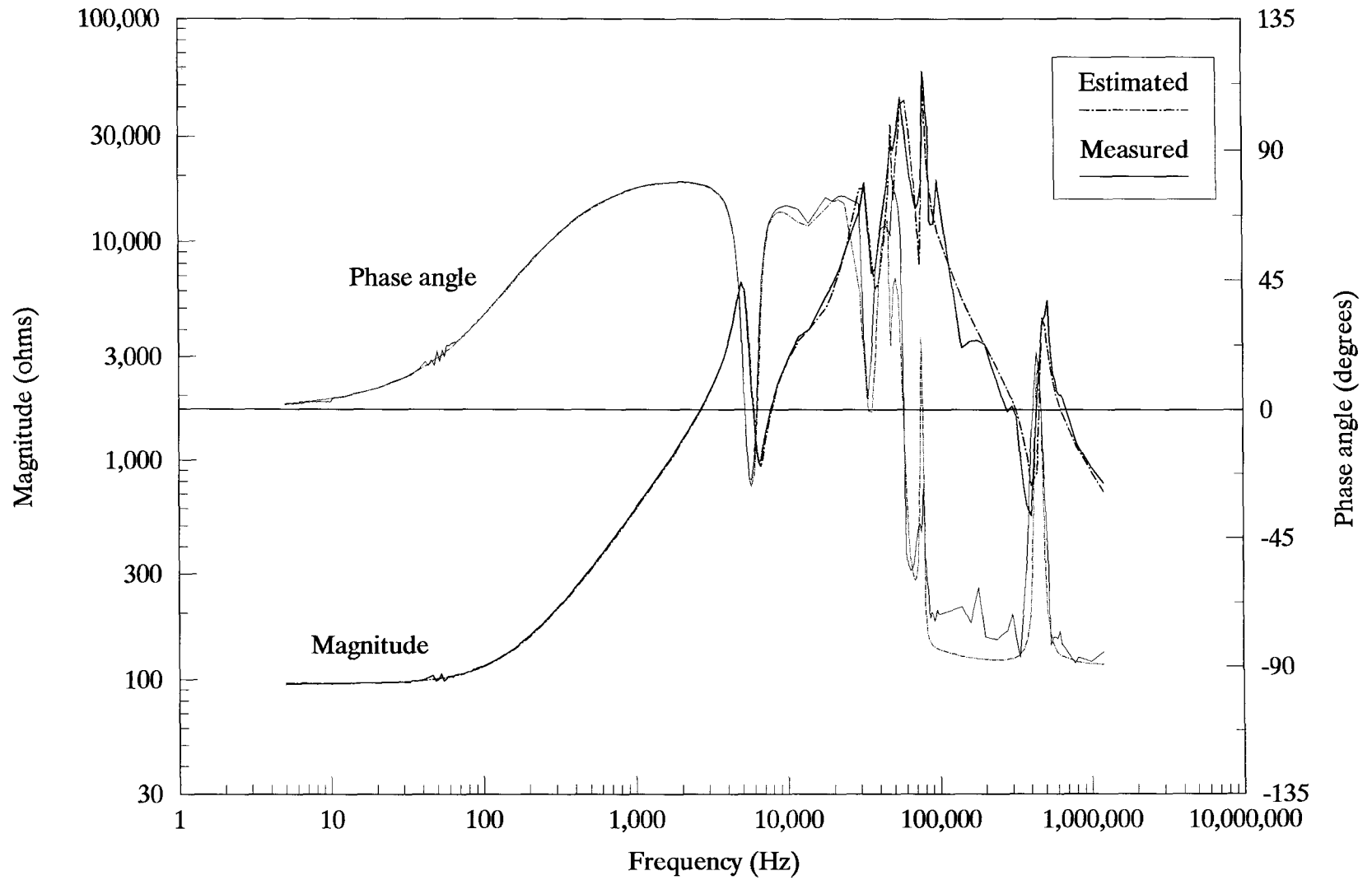


Fig. 6.22 Fitting of the sum of the low and tertiary-voltage winding impedances (zero-sequence).

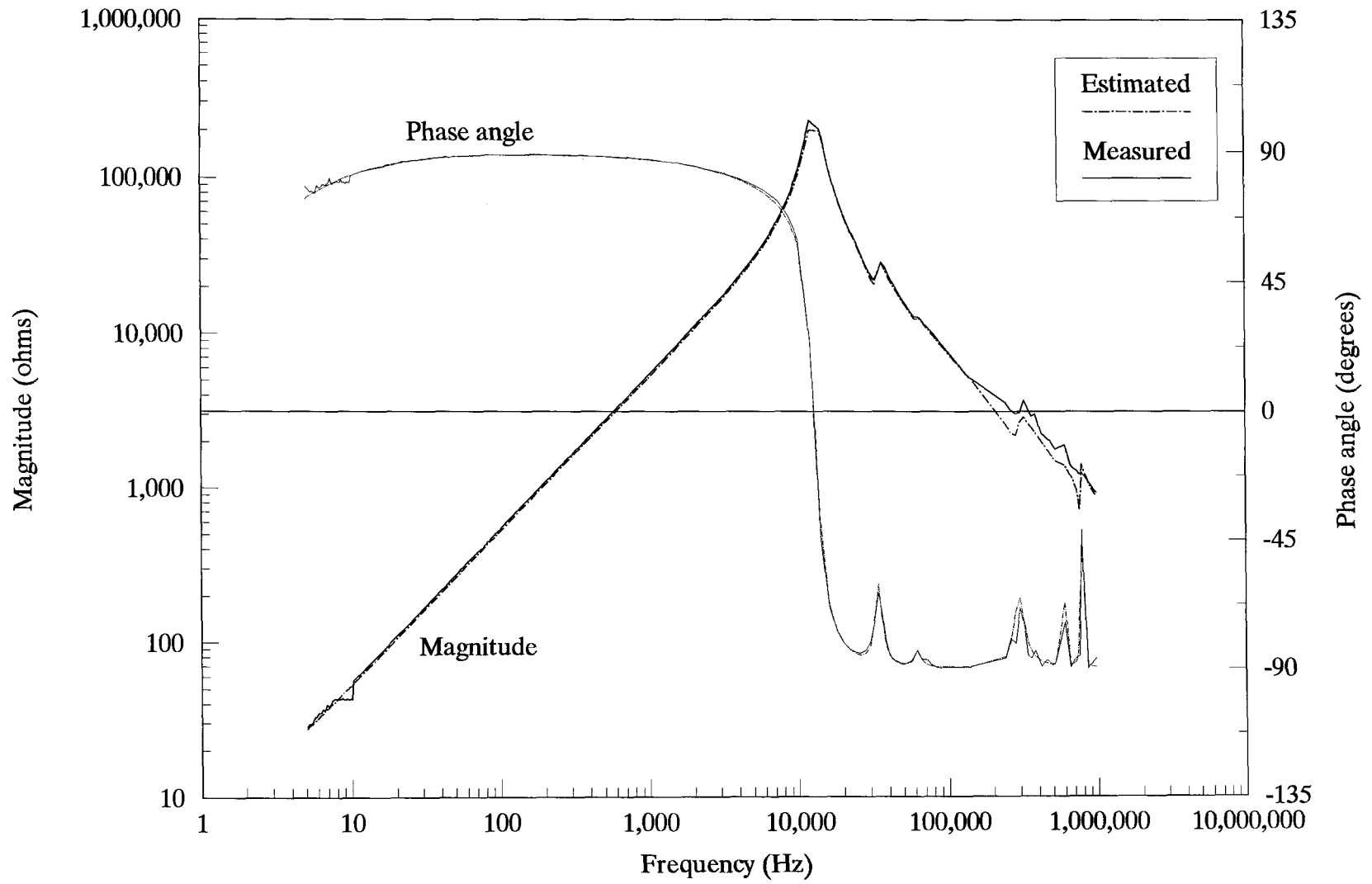


Fig. 6.23 Fitting of the sum of the high and low-voltage winding impedances (positive-sequence).

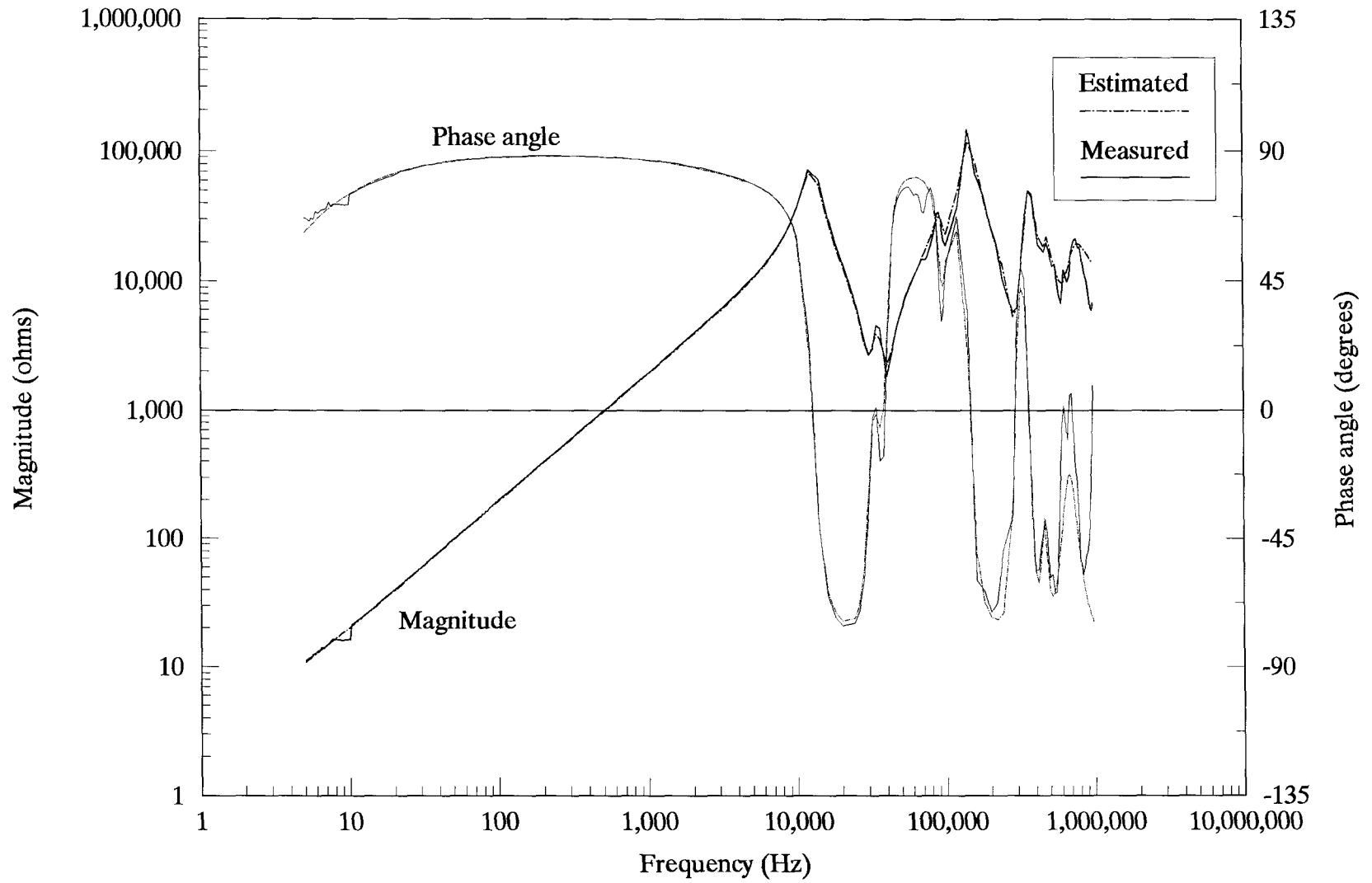


Fig. 6.24 Fitting of the sum of the high and tertiary-voltage winding impedances (positive-sequence).

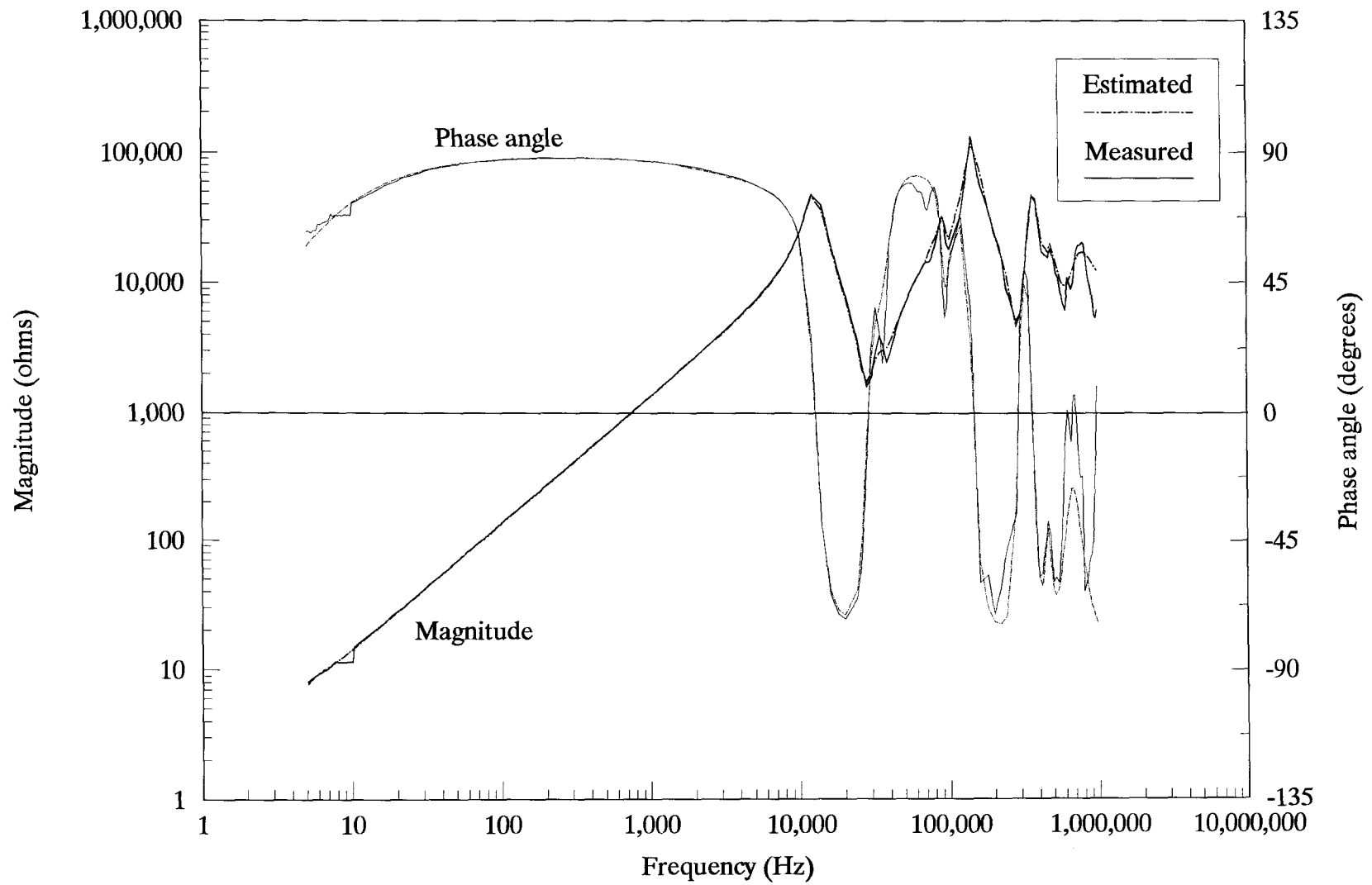


Fig. 6.25 Fitting of the sum of the low and tertiary-voltage winding impedances (positive-sequence).

Table 6.9 -- Parameters of the zero-sequence Z_{winding} impedance for the tested three-winding transformer
(per phase values referred to high-voltage side)

Case : Zo_HL					Case : Zo_HT					Case : Zo_LT				
Peak no.	C (farad)	$R_{\text{sk}} (\Omega)$	$R_1 (\Omega)$	$L_1 (\Omega)$	Peak no.	C (farad)	$R_{\text{sk}} (\Omega)$	$R_1 (\Omega)$	L_1 (henry)	Peak no.	C (farad)	$R_{\text{sk}} (\Omega)$	$R_1 (\Omega)$	L_1 (henry)
1	5.5878e-10	5.2597e+2	1.7928e+2	2.2965e-1	1	7.3880e-10	1.0235e+2	6.8885e+1	8.6127e-1	1	3.1390e-8	2.1268e+0	9.3466e+1	5.2827e-3
			3.8902e+3	9.4942e-2				1.9761e+2	3.7134e-2				1.1302e+1	6.1356e-3
			3.0746e+7	2.1162e-1				4.3893e+3	5.3395e-2				8.0051e+1	5.4825e-3
			-	-				1.4622e+7	1.4181e-1				8.4193e+4	2.8075e-2
2	2.6048e-9	-	5.8748e+4	3.5960e-1	2	6.8965e-9	2.4032e-2	2.5810e+4	1.4326e-1	2	9.7171e-9	2.8105e+1	1.4079e+3	1.2851e-2
3	1.1945e-9	-	2.0818e+4	2.0708e-2	3	2.5250e-8	5.1643e-2	2.1409e+3	3.1125e-4	3	1.4427e-9	6.6190e+1	1.7237e+4	1.7146e-2
4	3.4651e-9	-	1.3832e+4	3.1728e-3	4	3.6330e-9	3.0161e+0	7.6270e+3	1.1210e-3	4	6.9580e-9	-	2.3692e+4	1.5801e-3
5	4.8565e-10	-	2.9141e+4	1.5505e-2	5	3.0130e-9	4.4105e+1	4.8946e+3	4.3305e-4	5	3.9650e-10	-	4.5959e+4	1.8990e-2
6	9.1151e-10	-	2.0995e+4	4.5676e-3	-	-	-	-	-	6	1.4772e-9	-	5.1015e+4	2.8185e-3
7	4.7763e-10	-	4.9790e+3	2.3018e-4	-	-	-	-	-	7	8.9075e-10	-	4.2739e+3	1.2343e-4
High-frequency equivalent capacitance = 1.16971e-10 farad					High-frequency equivalent capacitance = 4.66133e-10 farad					High-frequency equivalent capacitance = 1.88918e-10 farad				

Table 6.10 -- Parameters of the positive-sequence Z_{winding} impedance for the tested three-winding transformer
(per phase values referred to high-voltage side)

Case : Zp_HL					Case : Zp_HT					Case : Zp_LT				
Peak no.	C (farad)	R _w (Ω)	R _l (Ω)	L _l (Ω)	Peak no.	C (farad)	R _w (Ω)	R _l (Ω)	L _l (henry)	Peak no.	C (farad)	R _w (Ω)	R _l (Ω)	L _l (henry)
1	2.3803e-10	7.3622e+0	5.5878e+1	1.6394e-2	1	7.1241e-10	3.5828e+0	7.0207e+0	6.4685e-3	1	1.0879e-9	2.3638e+0	5.5462e+0	5.5567e-3
			1.5984e+4	2.9495e-1				1.9539e+3	6.3287e-2				1.3610e+3	4.4632e-2
			4.8474e+8	5.2870e-1				1.1581e+5	2.0989e-1				7.9797e+4	1.3632e-1
2	3.0289e-9	2.3280e-1	1.2011e+4	7.0971e-3	2	5.9693e-9	5.1206e-3	3.0797e+3	3.5707e-3	2	6.0227e-9	7.7661e-3	1.7928e+3	3.5436e-3
3	1.8657e-8	2.4717e-1	1.2502e+3	3.5098e-4	3	6.7571e-10	1.3907e+0	1.6622e+4	4.3464e-3	3	7.3699e-10	1.8220e+0	1.6196e+4	3.9964e-3
4	2.3904e-9	-	1.1097e+3	1.1774e-4	4	5.2252e-11	2.0532e-1	1.2672e+5	2.3163e-2	4	5.6698e-11	1.3792e-1	1.2584e+5	2.1392e-2
5	2.1355e-8	-	5.3334e+2	3.2948e-6	5	7.4005e-11	4.7657e-2	5.0967e+4	2.5542e-3	5	8.0709e-11	2.2096e-2	4.8214e+4	2.3490e-3
6	7.1496e-9	-	9.5134e+2	5.8233e-6	6	2.9646e-10	7.9113e-2	1.1106e+4	3.8644e-4	6	3.2834e-10	4.8720e-2	9.6409e+3	3.4997e-4
					7	4.4640e-11	2.1277e-4	1.5070e+4	1.0495e-3	7	4.7813e-11	2.1277e-4	1.2842e+4	9.9546e-4
High-frequency equivalent capacitance = 1.92682e-10 farad					High-frequency equivalent capacitance = 1.62664e-11 farad					High-frequency equivalent capacitance = 1.77211e-11 farad				

2.2 Series Branch Impedance ($Z_{winding}$)

Before the measured impedances are used in the computation of the leakage impedances, the total capacitances derived from the fitting given in tables 6.7 and 6.8 have to be deducted from each of them. Equations 5.27, 5.28, 5.29 and 5.38 can then be applied to calculate the individual leakage impedance for each winding. After this, the three leakage impedances for the transformer model can be transformed into delta connection, as shown in fig. 2.9c. Part of the winding-to-winding capacitances can then be combined with the leakage impedances (as shown in fig. 2.10) to obtain the $Z_{winding}$ impedance to be synthesized with multiple RLC equivalent blocks. When this is done, the delta-connected winding impedances can then be converted back to their original configuration (fig. 9.2a).

The manipulations explained above, however, do not always result in winding impedances which are minimum-phase-shift functions. An alternative way was sought so that only minimum-phase-shift functions are dealt with in the fitting of impedances. It was found that the sum of two individual leakage impedances produces a minimum-phase-shift function. Physically, this may correspond to the fact that it is always possible to measure the sum of two leakage impedances of a transformer (if the windings can be disconnected) while it is not possible to directly measure the individual branches of the T circuit. The sum of two winding impedances (for both the zero and positive sequence) were fitted with RLC equivalent networks. The corresponding results are shown in figs. 6.20 to 6.25

and tables 6.9 and 6.10. For the reference purposes, the fitted results are named as follows:

Zero-sequence

Zo_{HL} :	Sum of the high-voltage and low-voltage winding impedances.
Zo_{HT} :	Sum of the high-voltage and tertiary-voltage winding impedances.
Zo_{LT} :	Sum of the low-voltage and tertiary-voltage winding impedances.

Positive-sequence

Zp_{HL} :	Sum of the high-voltage and low-voltage winding impedances.
Zp_{HT} :	Sum of the high-voltage and tertiary-voltage winding impedances.
Zp_{LT} :	Sum of the low-voltage and tertiary-voltage winding impedances.

Impedances for both the zero-sequence and the positive-sequence are referred to the high-voltage winding side.

The sum of the $Z_{winding}$ of two windings cannot be used right away since the model requires a separate series branch impedance for each winding. However, further fitting is not necessary because $Z_{winding}$ for each winding is related directly to those fitted results explained earlier. In terms of equations, the relationship can be written as follows:

$$Zo_{HL} = Zo_H + Zo_L \quad (6.1)$$

$$Zo_{HT} = Zo_H + Zo_T \quad (6.2)$$

$$Z_{o_LT} = Z_{o_L} + Z_{o_T} \quad (6.3)$$

where,

Z_{o_H} , Z_{o_T} and Z_{o_L} = the zero-sequence $Z_{winding}$ impedances for the high, tertiary and low-voltage windings, respectively. The impedances are referred to the high-voltage winding side.

Then, it can be shown that

$$\begin{aligned} Z_{o_H} &= \frac{1}{2}(Z_{o_HL} + Z_{o_HT} + Z_{o_LT}) - Z_{o_LT} \\ &= \frac{1}{2}Z_{o_HL} + \frac{1}{2}Z_{o_HT} - \frac{1}{2}Z_{o_LT} \end{aligned} \quad (6.4)$$

Similarly,

$$Z_{o_T} = \frac{1}{2}Z_{o_HT} + \frac{1}{2}Z_{o_LT} - \frac{1}{2}Z_{o_HL} \quad (6.5)$$

and

$$Z_{o_L} = \frac{1}{2}Z_{o_HL} + \frac{1}{2}Z_{o_LT} - \frac{1}{2}Z_{o_HT} \quad (6.6)$$

In terms of circuit representation, one-half impedance can be realised from the original impedance by simply reducing the constituent resistances and inductances to half their values and increasing the capacitances to double their values. Likewise, a negative impedance can be accomplished by replacing each and every parameter of the fitted result with a negative value of an equal magnitude.

The winding impedances for the positive-sequence model can be constructed exactly in the same manner.

However, if it happens that one of the winding impedances is a minimum-phase-shift function, it can be fitted and used to obtain the other two winding impedances by simple subtraction. For instance, it was found that the winding impedance for the high-voltage winding in the positive sequence of the tested three-winding transformer was a minimum-phase-shift function, as shown in fig. 6.26. Z_{p_T} and Z_{p_L} can be found as follows:

$$Z_{p_T} = Z_{p_HT} - Z_{p_H} \quad (6.7)$$

$$Z_{p_L} = Z_{p_HL} - Z_{p_H} \quad (6.8)$$

where,

Z_{p_T} and Z_{p_L} = the winding impedances of the tertiary and low-voltage windings, respectively.

Z_{p_H} = the winding impedance of the high-voltage winding which was found to be minimum-phase-shift and was previously fitted.

It is obvious that equations 6.7 and 6.8 are simpler than equations 6.5 and 6.6. Only two impedances are required to be connected in series to make up the winding impedances. Therefore, it is advantageous to use equations 6.7 and 6.8 whenever it is possible.

Figures 6.27 and 6.28 show the fitting results for the low-voltage and the tertiary-voltage Z_{winding} of the positive sequence model computed with equations 6.7 and 6.8, respectively.

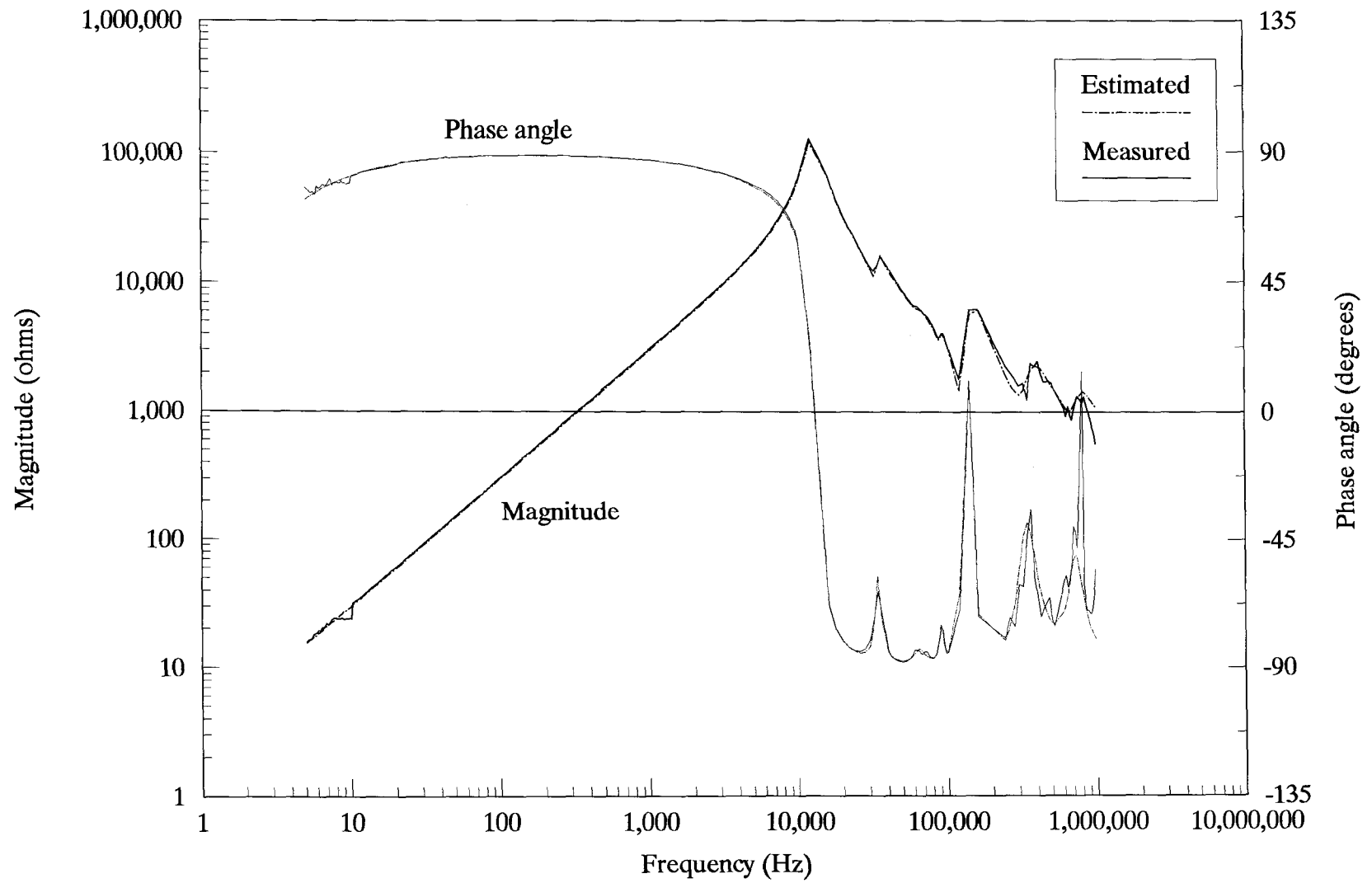


Fig. 6.26 Fitting of the winding impedance of the high-voltage winding (positive-sequence).

From the numerical examples for both the two-winding and the three-winding transformers presented in this chapter, it can be clearly seen that the proposed technique of impedance derivation to process the experimental data leads to very accurate results. Furthermore, it can be concluded that the developed transformer model is capable of producing satisfactory simulation results both in the frequency-domain and in the time-domain (experimental data was not available for the three-winding transformer in the time-domain).

3. Simulation of Transient Recovery Voltage

To compare the proposed frequency dependent transformer model with the constant-parameter model, a fault interruption case (Fig. 6.29) was simulated. The plots in Fig. 6.29 compare the voltage across contacts of the circuit breaker obtained with the proposed frequency dependent model (with parameters derived from the tested 50 MVA 115/23 kV transformer) and with a constant parameters model in which the short-circuit impedance is represented with the 60-Hz resistance and inductance. The same external capacitances network is used for both models. The difference in the results illustrate the importance of more accurate transformer modelling in fast switching transients.

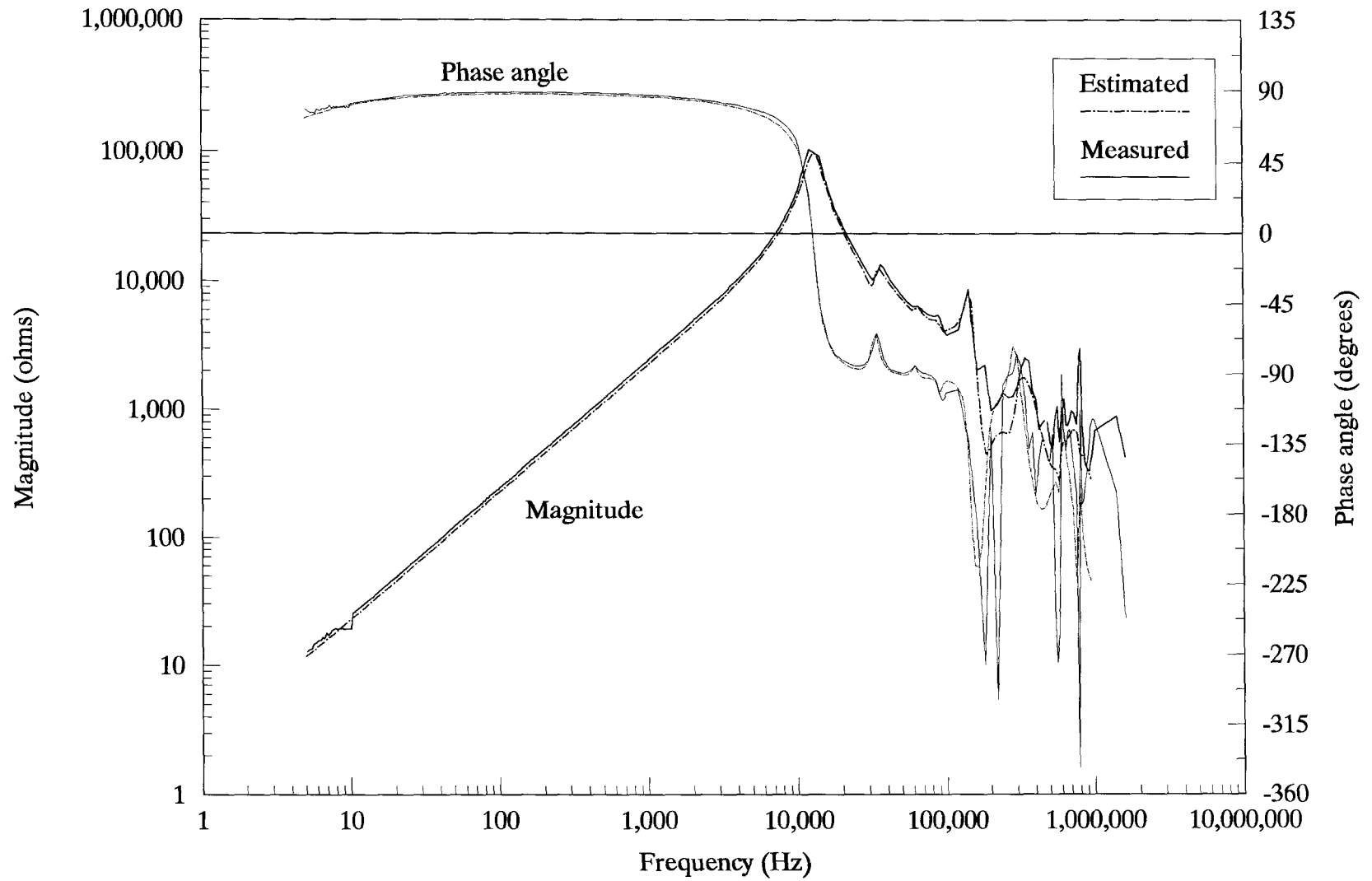


Fig. 6.27 Winding impedance of the low-voltage winding (positive-sequence).

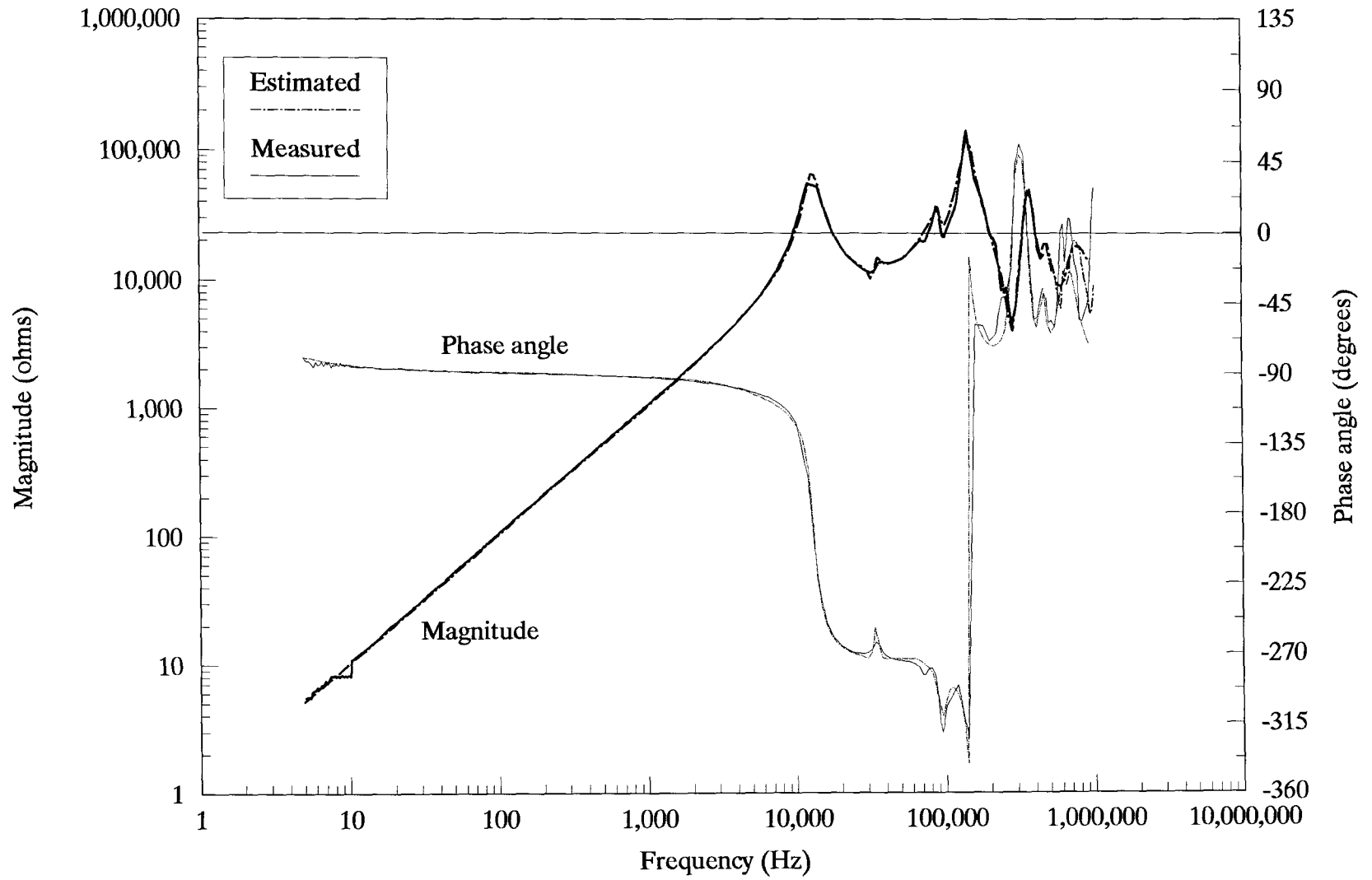


Fig. 6.28 Winding impedance of the tertiary-voltage winding (positive-sequence).

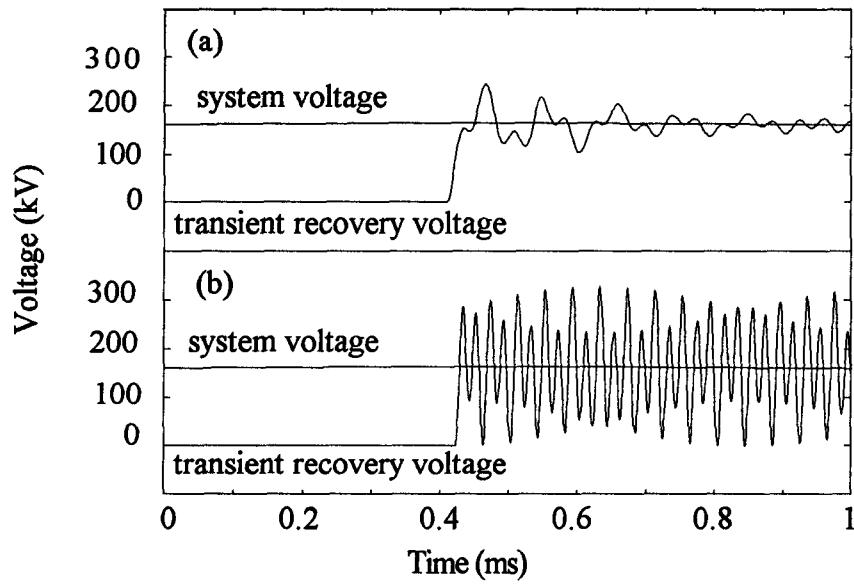
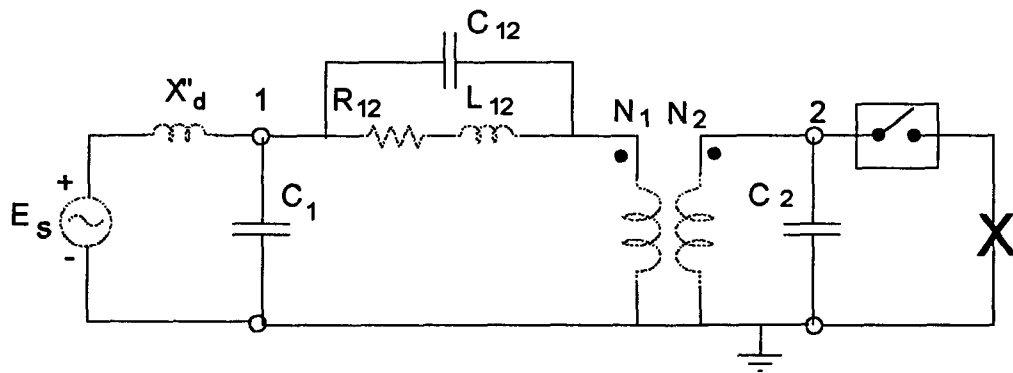


Fig. 6.29 Transient recovery voltage in a circuit breaker after clearing a fault. (a) Frequency-dependent model. (b) Constant-parameter model.

Chapter Seven

PROPOSED FUTURE WORK

Although much effort has been put into the research work for this thesis to make it as complete as possible, there are still a number of issues missing which might be considered worthwhile for continued future research. Three possible areas of further research are envisioned:

(1) Modeling of stray capacitances. Stray capacitances in the present model are assumed to be non-frequency dependent and lossless. It might be possible to model stray capacitances in more detailed by introducing dielectric losses into the model, as shown in fig. 7.1. In addition, some of the aspects in the measurement of stray capacitance may need to be improved. Since capacitances are modeled as separate entities from the rest of the model, balanced conditions for stray capacitances may not need to be assumed.

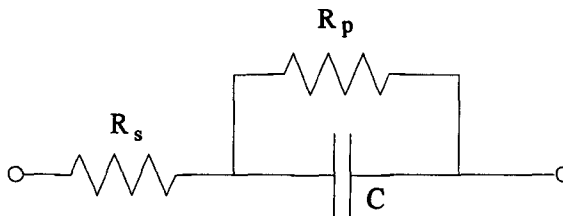


Fig. 7.1 Capacitance model with dielectric losses.

(2) Calculation of model parameters. As an alternative to measurements, it might be possible to determine the model parameters from the transformer physical dimension and construction. These data would have to be obtained from the manufacturer. Although most of the transformer data may be confidential, some manufacturers might still be willing to provide some useful information for educational purposes.

(3) Extend the capability of the model to cover any number of windings. It may not require much extra work to make the model valid for transformers having more than three windings. In this more general case, the concept of a T-equivalent circuit to model the coupling among N-coils ($N > 3$) may have to be abandoned in favor of "delta" branches connected among all nodes (similar to the connection in fig. 2.9c).

Chapter Eight

CONCLUSIONS

A wide-band general-purpose model has been developed for three-phase power transformer in the two and three windings per phase. Instead of using a $[Y(\omega)]$ matrix formulation for the transformer as seen from its external terminals, the model uses the classical 60-Hz T-circuit to represent the electric and magnetic interaction among coils belonging to the same phase. For three-phase common-core units, the mutual interaction among different phases is decoupled through a modal transformation matrix. Even though the concept is general, a balanced-system transformation matrix is assumed in order to simplify the modelling and the test data requirements. The decoupled sequence networks consist of a frequency dependent short-circuit branch and constant-valued terminal capacitances. These parameters were measured experimentally on a two-winding and a three-winding, three-phase core-type transformers. The two-winding transformer is rated at 50 MVA, 115/23 kV and the three-winding transformer is rated at 25 MVA , 115/22/11 kv. A technique was suggested that allows positive sequence impedance measurements to be made with a single-phase impedance analyser.

The model has been shown to give good results for both two-winding and three-winding transformers. Although the calculation of the series impedances from the

test data for the three-winding transformer is more complicated than for the two-winding case, the resulting impedances can still be synthesised with RLC networks with a high degree of accuracy.

As a result of the simplified topology, the frequency dependence modelling problem is reduced to the fitting of simple minimum-phase-shift impedances (the short-circuit impedances). Therefore, the possible numerical stability problems associated with the synthesis of the mutual terms in the $[Y(\omega)]$ formulation have been eliminated. Also, the model has fewer and simpler frequency dependent functions to synthesise, making it much faster than other models in time domain simulations.

Although the model presented in this thesis depends upon data obtained from measurements, the underlying concepts of the model are not limited to how the data is obtained. Once the data is available, regardless of its source, it can be processed in the same way explained in this thesis to get the parameters of the proposed model.

REFERENCE LIST

- [1] Morched, A. , Martí, L., Ottevangers, J.: "*A High Frequency Transformer Model for the EMTP*", IEEE Transactions on Power Delivery, vol. 7, No. 1, July 1992. pp. 1615-26.
- [2] D'Amore, M., and Salerno, M.: "*Simplified Models for Simulating Transformer Windings Subject to Impulse Voltage*", Paper A 79431-8, presented at IEEE PES Summer Meeting, Vancouver, British Columbia, Canada, July 1979.
- [3] P. T. M. Vaessen.: "*Transformer Model for High Frequencies*", IEEE Transactions on Power Delivery, vol. 3, No. 4, October 1988, pp. 1761-68.
- [4] R. C. Degeneff.: "*A Method for Constructing Terminal Models for Single-Phase n-Winding Transformers*", Paper A 78 539-9 presented at IEEE Pes Summer Meeting, Los Angeles California, July 1987.
- [5] T. Adielson, A. Carlson, H. B. Margolis, and J. A. Halladay.: "*Resonant Over-voltages in EHV Transformors - Modelling and Application*", IEEE Transactions on Power Delivery, vol. 1992 PAS-100, No. 7, July 1992 , pp. 3563-72.
- [6] CIGRE WG 33.02 (Internal Voltage): "*Guidelines for Representation of Network Elements When Calculating Transients*", CIGRE, 1989.
- [7] R. C. Degeneff.: "*A General Method for Determining Resoances in Transformer Windings*", IEEE Transactions on Power Apparatus and Systems, vol. PAS-96, No. 2, March/April 1977, pp. 423-30.
- [8] F. de León and A. Semlyen.: "*Complete Transformer Model for Electromagnetic Transients*", IEEE Transactions on Power Delivery, vol. 9, No. 1, January 1993, pp. 231-9.
- [9] Allan Greenwood.: "*Electrical Transients in Power Systems*", (Book) 2d ed., New York: John Wiley & Sons, Inc., 1991.

- [10] J. R. Martí. 1982.: *"Accurate Modelling of Frequency-Dependent Transmission Lines in Electromagnetic Transient Simulations"*, IEEE Transactions on Power Apparatus and Systems, vol. PAS-101, No. 1, January 1982, pp. 147-55.
- [11] William H. Press, Saul A. Teukolsky, William T. Vetterling and Brian P. Flannery.: *"Numerical Recipes in C : The Art of Scientific Computing"*, 2d ed. Cambridge: Cambridge University Press, 1992.
- [12] Clarke, Edith.: *"Circuit Analysis of A-C Power Systems, Volume I: Symmetrical and Related Components"*, (Book) New York: John Wiley & Sons, Inc., 1943.
- [13] H. Baher.: *"Synthesis of Electric Networks"*, (Book) New York: John Wiley & Sons, Inc., 1984
- [14] Hermann W. Dommel.: *"Electromagnetic Transients Program Reference Manual"*, Vancouver, B.C. , By the author, 1986.
- [15] J. R. Martí.: *"Modelling of Power Transformers (in Spanish)"*, Central University of Venezuela, Lecture note (1975).
- [16] Ross Caldecot, Yilu Liu and Selwyn E. Wright. 1990.: *"Measurement of the Frequency Dependent Impedance of Major Station Equipment"*, IEEE Transactions on Power Delivery vol. 5, No. 1, January 1990, pp. 474-80.
- [17] Yilu Liu, Stephen A. Sebo and Selwyn E. Wright.: *"Power Transformer Resonance - Measurements and Prediction"*, IEEE Transactions on Power Delivery, vol. 7, No. 1, January, 1992, pp. 245-53.
- [18] Francisco de Leon and Adam Semlyen.: *"Reduced Order Model for Transformer Transients"*, IEEE Transactions on Power Delivery, vol. 7, No. 1, January 1992, pp. 361-9.
- [19] P. T. M. Vaessen and E. Hanique.: *"A New Frequency Response Analysis Method for Power Transformer"*, IEEE Transactions on Power Delivery, vol. 7, No. 1, January 1992, pp. 384-91.
- [20] Richard L. Bean, Nicholas Chackan, Jr., Harold R. Moore, Edward C. Wentz. 1959.: *"Transformers for the Electric Power Industry"*, (Book) McGraw-Hill, 1959.

- [21] L. F. Blume, A. Bayajian, G. Camilli, T. C. Lennox, S. Minneci and V. M. Montsinger.: *"Transformers Engineering"*, (Book) 2d ed. New York: John Wiley & Sons, Inc., 1951

Appendix 1

FITTING OF THE IMPEDANCE FUNCTION

The frequency dependent part of the proposed transformer model is approximated with a series connection of several RLC network sections. One such section is shown in fig. 1. Each of the sections is used to duplicate one peak of the frequency response. The RL blocks can be viewed as representing the leakage inductance and associated losses,

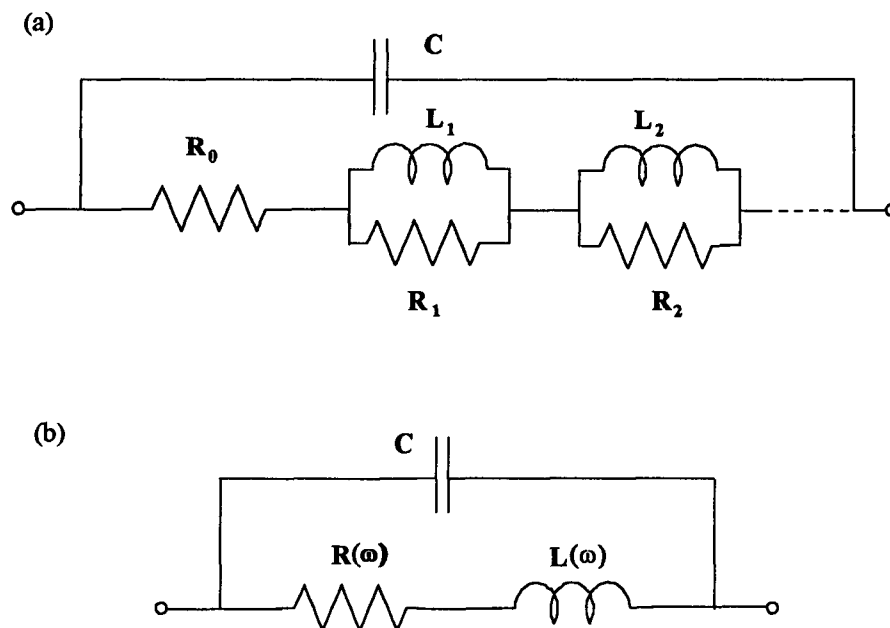


Fig. A1.1 Equivalent network representation of the frequency dependent branch of the sequence model. (a) A section representing any peak, (b) The frequency dependent resistance and inductance equivalent of (a).

which are both frequency dependent in nature due to skin effects in the transformer windings and associated physical enclosure. The capacitances of the synthesis blocks represent the interwinding capacitances which become reflected into the leakage impedance for modeling purposes. The combined impedance of the network of fig. 1 can be expressed as:

$$\begin{aligned}
 Z(\omega) &= \frac{[R(\omega) + j\omega L(\omega)]/j\omega C}{R(\omega) + j\omega L(\omega) + \frac{1}{j\omega C}} \\
 &= \frac{R(\omega) + j\omega L(\omega)}{[1 - \omega^2 CL(\omega)] + j\omega R(\omega)C} \quad (1)
 \end{aligned}$$

where,

$$R(\omega) = R_0 + \sum_{i=1}^n \frac{\omega^2 R_i}{\omega^2 + P_i^2},$$

$$L(\omega) = \sum_{i=1}^n \frac{R_i P_i}{\omega^2 + P_i^2},$$

and,

$$P_i = \frac{R_i}{L_i},$$

$$\begin{aligned}
 n &\geq 1 = \text{no. of RL parallel blocks for the principal peak,} \\
 &= 1 \quad \text{for remaining peaks.}
 \end{aligned}$$

The overall impedance of the frequency dependent branch is the sum of each block's impedance, as expressed in equation 1. To realize the parameters R_0 , R_i , P_i and C of each block, it is equally valid to fit either the magnitude or only the real part of the function

[1]. Since the impedance is a complex number, finding its magnitude involves operations of both squares and square roots of the real and imaginary parts. Furthermore, the magnitudes of two impedance functions cannot be added directly in order to get the total magnitude, while real parts of two functions can be combined by simple addition. Therefore, it is less complicated to fit the real part of the impedance function than it is to fit its magnitude. The real part of the combined frequency dependent impedance branch can be expressed as the sum of the real part of each impedance block. Multiplying both the denominator and numerator of equation 1 by the complex conjugate of the denominator, the real part of $Z(\omega)$ is found to be

$$\begin{aligned} \operatorname{Re}\{Z(\omega)\} &= \frac{R(\omega)}{[1 - \omega^2 CL(\omega)]^2 + [\omega R(\omega)C]^2} \\ &= \frac{R(\omega)}{Q(\omega)} \end{aligned} \quad (2)$$

where,

$$Q(\omega) = [1 - \omega^2 CL(\omega)]^2 + [\omega R(\omega)C]^2.$$

The Levenberg-Marquardt method (also called Marquardt method) for nonlinear functions [11] is used in the fitting of the real part of the impedance function. This method has been put forth by Marquardt based on an earlier suggestion by Levenberg. This method works very well in practice and has become the standard in nonlinear least-squares routines. The algorithm requires, at each iteration, an evaluation of partial derivatives of the model function with respect to each and every parameter on which the model

is dependent. The model function for the present problem is simply the sum of the real parts of all the blocks, which may be expressed as

$$F(\omega) = \sum_{i=1}^m \text{Re}\{Z_i(\omega)\} \quad (3)$$

where,

$$m = \text{no. of RLC impedance blocks or no. of peaks to be fit.}$$

Although $F(\omega)$ contains variables which come from all the impedance blocks, the partial derivatives of $F(\omega)$ with respect to the variables of one block will not include any variables from other blocks because all the blocks are independent of each other. The following are the partial derivatives of $F(\omega)$ with respect to R_o , R_i , P_i and C which are applicable to any block (from block # 1 to block # m) of the frequency dependent impedance of the transformer model:

$$\begin{aligned} 1) \frac{\partial F(\omega)}{\partial R_o} &= \frac{1}{Q(\omega)} \cdot \frac{\partial R(\omega)}{\partial R_o} - \frac{R(\omega)}{Q^2(\omega)} \cdot \frac{\partial Q(\omega)}{\partial R_o} \\ &= \frac{1}{Q(\omega)} - \frac{2R^2(\omega)\omega^2 C^2}{Q^2(\omega)} \\ 2) \frac{\partial F(\omega)}{\partial R_i} &= \frac{1}{Q(\omega)} \cdot \frac{\partial R(\omega)}{\partial R_i} - \frac{R(\omega)}{Q^2(\omega)} \cdot \frac{\partial Q(\omega)}{\partial R_i} \\ &= \frac{1}{Q(\omega)} \cdot \frac{\omega^2}{\omega^2 + P_i^2} \\ &\quad - \frac{R(\omega)}{Q^2(\omega)} \cdot \{2[1 - \omega^2 CL(\omega)][-\omega^2 C \frac{P_i^2}{\omega^2 + P_i^2}]\} \end{aligned}$$

$$\begin{aligned}
& + 2\omega^2 C^2 R(\omega) \frac{\omega^2}{\omega^2 + P_i^2} \} \\
3) \quad \frac{\partial F(\omega)}{\partial P_i} &= \frac{1}{Q(\omega)} \cdot \frac{\partial R(\omega)}{\partial P_i} - \frac{R(\omega)}{Q^2(\omega)} \cdot \frac{\partial Q(\omega)}{\partial P_i} \\
&= \frac{1}{Q(\omega)} \cdot \frac{-2\omega^2 R_i P_i}{(\omega^2 + P_i^2)^2} \\
&\quad - \frac{R(\omega)}{Q^2(\omega)} \cdot \{ 2[1 - \omega^2 CL(\omega)][-\omega^2 C \frac{\partial L(\omega)}{\partial P_i}] \\
&\quad + 2\omega^2 C^2 R(\omega) \cdot \frac{-2\omega^2 R_i P_i}{(\omega^2 + P_i^2)^2} \},
\end{aligned}$$

where,

$$\frac{\partial L(\omega)}{\partial P_i} = \frac{R_i}{\omega^2 + P_i^2} - \frac{2R_i P_i^2}{(\omega^2 + P_i^2)^2} .$$

$$\begin{aligned}
4) \quad \frac{\partial F(\omega)}{\partial C} &= \frac{1}{Q(\omega)} \cdot \frac{\partial R(\omega)}{\partial C} - \frac{R(\omega)}{Q^2(\omega)} \cdot \frac{\partial Q(\omega)}{\partial C} \\
&= \frac{R(\omega)}{Q^2(\omega)} \cdot \{ 2\omega^2 L(\omega)[1 - \omega^2 CL(\omega)] + 2C\omega^2 R^2(\omega) \}
\end{aligned}$$

In implementing the algorithm, all the peaks are initially approximated with simple blocks of RLC elements. The dc resistance R_0 is not initially included. The purpose of this simplification is to find a set of circuit parameters which will be used as an initial guess for further detailed fitting. For these simple blocks, there are only two unknown parameters to be fitted for each block: although there are three variables, i.e., R , L and C , the variables L and C can be assumed to be dependent. They are related to the resonant

frequency of the block, ω_0 , by the well known relationship $\omega_0^2 = (LC)^{-1}$. The resonant frequency of each block is readily obtainable from the test data. Therefore, the real part of each block can be reduced from the full expression

$$Re\{Z(\omega)\} = \frac{\omega^2 RL}{R^2(1 - \omega^2 LC)^2 + \omega^2 L^2} \quad (4)$$

down to

$$Re\{Z(\omega)\} = \frac{\omega^2 RL^2}{R^2 \left(1 - \frac{\omega^2}{\omega_0^2}\right) + \omega^2 L^2} \quad (5)$$

which contains only two parameters to be fitted, R and L . The initial value of R is assumed to be the peak value of the real part at the frequency where the resonance of the block occurs. The initial value for L is chosen from the $Z(s)$ function as follow. Let

$$Z(s) = \frac{s/C}{s^2 + \frac{s}{RC} + \frac{1}{LC}} \quad (6)$$

Then, in order for $Z(\omega)$ to have a resonant peak, the roots of the denominator of $Z(s)$ must be complex, or equivalently

$$\left(\frac{1}{RC}\right)^2 - \frac{4}{LC} < 0$$

which is the same as

$$\frac{1}{RC} < \frac{2}{\sqrt{LC}} \quad (7)$$

At resonance, it is already known that

$$\omega_0 = \frac{1}{\sqrt{LC}} \text{ and,}$$

and

$$\frac{1}{C} = \omega_0^2 L$$

Substituting into equation 7, one obtains

$$\frac{\omega_0^2 L}{R} < 2\omega_0$$

which implies that

$$L < \frac{R}{\pi f_0} \quad (8)$$

Based on equation 8, an initial value of L is taken as

$$L_{initial} = \frac{0.1R}{\pi f_0} \quad (9)$$

After the initial fit, the low frequency region before the principal peak is further refined by adding several RL parallel blocks. After removing the capacitance of the first

peak (obtained from the initial global fitting procedure), the asymptotic approximation technique of [1, 10] is used to fit the *magnitude* rather than the *real part* of the impedance function.

The RL parameter of the initial frequency region, together with the parameter for the peaks from the initial global fitting procedure are combined together as an initial guess for a re-optimization. This second optimization will now include dc resistances for all the impedance blocks. The initial values for these R_0 's can be any small numbers and are arbitrarily chosen to be 0.1 ohm each. The correct values will be given by the optimization result.

Since numerical stability is an important issue for the electromagnetic transients simulation program, the least-square fits must be constrained so that the result is numerically stable. At the same time, the result must be compatible with the test data. One of the advantages of parameters realization by fitting the real part of the impedance function is that the real part is always positive for a minimum-phase-shift function. Referring to equation 2, it is seen that $Q(\omega)$ is always positive due to the square operations. If the whole function is to be positive, then $R(\omega)$ must be positive too. One way that this condition can be satisfied, as indicated by equation 1, is to select all R_i as positive numbers. Since the synthesis impedance block consists of two branches, namely, the capacitance branch and the RL branch, the total network will be numerically stable if both branches are numerically stable themselves. The RL parallel network will be numerically stable if its pole (P_i) is positive. Keeping P_i positive and using only positive C 's makes the poles of

the rational function approximation positive, therefore guaranteeing that the overall function is numerically stable. The result of keeping P_i and R_i positive automatically leads to positive L_i . Having C and L_i positive makes it certain that $Q(\omega)$ has a minimum (equation 2) which will in turn cause the function $Re\{Z(\omega)\}$ to possess a maximum which is the objective of performing the fitting.